Morphological effects of buildings in a sandy beach environment

Daan Poppema

Daan Poppema
Morphological effects of buildings in a sandy beach environment

Invitation

To attend the public defense of the PhD thesis:

Morphological effects of buildings in a sandy beach environment

by Daan Poppema

On Friday 8 April 2022 at 14:30

In Waaier 4
(prof dr. Berkhoff room),
University of Twente,
Enschede

Contact:
Daan Poppema
d.w.Poppema@utwente.nl

Paranymphs:
Joost Kranenborg
j.w.m.kranenborg@utwente.nl

Wessel van der Sande
w.m.vandersande@utwente.nl

MORPHOLOGICAL EFFECTS OF BUILDINGS IN A SANDY BEACH ENVIRONMENT

Daan Willem Poppema

Graduation committee:

prof. dr. ir. H.F.J.M. Koopman	University of Twente, chairman and secretary
prof. dr. K.M. Wijnberg	University of Twente, promotor
prof. dr. S.J.M.H. Hulscher	University of Twente, promotor
dr. J.P.M. Mulder	University of Twente, co-promotor
prof. dr. D. van der Wal	University of Twente
prof. dr. ir. C.H. Venner	University of Twente
prof. dr. ir. T.K. Thiis	Norwegian University of Life Sciences
prof. dr. A. Kroon	University of Copenhagen
dr. ir. S. de Vries	Delft University of Technology

The presented research is carried out at the Water Engineering and Management (WEM) group, Civil Engineering, University of Twente, The Netherlands. This work is part of the research programme ShoreScape, which is (partly) financed by the Dutch Research Counsil (NWO).

ISBN: 978-90-365-5352-0
DOI: 10.3990/1.9789036553520
Cover design: Daan Poppema
Printed by: Ipskamp Printing

MORPHOLOGICAL EFFECTS OF BUILDINGS IN A SANDY BEACH ENVIRONMENT

DISSERTATION

to obtain
the degree of doctor at the University of Twente,
on the authority of the Rector Magnificus
prof. dr. ir. A. Veldkamp,
on account of the decision of the Doctorate Board,
to be publicly defended
on Friday 8 April 2022 at 14.45 hours

by

Daan Willem Poppema

born on 14 August 1993
in Groningen, The Netherlands

This dissertation has been approved by:

prof. dr. K.M. Wijnberg	Promotor
prof. dr. S.J.M.H. Hulscher	Promotor
dr. J.P.M. Mulder	Co-promotor

The wind was not the beginning. There are neither beginnings nor endings to the turning of the Wheel of Time. But it was a beginning.

– *Robert Jordan*

Contents

Preface

De afgelopen vier jaar heb ik onderzocht hoe gebouwen op zandstranden hun omgeving beïnvloeden. Het is een cliché, maar deze periode is voorbij gevlogen! Dit proefschrift had er niet gelegen zonder een groot aantal mensen, die ik graag wil bedanken.

Als eerste mijn begeleiders. Kathelijne, bedankt voor je eindeloze ideeën in mijn onderzoek en de kritische blik waarmee je me pushte om altijd door te vragen hoe iets nu eigenlijk werkt. Ik waardeer onze wekelijkse overleggen, en hoe je ook daarbuiten iedere keer weer tijd voor me wist te maken. Ik heb genoten van ons veldwerk op Terschelling, de Zandmotor en de kleinere uitstapjes met de drone en de gesprekken over carrièreplannen in de auto ernaartoe. Jan, mijn begeleider 'op afstand': bedankt voor alle hulp en je aanstekelijke enthousiasme. Je was niet alleen onmisbaar bij alle veldexperimenten, maar ook bij uitstek degene die het Shorecape project als geheel bij elkaar bracht. Daarnaast heb ik kunnen genieten van je tegeltjeswijsheden en de achterliggende les om bij ieder idee of maatregel eerst het doel vast te stellen. Suzanne: je begeleidde me al bij mijn afstuderen, en ik ben erg blij dat je me daarna de kans hebt gegeven deze PhD te doen. Ook al was onze samenwerking wat minder direct, jouw aandacht voor projectmanagement heeft me een hoop geholpen en je feedback op de papers hielp iedere keer weer om het doel en verhaal scherp te krijgen.

Aan mijn co-auteurs, Sander en Andreas: bedankt voor de fijne samenwerking, jullie bijdragen en expertise hebben de papers duidelijk sterker gemaakt. Ik heb niet alleen inhoudelijk een hoop van jullie geleerd, maar ook qua schrijfstijl en presentatie van mijn werk.

Then I have a large number of people to thank for their help with the field experiments. For even though pursuing a PhD is mostly an individual endeavour, the field experiments were anything but. Als eerste: Jan Willem. Onze eerste kennismaking was bij je afstuderen waar ik je begeleidde, maar ik heb je vooral leren kennen tijdens meerdere weken aan veldwerk. Jouw enthousiasme en praktisch inzicht maakten je tot een fantastische hulp op het strand, maar ik heb zeker zulke goede herinneringen aan alle gezelligheid en spelletjes, op Terschelling en bij de Zandmotor. Then I want to thank all colleagues, students and others for helping and working together at the beach. Paran, Geert, Janneke, Sander, Mieke, Christa, Wessel, Vera, Weiqiu, Sara, Sam, Mariëlle, Andrea and Ton: I appreciate the help and enjoyed working with you and getting to know you in a different environment! For all of you that were scheduled to help, but not needed for a lack of wind: your enthusiasm was still very much appreciated.

To Paran and Janneke, my fellow members in het ShoreScape project: I enjoyed our shared discussions, even when we had some difficulties coming to a shared lingo between engineering and spatial design. Luckily our shared chapters in the Rius book helped to bring our language and arguments together. Our shared time during the experiments at Terschelling, Kijkduin and Noordwijk remain a highlight of my PhD.

Also a big thanks to all other colleagues, for fun coffee breaks and lunch walks at the UT, but especially for pub quizzes, 'daghappen', playing squash, the Batavierenrace, barbecues and all other activities that gave me the energy to do my research and that make WEM such a nice group to work at. Een speciale vermelding voor Koen, Koen en Geert voor de fantastische congres- en reiservaringen in Shanghai, Tampa en Cuba. Joost en Wessel: ik ben ontzettend blij met al onze frisbeepauzes in het Van Heekpark tijdens de lockdown. Anke, Monique, Dorette and Joke: dank voor alle hulp als ik dingen geregeld moest hebben. Jullie kregen het altijd voor elkaar, ook als er vanwege experimenten en voorspelde wind weer eens grote haast achter zat. Vera, Weiqiu: we have been office mates since the start of our PhD's and I am really happy that we could finish it together back at the office as well. I don't remember any of the Chinese we had on our whiteboard for over two years, but I enjoyed the conversations on China, work, weekend activities and of course our annual Christmas decorations.

Then I have all my friends to thank for their support and interest in my work, but especially for all-important distractions and fun moments outside of work. To my current and former housemates: I enjoyed living together, from the daily conversations after work to the international cooking and the project to upgrade our garden. Aan alle Vakgerichters: de sportieve uitlaatklep, het borrelen, ouwehoeren, spelletjesavonden, toernooien en talloze andere activiteiten waren altijd mooi. Dankzij jullie kon ik me nog een tijd langer half student voelen. Aan de 'avond Assen' crew: de avonden Assen waren altijd fantastisch, zelfs als ze niet in Assen waren. 'Duinen voor dummies' is het helaas niet geworden. Tom, Ruud, Ivo: het fietsen, geocachen, de vakanties en barbecues waren altijd gezellig, dat er nog vele mogen volgen!

Mijn laatste dankwoord gaat naar mijn familie. Papa, mama, Joost, Miriam en Omi, bedankt voor alle vragen over mijn onderzoek, de krantenknipsels over water en jullie bezoek bij mijn werk op de Zandmotor. En bovenal: bedankt voor de fijne weekenden in Eenrum en dat jullie er altijd voor me zijn.

Enschede, maart 2022

Summary

The worldwide popularity of sandy beaches for tourism and recreation leads to an increasing presence of buildings at the beach: from houses for vacation or permanent inhabitation to restaurants, changing cabins, and buildings for lifeguards and rescue services. All these buildings affect their environment: buildings alter the airflow in their surroundings and thereby the windblown sediment transport. This causes patterns of deposition and erosion around buildings, which can for instance block roads, walkways or beach entrances. This can also have repercussions for the larger beach environment. Dune growth, which is required to balance natural storm erosion and sea level rise, only occurs with a healthy sediment influx into the dunes. Deposition patterns around a building mean that windblown sand transport is intercepted. For buildings placed in front a dune this implies a reduced sand influx into the dunes, thereby affecting coastal safety.

Coastal managers are responsible for defining the regulation that beach buildings should adhere to, and decide where, when and if buildings can be placed. This requires a proper understanding of how beach buildings shape their environment, and how this specifically depends on the building properties that can be addressed by regulation. Therefore, this thesis aims to determine and understand quantitatively how buildings at a sandy beach affect the wind-driven morphological development of the beach environment.

To examine the initial deposition and erosion patterns that develop around a building, field experiments were conducted with scale models of buildings placed at the beach. These showed that deposition occurs at a small distance upwind of a building, as well as in two deposition tails extending outward obliquely behind a building. Lateral deposition can occur at the building sides, connecting the upwind and downwind deposition to form a continuous horseshoe shape. Scour can also occur, directly along the upwind wall and side walls, and especially at the upwind building corners. For wind perpendicular to a building, the sheltered lee directly behind a building often shows little bed level change, as a lack of sediment flow into this area limits deposition, while local airflow is too weak to cause erosion. If sediment does enter the lee, deposition due to the low windspeed and flow circulation can over time result in the formation of a substantial deposition ridge in the lee behind a building.

Next, the deposition size and the dependency of the deposition size on building geometry were examined. The horizontal size of the initial deposition appears to depend on the width and height of the wind-facing wall. A new building factor $B = w^{2/3}h^{1/3}$ was established, which, by combining the effect of the building width w and height h, linearly relates the building geometry to the horizontal extent of the deposition. In addition, deposition size depends on the wind speed. Especially the initial downwind deposition length is affected, and increases approximately linear with wind speed.

For wind at an oblique angle to a building, the general picture of bed level change remains the same as for wind perpendicular to a building, with upwind deposition, two downwind deposition tails obliquely behind the building and local scour directly around the building. However, wind and sand diverted around a building are now split unevenly between both sides of a building. This creates downwind deposition tails that are asymmetrical, i.e. one tail that is longer than the other. The difference in length is determined by the orientation of the wind-facing walls, and their effective width measured perpendicular to the wind direction.

For configurations with multiple buildings, the building spacing largely determines the morphological patterns that develop. Buildings placed close together create resistance to airflow and sediment transport through the gaps between buildings. For buildings with approximately equal width and height, and wind perpendicular to the buildings, this results in higher and longer upwind deposition areas for a gap width of 0.5w compared to a gap width of at least 1w. Downwind, it means that smaller building spacing results in smaller deposition tails behind the gaps, but larger deposition tails at the outside of a building group. For gap widths of up to 2w, the bed level pattern around a building differs substantially from observations for stand-alone buildings, indicating a different type of airflow pattern developing between buildings. For larger gap widths, the pattern is similar to that of stand-alone buildings, with deposition tails being the sum of the individual building effects where they overlap.

Next, interactions of building-induced bed patterns with natural aeolian bedform dynamics are studied using a cellular automaton (CA) model. New CA rules are developed to include the sediment transport dynamics around building in an existing CA model for self-organized aeolian morphodynamics. Based on a comparison of CA model results and field experiments, the model successfully captures the morphodynamics around buildings, with good agreement in terms of the shape of deposition and erosion patterns around individual buildings as well as the interactions that occur around building groups. Model results further demonstrate that building-induced effects interact with aeolian bedform dynamics and can alter dune shape, growth and migration.

Overall, this study has revealed that systematic relations exist between the geometric characteristics of buildings – individual buildings and building groups – and the induced aeolian deposition and erosion patterns. Quantitative relations were derived for the horizontal extent of the initial deposition patterns and for the asymmetry of the deposition tail lengths. For building groups, three building spacing regimes were identified, each with different morphological patterns around buildings. The long-term simulations illustrate how interactions of building-induced effects with aeolian bedform dynamics can alter dune development. These findings contribute to the much-needed scientific support for regulations for permitting buildings on the beach.

Samenvatting

Door een wereldwijde vraag naar strandrecreatie en toerisme is er steeds meer bebouwing op stranden aanwezig. Van woonhuizen en vakantiehuisjes tot restaurants, kleedkamers, en gebouwen voor de strand- en kustwacht: al deze gebouwen beïnvloeden hun omgeving. Ze veranderen de windpatronen in hun omgeving en daarmee ook het eolisch zandtransport. Dit veroorzaakt patronen van depositie en erosie om gebouwen, die vervolgens wegen, paden en strandopgangen kunnen blokkeren. Dit alles heeft ook gevolgen voor de waterveiligheid. Als compensatie voor natuurlijke stormerosie en zeespiegelstijging is namelijk duinaangroei nodig. Dit vereist voldoende sedimenttransport van het strand naar de duinen. Depositie rondom gebouwen impliceert dat er sediment wordt onderschept. Voor strandbebouwing die voor het duin staat, houdt dit een reductie van de zandaanvoer richting het duin in, en daarmee een negatief effect op waterveiligheid.

Kustbeheerders zijn verantwoordelijk voor het vaststellen van de regelgeving waaraan strandbebouwing moet voldoen. Ze bepalen waar, wanneer en óf het plaatsen van gebouwen is toegestaan. Dit vereist een gedegen begrip van de invloed van strandbebouwing op haar omgeving, en vooral van hoe dit afhangt van gebouweigenschappen waar men met regelgeving op kan sturen. Het doel van dit proefschrift is daarom om kwantitatief te bepalen en begrijpen hoe strandbebouwing de eolische morfologische ontwikkeling van de strandomgeving beïnvloedt.

De initiële depositie- en erosiepatronen rondom gebouwen zijn onderzocht op basis van veldexperimenten, met schaalmodellen van gebouwen op het strand. Deze experimenten toonden aan depositie plaatsvindt op een kleine afstand bovenwinds van het gebouw en in twee depositiestaarten schuin achter het gebouw. Vlak naast het gebouw vindt soms depositie plaats, in welk geval de bovenwindse en benedenwindse depositie worden verbonden tot één hoefijzervormig geheel. Ook treedt er regelmatig scour op, direct langs de bovenwindse muur en zijmuren en vooral rond de bovenwindse gebouwhoeken. Als de wind recht op een gebouw staat, treedt er in de luwte achter het gebouw over het algemeen weinig depositie of erosie op: depositie wordt beperkt door de geringe sedimentaanvoer terwijl de lage windsnelheden te zwak zijn om erosie te veroorzaken. Maar als er toch sediment wordt aangevoerd, zal dit neerslaan door de windcirculatie en lage windsnelheid achter het gebouw. Dit kan uiteindelijk een substantiële depositierichel vormen.

Vervolgens heb ik gekwantificeerd hoe de afmetingen van deze depositiepatronen afhangen van de gebouwgeometrie. De horizontale afmetingen van de initiële depositie hangen af van de gebouwhoogte h en breedte w. En nieuwe gebouwfactor $B = w^{2/3} h^{1/3}$ is vastgesteld, die de horizontale depositieafmetingen lineair linkt aan deze gebouwafmetingen. Daarnaast hangen de depositieafmetingen ook af van de windsnelheid. Dit geldt het sterkst voor de depositiestaarten, die in lengte ongeveer lineair schalen met de windsnelheid.

Als de wind schuin op een gebouw staat, blijft het algemene beeld qua bodemveranderingen hetzelfde. Dus depositie bovenwinds en in twee staarten benedenwinds schuin achter het gebouw, en lokale scour direct voor en naast het gebouw. Echter, wind en zandtransport worden nu niet langer gelijkmatig langs de linker- en rechterkant van een gebouw geleid. Hierdoor ontstaat asymmetrische depositie, waarbij de ene depositiestaart langer is dan de andere. Het verschil in lengte wordt bepaald door de oriëntatie van de muren en hun effectieve breedte loodrecht op de wind.

Voor groepen van meerdere gebouwen is de tussenafstand bepalend voor wat voor morfologische patronen er ontstaan. Als gebouwen dicht bij elkaar staan, creëert dit weerstand voor de luchtstroming en het zandtransport tussen gebouwen door. Bij gebouwen die ongeveer even breed als hoog zijn, resulteert dit in sterkere bovenwindse depositie (hoger en langer) voor een tussenafstand van 0.5w dan voor een afstand van 1w of meer. Benedenwinds, achter de gebouwen, is het gevolg dat depositie achter de gaten tussen gebouwen afneemt naarmate deze gaten kleiner worden, terwijl de depositie aan de buitenkant van de groep juist toeneemt. Bij tussenafstanden tot 2w verschilt het bodempatroon rondom een gebouw in een groep substantieel van het patroon rondom een alleenstaand gebouw. Dit geeft aan dat ook de windpatronen wezenlijk verschillen. Bij grotere tussenafstanden gaan de patronen rondom alleenstaande gebouwen en gebouwgroepen meer op elkaar lijken, waarbij voor overlappende gebouweffecten de verwachte depositie gesommeerd kan worden.

Ten slotte zijn interacties van de morfologische patronen rond gebouwen met natuurlijke eolische bedvormdynamiek onderzocht, met behulp van een cellulaire automaat (CA) model. Nieuwe CA regels voor sedimenttransport rondom gebouwen zijn ontwikkeld en toegevoegd aan een bestaand model voor natuurlijke morfodynamiek. Uit vergelijking van de CA resultaten met onze veldexperimenten blijkt dat het model de morfodyamica rondom gebouwen succesvol beschrijft. Dit geldt zowel voor de vorm van de depositie- en erosiepatronen rondom alleenstaande gebouwen als voor de interacties rond gebouwgroepen. Daarnaast tonen simulaties aan dat interactie van deze patronen rond gebouwen met natuurlijke bedvormdynamiek de vorm, groei en migratie van duinen kan beïnvloeden.

Al met al heeft dit onderzoek systematisch relaties vastgesteld tussen de geometrie van bebouwing – dus van individuele gebouwen en gebouwgroepen – en de resulterende depositie- en erosiepatronen. Er zijn kwantitatieve relaties afgeleid voor de horizontale afmetingen van initiële depositiepatronen en voor de asymmetrie van depositiestaarten achter gebouwen. Voor gebouwgroepen zijn drie verschillende regimes aangetoond, elk met een ander type morfologische patroon. De lange-termijn simulaties geven aan hoe interacties tussen gebouweffecten en natuurlijke eolische bedvormdynamiek ingrijpen op duinontwikkeling. Daarmee dragen deze bevindingen bij aan de hoognodige wetenschappelijke onderbouwing van regelgeving voor het toestaan van strandbebouwing.

1

General introduction

1

General introduction

Figure previous page: Deposition behind beach houses at Julianadorp, The Netherlands.

1.1 Background

Beaches are among the most popular destinations for recreation and tourism, for walking, swimming, sunbathing, surfing and numerous other activities. This results in the presence of buildings such as restaurants, bars, hotels, bath houses and changing cabins to cater to beach visitors; buildings for lifeguards and rescue services; and houses for both vacation and permanent inhabitation (Fig. 1.1). Simultaneously, beaches also provide other ecosystem services. Together with the dunes, beaches act as a buffer to provide safety against floods, locally at the coast, but also for the hinterland. Moreover, the rich and dynamic nature of beaches and dunes represents essential ecological values, adds to the appeal of the coast for tourism (Dwyer & Edwards, 2000; Hall, 2001) and, in the form of vegetation capturing sediment and building up the coast (Feagin et al., 2015; Ruggiero et al., 2018), supports coastal safety.

All these beach activities and functions are interconnected. Buildings are *not* just passive structures placed at the beach for us humans to enjoy their benefits. Their presence and usage have consequences for their surroundings: buildings affect airflow, windblown sediment transport, morphology and vegetation development in their surroundings (Hunt, 1971; Jackson & Nordstrom, 2011; Luo et al., 2012; Mitteager et al., 2006) and, conversely, buildings are affected by the dynamics of their environment (Sherman & Nordstrom, 1994). Moreover, beaches are part of a larger coastal system, with the intertidal area at one side, and (often) dunes at the other side. The exchange of sediment between these areas allows the beach and dunes to accrete, as needed to recover from storm erosion (Morton et al., 1994) or keep up with (relative) sea level rise (De Winter & Ruessink, 2017; Keijsers et al., 2016). Therefore, any effect of buildings on the sediment exchange with the dunes can eventually have repercussions for coastal safety.

Local authorities and coastal managers have to decide *if* and *where* they allow buildings at the beach, and set any regulation these buildings should adhere to, in the form of for

Figure 1.1: Examples of Beach buildings. Left: beach houses in Julianadorp, NL. Right: Beach restaurants in Katwijk, NL (© Thomas Steenvoorden).

instance the allowed building size, building spacing and building location (Nordstrom & McCluskey, 1984). Setting these rules requires a proper understanding of how buildings shape their surroundings. This entails a general understanding of the building effects and long-term consequences for both coastal safety and other coastal functions, but especially also knowledge of how this depends on the building characteristics that can be addressed by regulation. This knowledge is extra relevant in the present-day context of increasing demand for coastal tourism (Hall, 2001; Moreno & Amelung, 2009; Orams & Lück, 2014) and buildings on the beach (Malavasi et al., 2013; Schlacher et al., 2008), while climate change and (relative) sea level rise threaten coastal safety.

Therefore, this thesis studies the morphological effects of buildings in a sandy environment. The remainder of this chapter describes the pre-existing knowledge of how these buildings affect their environment; followed by the knowledge gap; research aim and questions; the approach for answering these questions; and finally the outline of the thesis.

1.2 Effects of buildings on a sandy environment

Any obstacle or topographic variation in a sandy landscape will affect the wind flow and thereby aeolian sand transport, whether it is a natural bedform such as a dune, vegetation, or a manmade object like a building. Dunes affect the incoming wind by inducing wind deceleration in front of the dune; wind acceleration from streamline compression over the stoss slope a dune and deceleration, flow detachment and recirculation behind the dune (Smith et al., 2017a; Wiggs et al., 1996). The downwind flow deceleration and recirculation cause deposition that is essential for dune growth and migration (Baas, 2007; Werner, 1995). In addition, the presence of dunes leads to changes in the local wind direction, bed shear stress and turbulent intensity (Bauer et al., 2012; Hesp et al., 2015; Smith et al., 2017a). Likewise, vegetation affects the local airflow, with as main effect flow deceleration and increased sedimentation that cause shadow dune formation (Charbonneau et al., 2021; Hesp, 1981; Wiggs et al., 1994), but also a potential for local wind acceleration, especially directly to the side of plants (Ash & Wasson, 1983; Leenders et al., 2007) or under tree canopies (Cheng et al., 2020).

On the same principles, buildings affect the airflow in their surroundings. However, an essential difference is that buildings are (usually) bluff objects, i.e. they have sharp edges and angles compared to more aerodynamic shape of a dune. As a result, airflow cannot exactly follow the bed surface and building shape, so flow detachment and recirculation occur (Fig. 1.2). The resulting airflow pattern has been studied extensively (Baskaran & Kashef, 1996; Beranek, 1984; Castro & Robins, 1977; Gao & Chow, 2005; Hunt, 1971; Kothari et al., 1986). A building obstructing the wind flow effectively creates a horseshoe vortex around the building. Wind is decelerated and detaches from the bed and forms a rolling vortex in front of the building . This vortex is wrapped around the building, forming a

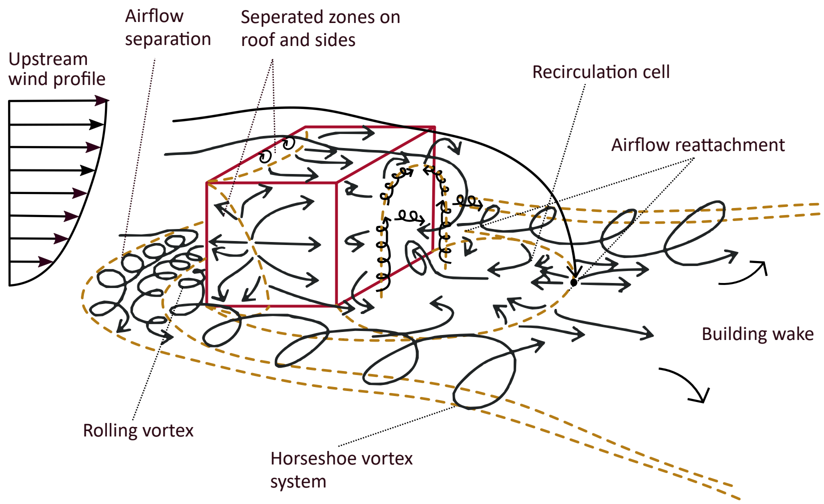

Figure 1.2: The mean streamline patterns around a cuboid building oriented perpendicular to the wind, modified from Hunt et al. (1978) and Blocken et al. (2011).

horseshoe shape. In the horseshoe vortex tails, besides and obliquely behind the building, airflow is accelerated. In the lee behind the building, airflow deceleration and recirculation occur.

In a sandy environment – being a beach, coastal dune or desert – these wind flow patterns around buildings shape the local morphology. Wind usually causes scour along the sides of a building (Jackson & Nordstrom, 2011), at the upwind wall and especially upwind corners (Iversen et al., 1991; Iversen et al., 1990; McKenna Neuman et al., 2013; Tominaga et al., 2018). Upwind deposition forms a small distance upwind of the building, as visible in (Fig. 1.3), or as a ramp against the upwind building wall (Canning, 1993; Jackson & Nordstrom, 2011; Nordstrom & Jackson, 1998). This is caused by the rolling recirculation vortex upwind of a building, which decelerates sand or blows it against the general wind direction. This initially creates deposition a small distance upwind of the building, which can eventually grow against the building face, similar to the echo dunes and climbing dunes that occur in front of natural cliffs (Qian et al., 2011; Tsoar & Blumberg, 1991; Tsoar, 1983). Based on wind tunnel experiments, deposition is reported to occur in the sheltered lee behind buildings, while erosion occurs at the horseshoe vortex tails obliquely behind the building (Fig. 1.2) due to increased wind speed and vorticity (Iversen et al., 1991; Iversen et al., 1990; McKenna Neuman et al., 2013; Tominaga et al., 2018). Conversely, in field experiments on snow accumulation, deposition was observed in the areas obliquely behind the buildings, as well as occasional deposition along the building sides (Liu et al., 2018; Thiis, 2003; Thiis & Gjessing, 1999). Nordstrom and McCluskey (1984) reported deposition as the primary effect around buildings, describing houses built on the ground as sediment traps.

Figure 1.3: Deposition in front of a row of holiday houses at the beach (Katwijk, The Netherlands)

On a larger scale, urban development can disconnect dunes from the beaches that serve as source area for sand blown into the dunes or completely cover the source areas, such that they are no longer available (Malvárez et al., 2013). Urban areas can also substantially alter wind speed, wind direction, and turbulent intensity, and thus the sediment flux potential (Hernández-Calvento et al., 2014; Smith et al., 2017b). For example: such flow perturbations at Maspalomas, Spain, resulted in a decrease of dune dynamics and erosion in the lee behind the urban development, while adjacent to the urban development wind was accelerated, increasing erosion and expanding deflation surfaces (Smith et al., 2017b).

The effect of buildings located at the beach-dune interface on sediment transport volumes to the dunes was examined in professional reports, written for Dutch water managers and regional authorities. Deposition occurred in front of buildings, which lowered transport rates to the dunes, thereby resulting in decreased deposition or even erosion behind buildings (Hoonhout & Van Thiel de Vries, 2013; Van der Valk & Van der Meulen, 2013). This was especially clear for semi-continuous structures such as rows of holiday homes and even the case for buildings only present in summer. High-resolution aerial drone measurements, taken around multiple buildings over one year (De Zeeuw, 2017) further showed varying patterns of deposition and erosion directly around buildings, but in all cases a negative effect on the dune growth volumes.

1.3 Knowledge gap

Although it is clear that buildings at the beach cause sedimentation and erosion (Nordstrom & McCluskey, 1984, 1985) and thereby affect aeolian sediment transport and beach-dune development (García Romero et al., 2016; Smith et al., 2017b), quantitative knowledge of how buildings affect their surroundings is limited. This lack of knowledge especially concerns systematic knowledge of how these effects depend on the building geometry (principally building size and shape) and building configuration (most notably the distance to other buildings and wind direction relative to the building) (Hoonhout & Van Thiel de Vries, 2013; Hoonhout & Waagmeester, 2014; Nordstrom & McCluskey, 1984). For instance, to model cross-shore sediment transport, Hallin et al. (2019) assumed conservatively that beach houses completely prevent aeolian sediment transport to the dunes, because it was unknown to what degree buildings intercept local sediment transport and how this depends on the building design and configuration.

Moreover, it remains unknown how interaction between local deposition and erosion around buildings and natural aeolian beach-dune dynamics affects the longer-term morphological development of the larger beach-dune system. Beaches are not static flat environments, due to various types of dynamic bedforms, including megaripples and sand dunes such as transverse dunes or barchans (Bagnold, 1941; Pye & Tsoar, 2008). The dynamics of these bedforms affect the sediment transport into the dunes (Nield et al., 2011). So when natural aeolian bedforms interact with building-induced deposition and erosion, this can over time (years to decades) change both the local morphology around a building and the sediment transport into the dunes.

1.4 Research aim and questions

The aim of this thesis is *to determine and understand quantitatively how buildings at a sandy beach affect the wind-driven morphological development of the beach environment.*

To achieve this aim, this research starts fundamentally, by characterizing the initial effect of buildings on a flat sandy bed, purely looking at aeolian sediment dynamics and excluding other processes (research question 1 to 3). By looking at the initial effect that occurs on the timescale of a wind event on a flat bed, the direct effect of a building itself can be examined, under uniform wind conditions and without topographic constraints or interactions with dunes or vegetation. This is also the reason that effects are examined on the scale of a single building or small building group, rather than on a city scale. Research question 1 starts with a general characterization of the deposition and erosion patterns that occur around buildings at a sandy beach. Next, research question 2 and 3 aim specifically for the systematic knowledge that was lacking, so how building effects (i.e. the erosion and deposition patterns around buildings) depend on the building geometry and configuration. These three steps focus on building effects on a static flat beach, but natural beaches are dynamic environments, and include bedforms interacting with the local building effects. Therefore, research question 4 extends the research to longer term (annual to decadal) evolution of building-induced bed patterns and the interaction of building-induced effects with the natural bedform dynamics of the beach.

Q1 *Which morphological patterns arise on the timescale of a wind event around a single* *building on a sandy beach?*

Q2 *How does the initial size of the deposition pattern around a single building depend on the building geometry?*

Q3 *How do initial morphological patterns depend on the spatial configuration of buildings?*

Q4 *How do building-induced morphological patterns interact over time with natural aeolian bedform dynamics?*

1.5 Research methodology

To examine the local deposition and erosion patterns around buildings at the beach (research question Q1-Q3), field experiments with cuboid scale models of buildings were used. The experimental approach allowed for systematically varying separate properties of the building design and spatial configuration, to determine how they affect the size and shape of the deposition and erosion patterns. By conducting the experiments on the beach rather than in a wind tunnel, the experiments could take place under real conditions and automatically included all spatial and temporal variability of real field conditions that are essential for wind-driven sediment transport. With respect to the sediment properties, this includes spatial grain size variation and supply limitations from vertical sorting of the bed (Hoonhout & De Vries, 2019), surface moisture (Namikas & Sherman, 1995), and wetting and drying (Bauer et al., 2009) of the beach. For the wind conditions, both short-term fluctuations (e.g. turbulence) and longer-term variations (e.g. slightly changing wind directions) were automatically included in the experiments as well. In combination with the large fetch lengths possible in the field, this allowed incoming sediment transport to be in equilibrium with the local conditions (Delgado-Fernandez, 2010), thereby ensuring that any changes to the wind field resulted in realistic changes to the sediment flux and beach morphology.

Scale models of buildings were used rather than full-scale models to make it feasible to place multiple models on the beach at the same time and easily position them at any desired orientation to the wind. Hereby, enough observations could be obtained to draw quantitative conclusions that would be difficult to achieve from only a few large scale models. The scale models used were between approximately 0.5 and 1.5 m in width, height and length, so about a 1:10 to 1:3 scale for a beach house of $3 \times 6 \times 3$ m. These models are larger than what would be possible in most wind tunnels, but the combination of smaller-than-real-life buildings and an unscaled environment (i.e. natural wind conditions and sediment properties) could still introduce scaling issues. Due to the limited scaling factor that was used and experiences from similar experiments in snow (Liu et al., 2018; Oikawa & Tomabechi, 2000), scaling issues were not expected to play a role in our experiments. This was checked by comparing the results around a small scale model with those around a full-scale model, placed at the beach simultaneously.

Three sets of experiments were conducted in order to answer the first three research questions (Fig. 1.4). First, cuboid scale models of varying width, length and height were placed at the beach for a day, all oriented approximately perpendicular to the wind. In *chapter 2*, this experiment is used to qualitatively examine the erosion and deposition pattern around buildings, with the focus on the various locations where deposition and erosion can occur. In *chapter 3*, the results from the same experiment are analysed quantitatively to determine how the size of the initial deposition pattern depends on building geometry and wind speed. Furthermore, as a second experiment, a small scale model (w, l, h of $0.5 \times 2 \times 0.5$ m) and full-scale model ($2.5 \times 12 \times 2.5$ m) were placed at the beach simultaneously for a period of approximately 5 weeks. This experiment is also analysed in *chapter 3*, to determine how well the deposition and erosion patterns match between small scale models and full-scale buildings; and to compare the initial effect of a building after a single wind event to the longer-term effect after 5 weeks. In *chapter 4*, a third set of experiments is used to determine the effect of the spatial configuration of buildings. Hereto, individual scale models and triplets of scale models were placed at the beach while varying scale model spacing and their orientation to the wind.

To examine the interaction of building-induced deposition and erosion patterns with natural bedform dynamics (Q4), computer modelling was used. Hereto a cellular automata (CA) model for aeolian landscape dynamics was extended with buildings effects, based on the insights and results obtained in the experiments. In morphodynamic CA models, rules are used to capture the essence of physical processes (Coulthard et al., 2007; Fonstad, 2013). Based on these rules, self-organisation emerges at the landscape scale from interactions between local topography, sediment transport and vegetation dynamics. This type of model is chosen because CA models excel in capturing the feedbacks and interactions between the processes that shape landscapes (Baas, 2002; Fonstad, 2013). In a sense they focus on the spatial distribution of sediment for a given sediment flux, whereas process-based aeolian models such as Aeolis (Hoonhout & De Vries, 2016), the Coastal Dune Model (Duran & Moore, 2013) and Duna (Roelvink & Costas, 2019) focus more on determining the amount of sediment flux.

More specifically, the DECAL model by Baas (2002) was used in this study. This model, and its successor Dubeveg by Keijsers et al. (2016), have been used previously to model the morphodynamics of natural sand deserts and beach-dune systems (Baas, 2007; Galiforni Silva et al., 2018; Nield & Baas, 2008b). They capture a range of relevant coastal processes, including aeolian sediment transport, groundwater, vegetation dynamics and hydrodynamics. In addition, the relatively simple model set-up allows for efficient modelling of long-term (annual to decadal) morphodynamic evolution (Baas, 2002; Nield & Baas, 2008a).

Chapter 5 describes how the CA model is extended with new rules to describe how buildings alter the sediment flow in their surroundings, with a novel horizon-scanning approach to

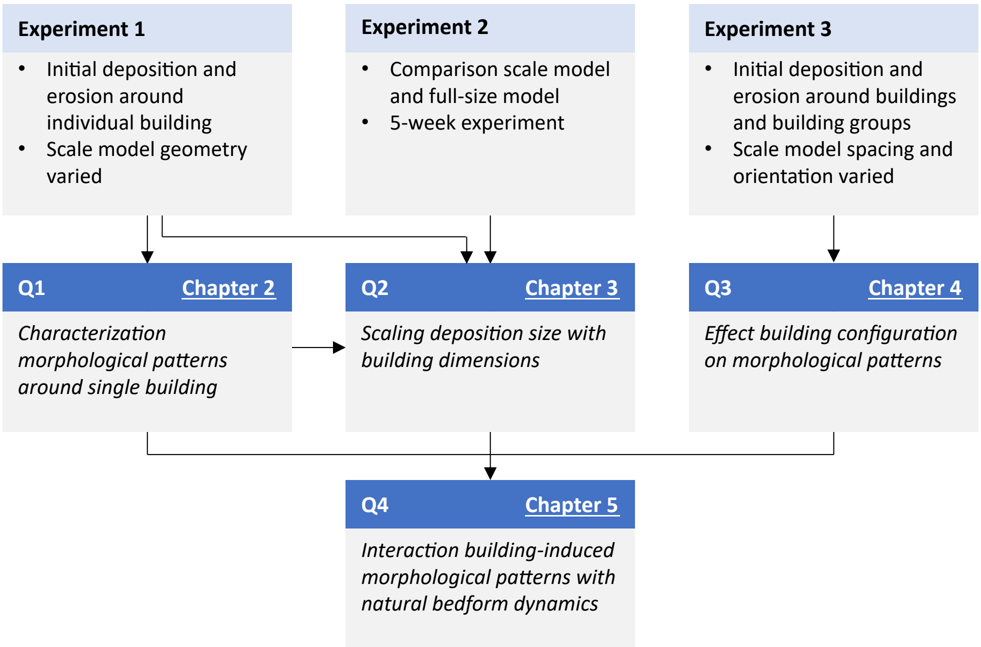

Figure 1.4: Thesis outline with the research question answered in each chapter.

capture the dependency on building size and the proximity to buildings. The effect of these new rules on the emerging morphology is tested by comparing the CA model results to observations from the field experiments. Next, longer-term model runs of up to 15 years are used to study how building-induced deposition and erosion patterns interact over time with natural aeolian bedform dynamics.

1.6 Thesis outline

The four research questions (Q1-Q4) are answered in chapter 2 to 5 (Fig. 1.4). Chapter 2 starts with a qualitative description of the initial deposition and erosion patterns around individual buildings, based on field experiments (Q1). Chapter 3 examines these patterns quantitatively, to assess how building dimensions and wind speed determine the size of deposition patterns (Q2). In chapter 4, more complex building configurations are tested, to examine how deposition patterns are affected by building orientation and building spacing (Q3). Next, chapter 5 uses the insights and results obtained in the field experiments of chapter 2-4 in order to model the effects of buildings and examine interactions between natural bedform dynamics and building-induced deposition and erosion (Q4). The obtained knowledge is put into perspective in the discussion (chapter 6), followed by the main conclusions and recommendations in chapter 7.

2

Morphological patterns around beach buildings

2

Morphological patterns around beach buildings

Abstract: Worldwide, buildings are present at the beach and in the dunes for recreation or habitation. Their presence can affect the beach-dune development, because they affect the airflow and aeolian sediment transport in their surroundings. This might eventually have repercussions for coastal safety. We start examining these effects by studying the local sedimentation and erosion patterns around buildings. Hereto, we placed scale models of buildings on the beach. The sedimentation and erosion patterns around the models were measured using structure-from-motion photogrammetry. In general, the airflow around bluff bodies like buildings forms a horseshoe vortex. This creates deposition and erosion patterns in a horseshoe shape. For nearly all scale models, the upwind part and downwind tails of the horseshoe showed deposition. The horseshoe deposition at the building sides was sometimes visible, also depending on building orientation. Frequently, smaller erosion and/or deposition areas also developed between the horseshoe deposition and the building.

Figure previous page: Deposition around a single scale model.

This chapter is published as Poppema, D.W., Wijnberg, K.M., Mulder, J.P.M., & Hulscher, S.J.M.H. (2019). Scale experiments on aeolian deposition and erosion patterns created by buildings on the beach. *Coastal Sediments 2019* (pp. 1693-1707): World Scientific. DOI: 10.1142/9789811204487_0146

2.1 Introduction

WORLDWIDE, URBANIZATION and a demand for recreation have led to buildings being built at the beach-dune interface. This occurs in the form of houses for recreational seasonal use or permanent habitation, hotels, restaurants and commercial stalls (Jackson & Nordstrom, 2011). In the Netherlands, there is an increasing demand for these buildings and a shift to more year-round present restaurants (Hoonhout & Waagmeester, 2014). A similar trend is found in other countries, both for coastal tourism in general (Hall, 2001; Moreno & Amelung, 2009) and the number of buildings at the beach-dune interface (Malavasi et al., 2013; Schlacher et al., 2008).

All these buildings alter the wind field and the related wind-driven sediment transport in their vicinity. They can decrease the wind speed and promote sedimentation in their surroundings, for instance in front of buildings and at the lee side of buildings (Jackson & Nordstrom, 2011; Nordstrom, 2000; Smith et al., 2017b). Conversely, airflow in between buildings can also be accelerated, causing local erosion and increased sediment transport (Jackson & Nordstrom, 2011; Nordstrom, 2000). The same effect can be seen under houses on pilings, where a scour zone can commonly be found (Jackson & Nordstrom, 2011; Nordstrom & McCluskey, 1985). Furthermore, an increased turbulent intensity in the wake of houses can promote an increase in sediment transport (Smith et al., 2017b). Continuous lines of buildings can also form a barrier for sediment transport, separating dunes from their beach or foredune sediment sources and thereby causing fetch segmentation (Jackson & Nordstrom, 2011; Smith et al., 2017b).

Aeolian sediment transport from the beach to the dune zone is essential for long-term coastal safety. Dunes protect the hinterland against flooding and provide a high ground to live on. They need an influx of sand to balance natural dune erosion caused by storms (Keijsers, 2015; Morton et al., 1994), to keep step with (relative) sea level rise, and to compensate for the expected increase in hydrodynamic erosion due to climate change (Carter, 1991; De Winter & Ruessink, 2017; Keijsers, 2015).

The combination of 1) a worldwide presence and demand for buildings at the beach-dune interface; 2) their effect on the aeolian sediment transport and beach-dune morphology; and 3) the importance of aeolian sediment transport for coastal safety, necessitates a proper understanding of how buildings on the beach-dune interface affect their environment. The first step in this research is to describe the local erosion and sedimentation patterns around a building and define generic patterns from these observations. To determine these erosion and deposition patterns, scale experiments on the beach were used, with various building geometries. The first of these field experiments were conducted in the fall of 2018, examining single buildings in isolation, placed directly on the ground.

In this chapter, we first describe the airflow around buildings and the expected sedimentation and erosion patterns (the theory section). Next, in the methodology we specify the set-up of our experiments. The results section gives a qualitative overview of the different types of sedimentation and erosion patterns that occurred during the experiment. Finally, the chapter ends with a discussion and conclusion.

2.2 Theory

The wind around a bluff object like a building forms a horseshoe vortex (see Fig. 1.2 and Hunt, 1971; Martinuzzi & Tropea, 1993; Peterka et al., 1985). A stagnation zone exists around 2/3 to 3/4 of the building height. Above this zone, wind is diverted upward and to the sides. Below this zone, the pressure caused by the wind profile diverts the wind downward and to the sides (Peterka et al., 1985). These upward and sideward flows separate from the front of the building at the edges. Upwind of the building, the increased pressure and downward flow cause a reverse flow close to the ground. This creates a rotating vortex in front of the building, that is wrapped around the building in a horseshoe shape (Hunt, 1971; Martinuzzi & Tropea, 1993; Peterka et al., 1985).

The separated flow over the building edges can reattach at the top and side of the building before it reaches the back of the building. Whether it reattaches depends on the building's length-to-width and length-to height ratio and on the turbulent intensity (Hunt, 1971; Peterka et al., 1985). If flow reattachment does not occur, the flow at the side and top of the building forms one big recirculation cell with the flow behind the building. If flow reattachment occurs, a separate recirculation cell is formed behind the downwind edges of the building. Within the recirculation cell, two standing vortices occur at the building corners, forming an arch behind the building (Martinuzzi & Tropea, 1993; Peterka et al., 1985).

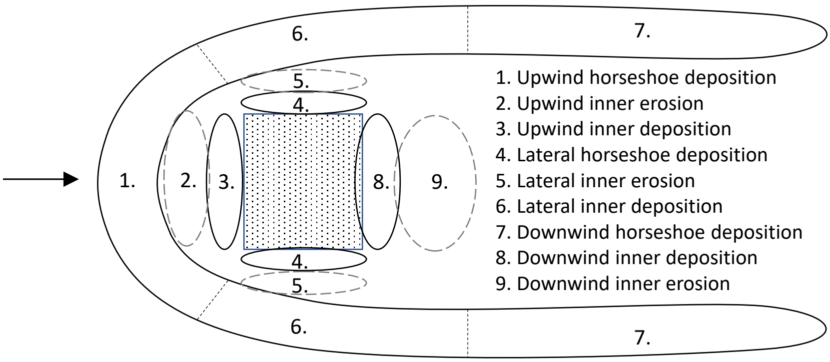

Figure 2.1: The locations and names of possible aeolian erosion and deposition features around a cube or building.

Deposition and erosion patterns around buildings are the direct effect of these wind flows and often follow the horseshoe shape. Although little research exists on the aeolian erosion and deposition of sand around buildings, multiple experiments on the deposition and erosion of snow were conducted (Liu et al., 2018; Oikawa & Tomabechi, 2000; Thiis, 2003; Thiis & Gjessing, 1999). Although there are some differences with sand – most notably the lower density and cohesion of snow and the possibility of snow fall – the wind field and processes are similar, so these experiments still provide insight on the aeolian erosion and deposition of sand around bluff bodies like buildings.

In field experiments on the snow drift around a cube with sides of 2.5 m, Thiis and Gjessing (1999) observed a deposition horseshoe. Following the nomenclature of Fig. 2.1, the upwind horseshoe deposition was clearly separated from the building front. Lateral horseshoe deposition was absent and the downwind horseshoe depositions were present. These downwind deposition areas, also called deposition tails, differed in length due to an oblique wind angle. Close to the building no (inner) deposition was observed. The lack of a downwind inner deposition was probably caused by the windspeed, which was too low to cause suspensive transport that could be blown over the cube. In a later study of Thiis (2003), downwind inner deposition developed especially after a stronger wind event (15 m/s). Lateral horseshoe deposition was again barely visible.

In several other experiments, snow accumulation was observed around cubes under conditions of combined snow drift and snow fall. Using cubes of 0.5 m and wind speeds from 0.5 to 4.5 m/s, Liu et al. (2018) found that at low wind speed (1.5 m/s), a deposition horseshoe developed, touching the front of the building and the back corners. At 3.5 m/s, two elevation maxima developed upwind of the cube (so indicating upwind horseshoe deposition and upwind inner deposition). At 4.5 m/s, these areas were actually separated by an upwind erosion area. Upwind of the cube, Oikawa and Tomabechi (2000) found that the inner erosion depth and horseshoe deposition depth increased with wind speed, based on an experiment with 1m-sized cubes and day-averaged wind speeds from 1.5 to 5 m/s. Below the threshold velocity (4 m/s), wind speed also had a positive effect on the upwind inner deposition depth. At the sides of the cube, Liu et al. (2018) observed that the distance between the cube and lateral horseshoe deposition increased from 1.5 to 3.5 m/s wind speeds, while the lateral horseshoe deposition disappeared completely at 4.5 m/s. Downwind of the cube, they found a minimal amount of inner deposition at the lowest windspeed – possibly aided by the presence of snow fall – which became more significant at higher wind speeds. Oikawa and Tomabechi (2000) found not only downwind inner erosion and deposition directly behind the cube, but also downwind deposition further away (at more than twice the cube height away).

Figure 2.2: A photo of one of the set-ups, testing the effect of building width and height (12-10-2018)

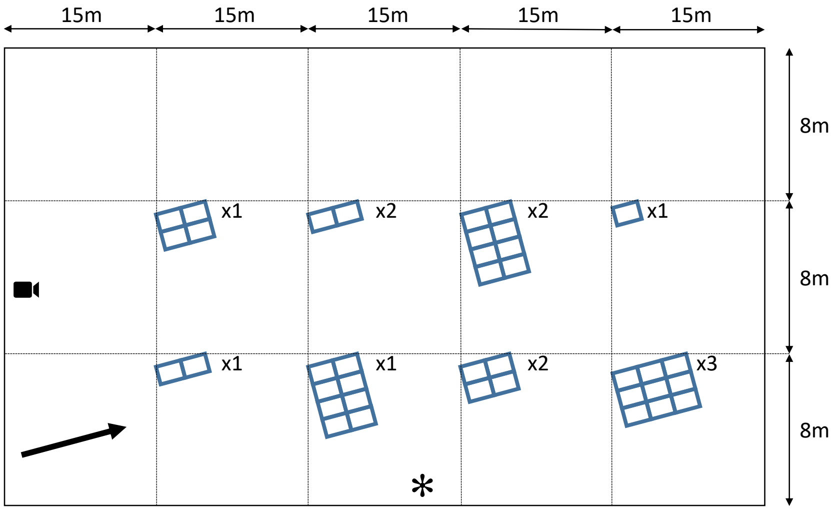

Figure 2.3: A sketch (not to scale) of the set-up shown in Fig. 2.2. The arrow indicates wind direction, the camera icon the camera for the timelapse video, $\ast$ the Windsonic and Wenglors and x1/x2/x3 the number of boxes stacked upon each other.

2.3 Methodology

Scale models of buildings were placed at the beach to determine the aeolian sedimentation and erosion patterns of sand around buildings (Fig. 2.2, 2.3). The scale models were cuboid stacks of cardboard boxes. These stacks varied in size and shape, in order to determine the effect of building geometry. The boxes used were 32×50×35 cm (w, l, h) and the model length, width and height were varied between 1 and 4 boxes. Boxes were filled with a sand bag to prevent them from being blown away.

Field experiments at the beach were chosen over wind tunnel experiments, because field experiments allow to test under natural conditions and at a natural scale. Wind tunnels – while suitable for examining airflows around buildings – have difficulties simulating sediment transport and bed development. The problem here mainly concerns scaling and irreconcilable dimensionless numbers (Duthinh & Simiu, 2011; White, 1996), further complicated by the introduction of buildings. In addition, turbulent field conditions are notoriously difficult to mimic in wind tunnels (Duthinh & Simiu, 2011), while simultaneously important for the flow structure around buildings (Peterka et al., 1985; Smith et al., 2017b). Placing models at the beach allowed for using larger sizes than what could be tested in a wind tunnel (especially when considering configurations of multiple buildings). Nonetheless, some degree of scaling was applied in our field experiments (approximately a 1:10 to 1:3 scale) to make the set-up more flexible and manageable.

Scale models were placed at the beach in the morning, so that sedimentation and erosion patterns could develop during the day. They were oriented approximately perpendicular to the wind. Figure 2.2 and 2.3 show an example of the set-up. During the day, the wind speed and wind direction were measured at a 1s interval using a WindSonic 2D ultrasonic anemometer placed at a height of 1.8 m. A vertical array of 10 Wenglor laser particle counters (see Goossens et al., 2018; Hugenholtz & Barchyn, 2011) was used to monitor the height of the transport layer. The sensors were located between approximately 5 cm and 1 m above the surface, with the highest elevations varying slightly to ensure that at least 1 sensor was located higher than the model height. In addition, a time-lapse video with a 10-second interval was made with a camera located at a height of 5 m, in order to record the experiment and to be able to identify interesting events such as streamers or natural bedforms migrating into the experiment area.

At the end of the day, the sedimentation and erosion patterns around the models were recorded and the models were removed. The sedimentation and erosion patterns were measured using structure-from-motion photogrammetry (see e.g. Van Puijenbroek et al., 2017). A telescopic stick was used to take photos all around the models, from a height of approximately 5 metres. These photos were computationally combined to form a digital elevation model (DEM) and orthophoto (a distortion-free top view) using Agisoft Photoscan (in December 2018 renamed to Agisoft Metascan). In Photoscan the accuracy was set to high for photo alignment and dense cloud generation, resulting in a horizontal resolution of approximately 2 mm for the DEM and orthophoto. The orthophoto and DEM were used to determine the erosion and deposition patterns and measure their dimensions.

The experiments were mainly conducted at the Sand Motor in the Netherlands (Fig. 2.4). At this mega beach nourishment, the beach is more than 500 metres wide, thus ensuring that there are always locations with large fetch lengths, independent of the wind direction. The median grain size is 335 μm (Hoonhout & De Vries, 2019). One experiment took place at the beach near Formerum, Terschelling. Here the beach is approximately 300 metres wide, so in combination with the almost shore-parallel wind that occurred enough for good aeolian sand transport. Here, the median grain size is approximately 200 μm (Guillén &

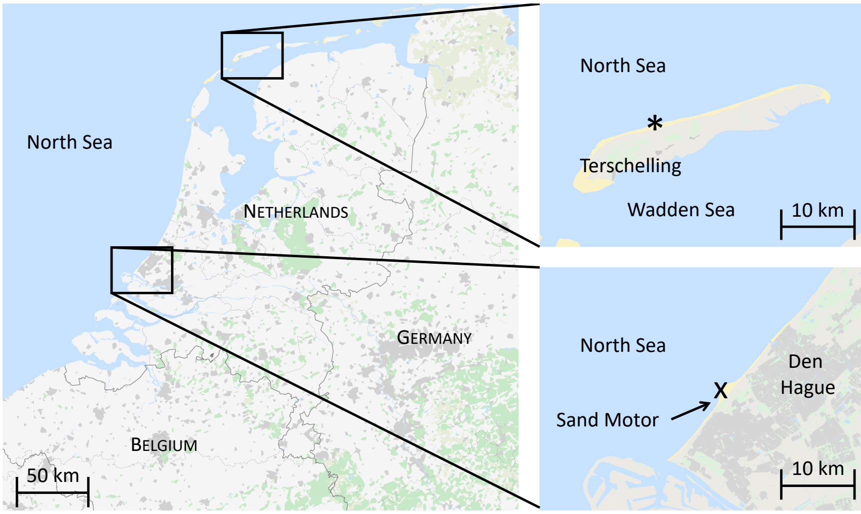

Figure 2.4: A map with the locations of the experiments, with the ∗ indicating the experiment at Terschelling and the X the experiments at the Sand Motor.

Hoekstra, 1997). In total there were seven days during which sedimentation and erosion patterns around models were recorded. On average, 6 to 10 models (i.e. 6 to 10 stacks of different dimensions) were placed on the beach simultaneously, making for a total of 59 observations. Table 2.1 shows an overview of the conducted experiments.

2.4 Results

Figure 2.5 shows the sedimentation patterns around two models. The horseshoe-shaped deposition is clearly visible. For the right model, this horseshoe is almost continuous (marked

Table 2.1: A concise overview of the conducted experiments

Date	Location	# of scale models	Wind speed [m/s]	Remarks
29-05-2018	Terschelling	6	6.8	
11-10-2108	Sand Motor	9	5.9	Bed moist, less erodible
12-10-2018	Sand Motor	8	6.9	Bed moist, less erodible
23-10-2018	Sand Motor	10	9.5	
24-10-2018	Sand Motor	8	6.5	Light rain
19-11-2018	Sand Motor	9	7.6	
20-11-2018	Sand Motor	9	7.0	

as nr. 1, 4 and 7 on Fig. 2.5, following the numbering of Fig. 2.1): it is only interrupted at the upwind corners of the model. The model at the left is positioned slightly oblique to the wind, with the right side angled windward and the left side leeward. Here, the lateral horseshoe deposition (nr. 4) is continuous at the right, but absent at the left. Zooming in on the models, some additional features become visible. At the left model, upwind inner deposition occurred (nr 3). Furthermore, the left model shows a hint of downwind inner deposition (nr. 8), while the right model exhibits a clearer triangular-shaped downwind inner deposition. The left model also shows erosion to the outside of (what would be) the lateral horseshoe deposition (nr. 10). We term this erosion, noticeable from the shells that remained after the sand was eroded, lateral outer erosion. The moist surface prevented the occurrence of upwind and lateral inner erosion, but both models show areas without deposition that might otherwise be eroded. Another interesting feature visible for both models is the double sedimentation ridge at the downwind edge of the upwind horseshoe deposition.

The patterns described above are fairly representative for patterns observed around other models and at other days. The upwind and downwind horseshoe deposition are present around virtually all models, with occasionally a larger distance between the downwind model corners and the start of the downwind horseshoe deposition (see Fig. 2.6a for an extreme case). The lateral horseshoe deposition shows more variation: often it is absent (Fig. 2.6a, b), sometimes it is present at one side (Fig. 2.5b, c and d) or at both sides (Fig. 2.5c: still interrupted at the upwind corners, Fig. 2.6e: fully present). For models oriented obliquely to the wind (due to inaccurate positioning or changing wind conditions), the lateral horseshoe deposition is often limited to the windward side. During three of the seven days, several models showed a double sedimentation ridge at the downwind edge of the upwind horseshoe deposition.

Some light upwind inner deposition occurred in almost half of the cases (e.g. Fig. 2.6d). Light downwind inner deposition occurred slightly more than half of the time. The presence or absence of this area was generally quite consistent for the different models tested during a day, with little effect from the model height. In case of models oriented obliquely to the wind, this downwind inner deposition occasionally formed one continuous deposition area together with the lateral leeward inner deposition (Fig. 2.6c, nr. 6 and 8). Remarkably, all model set-ups used on the one day at Terschelling showed erosion instead of deposition directly downwind of the model (Fig. 2.6b). The upwind and lateral inner erosion also occurred a bit more than half of the time, with occurrence also depending on wind speed and surface erodibility. On 23-10-2018, the high wind speed (9.5 m/s) not only caused inner erosion at the front and sides, but also undercutting at the corners (Fig. 2.6e and f). Lateral outer erosion was occasionally visible: around all of the models at 29-05-2018 and the majority of the models on 12-10-2018 (e.g. Fig. 2.6b: with at the left side separate lateral outer and inner erosion and at the right side only lateral outer erosion).

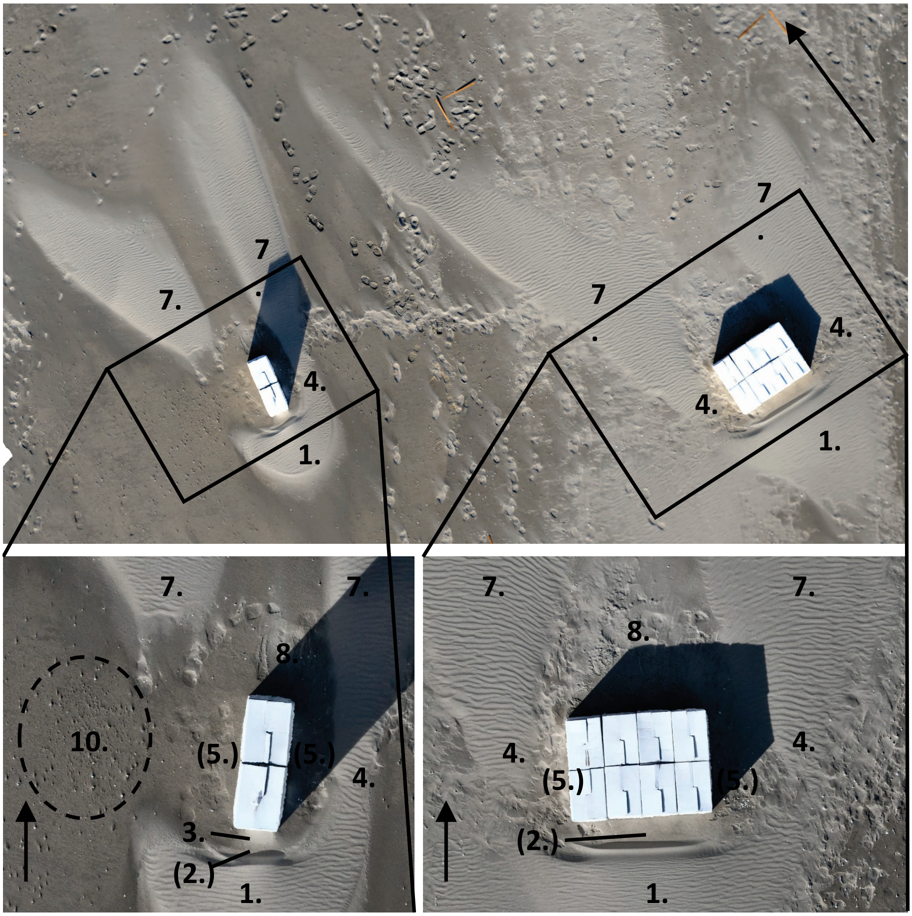

Figure 2.5: Orthophoto of the sedimentation and erosion around 2 models. Left model 1x2x2 boxes (32x100x70 cm), right model 4x2x1 boxes (128x100x35 cm), recorded at 12-10-2018. Numbers indicate sedimentation and erosion areas as presented in Fig. 2.1, number between brackets indicate a lack of sedimentation on what is indicated as erosion area in Fig. 2.3. Arrows indicate wind direction. Number 10 indicates an area with erosion.

Figure 2.6: Notable erosion and sedimentation structures around scale models, with arrows indicating the wind direction. a) Orthophoto showing a large distance between the model and the start of the downwind horseshoe deposition. b) Orthophoto showing lateral inner and outer erosion and downwind inner erosion. c) Photo of a model oriented obliquely to the wind, showing lateral inner deposition d) Photo of model a oriented obliquely to the wind, showing upwind inner deposition and asymmetric lateral deposition. e) Photo showing continuous lateral deposition. f) Zoom of 6e, showing erosion around model and under model corners.

2.5 Discussion

The deposition and erosion patterns found in the experiment are similar to the snow accumulation patterns around buildings reported in literature. However, there are some differences. The negative effect of the wind speed on the presence of lateral horseshoe deposition, as reported in Liu et al. (2018), is not confirmed. On the contrary, continuous lateral horseshoe deposition at both sides of the model was especially present at the day with the highest wind speed (9.5 m/s). At low wind speeds, Liu et al further observed continuous upwind snow deposition from the horseshoe to the building front. In our experiments, there was an area showing either a lack of deposition or even erosion between the upwind horseshoe deposition and the front of the model. However, the lowest wind speed that Liu et al. observed (1.5 m/s) was lower than the critical wind speed, so no erosion could occur. At this wind speed, snow transport consists of the convection of snow fall. This snow fall is blown against the front of the building, but the reverse flow of the horseshoe vortex lacks the strength to cause erosion. At the beach, sand/snow fall does not exist as supply mechanism. Hence, sand transport can only occur at higher wind speeds that induce motion at the bed. At this wind speed, the reverse flow in front of our models caused an area without sedimentation (or even erosion) between the upwind horseshoe deposition and the model front.

A new observation in this experiment is the occurrence of erosion further outward from the sides of the model. In some cases a distinct lateral outer erosion area formed outside of the normal horseshoe sedimentation. In other cases, erosion already started near the model, but extended further than where the horseshoe sedimentation would be expected to form.

The experiment also showed the effect of the wind direction. The models that were oriented slightly oblique to the wind tended to only show lateral horseshoe deposition at the windward side, and not at the leeward side. This agrees well with the pattern that Liu et al. (2018) found for snow accumulation around a cube oriented slightly oblique to the wind under higher wind speeds (10° angle, 4.5 m/s wind speed). However, the presence and clearness of the lateral horseshoe deposition we observed, also showed strong variation for models oriented perpendicular to the wind, so the interplay between orientation, wind speed and lateral horseshoe deposition remains a subject for further research.

In this chapter, we described generic patterns of deposition and erosion around scale models of buildings. The wind speed and differences in the erodibility of the bed are only mentioned where especially relevant. A more systematic analysis of the effect of these factors on the type of sedimentation and erosion patterns should be conducted in the future. This is especially relevant for the lateral horseshoe deposition and downwind inner deposition, for which previous experiments on snow accumulation (e.g. Liu et al., 2018; Thiis, 2003) suggest an effect from the wind speed. Furthermore, the effect of the model size and shape on the dimensions of the sedimentation and erosion patterns will be examined in future research.

2.6 Conclusion

To determine the aeolian erosion and deposition patterns around buildings on the beach, a scale experiment was conducted. This experiment, conducted at the beach, showed that the deposition and erosion patterns formed by sand are quite similar to the patterns of snow accumulation around buildings. Deposition patterns follow the horseshoe vortex that the wind forms around a building. The deposition area upwind of the building and the deposition tails downwind of the building (downwind horseshoe deposition) are almost always present if the wind is strong enough to cause sand transport. The presence of horseshoe deposition to the side of the building (lateral horseshoe deposition) and of deposition and erosion between the horseshoe and the building itself is more variable, and depends on wind speed, wind direction, and the erodibility of the bed. In contrast to earlier research on snow accumulation, we did not observe a clear effect of the wind speed on the lateral horseshoe deposition. In addition, our upwind deposition was always located some distance upwind of the building, while upwind snow accumulation continued up to the building front for the lowest wind speeds. A further analysis of the experimental data is needed to draw more quantitative conclusions on the effect of building size and shape on the dimensions of the sedimentation and erosion patterns.

2.7 Acknowledgements

This research forms part of the ShoreScape project (Sustainable co-evolution of the natural and built environment along sandy shores), funded by the Netherlands Organization for Scientific Research (NWO), contract number ALWTW.2016.036, co-funded by Hoogheemraadschap Hollands Noorderkwartier and Rijkswaterstaat, and in kind supported by Deltares, Witteveen+Bos, and H+N+S. We also want to thank Rijkswaterstaat for the logistic support during the experiment at the Sand Motor. Furthermore, we thank Jan Willem van Dokkum for his great help during the preparation and execution of the experiments. In addition, we are grateful to Janneke van Bergen, Sara Dionísio António, Weiqiu Chen, Joost Kranenborg, Mariëlle Rotteveel, Sam de Roover, Ton van der Heide and the organization of the Oerol festival for their assistance with the experiments.

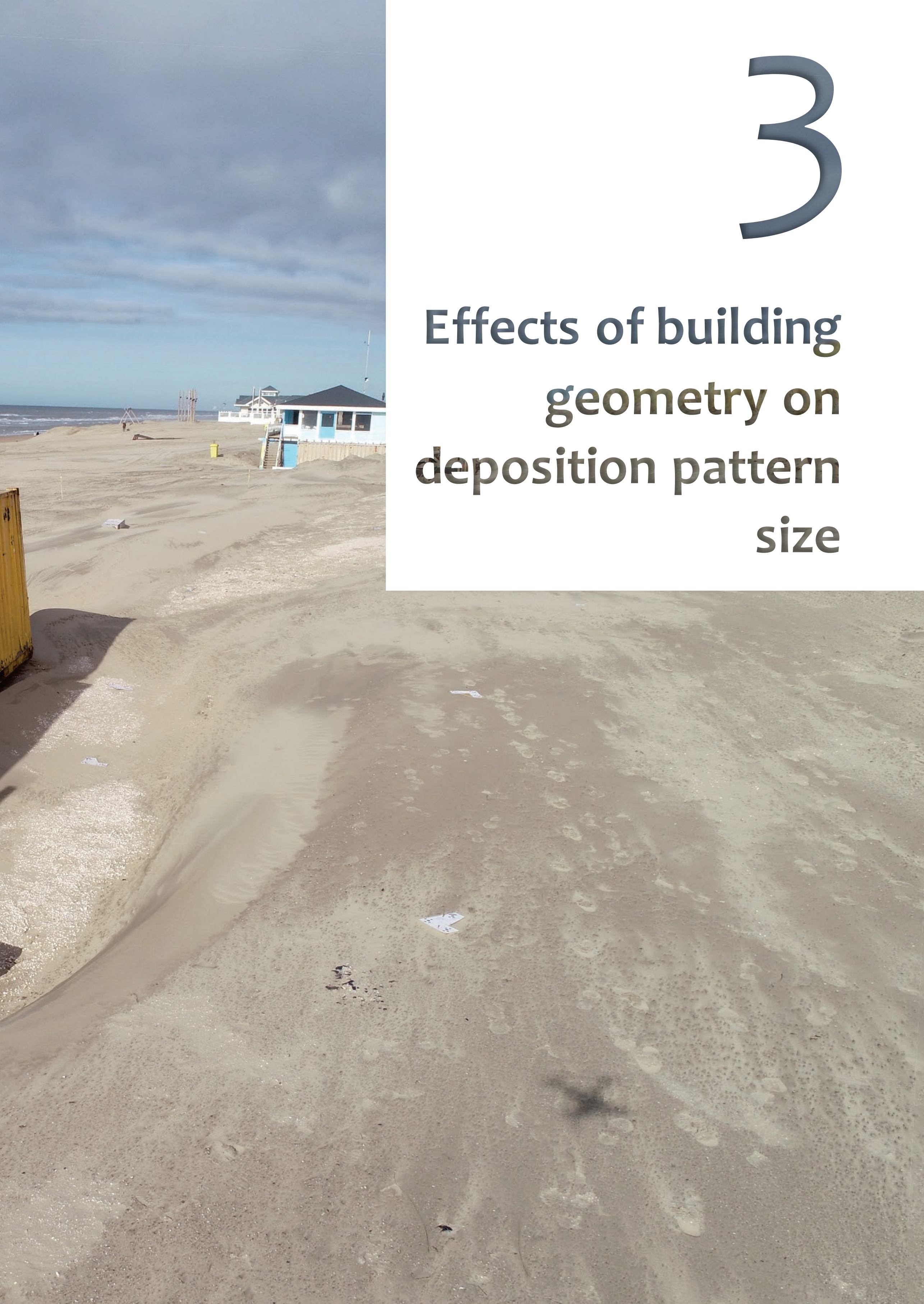

3

Effects of building geometry on deposition pattern size

3

Effects of building geometry on deposition pattern size

Abstract: In sandy environments, like the beach-dune system, buildings not only affect the airflow, but also the aeolian sediment transport in their surroundings. In this study, we determine how the horizontal size of sediment deposition patterns around buildings depends on the building's dimensions. Four one-day experiments were conducted at the beach using box-shaped scale models. We tested 32 building geometries, where scale model height, width and length ranged between 0.3 and 2.0 metres. The deposition patterns were substantial in size: the total length and width of the deposition area were up to an order of magnitude larger than the horizontal building dimensions. It was found that the size of upwind and downwind deposition patterns depended more on the building width perpendicular to the wind direction (w), than on the building height (h). Building length had little influence. Especially the combined effect of w and h correlated well with horizontal deposition size. This is expressed in a new scaling length B for deposition around buildings, with $B = w^{2/3}h^{1/3}$. As a first validation, the spatial dimensions of the initial deposition patterns observed around a scale model of 2.5×12×2.5 metres, placed at the beach for five weeks, showed good agreement with those predicted based on B

Figure previous page: The full-size model at Noordwijk after 3 weeks.

This chapter is published as Poppema, D.W., Wijnberg, K.M., Mulder, J.P.M., Vos, S.E., & Hulscher, S.J.M.H. (2021). The effect of building geometry on the size of aeolian deposition patterns: scale model experiments at the beach. *Coastal Engineering*, 103866. DOI: 10.1016/j.coastaleng.2021.103866

3.1 Introduction

All over the world, people enjoy recreation at the beach. As a result, more and more buildings like restaurants, beach huts and houses are built at the beach-dune interface (Hoonhout & Waagmeester, 2014; Malavasi et al., 2013, see Fig. 3.1 for some examples). However, sandy coasts are vulnerable areas where beaches and dunes represent important natural and recreational values and, especially in low lying countries like the Netherlands, dunes serve as primary flood protection. Buildings affect the wind-driven sand transport in their surroundings and thereby affect the natural development of the very same dunes (Jackson & Nordstrom, 2011). In addition, sediment deposition and erosion around buildings can be a hindrance to building owners and beach visitors.

Buildings at the beach or in the beach-dune interface reduce the source area for windblown sediment transport (García Romero et al., 2016; Morton et al., 1994) and alter the wind field in their surroundings (Jackson & Nordstrom, 2011; Nordstrom & McCluskey, 1984; Smith et al., 2017b). In the front and lee of buildings, flow deceleration and reversal can decrease sediment fluxes, leading to sedimentation. Conversely, the deflection of wind around buildings or underneath elevated buildings can create an acceleration zone with increased sediment transport and erosion (Jackson & Nordstrom, 2011; Smith et al., 2017b). The sediment transport can be increased further by the higher turbulent intensity of the wind behind buildings (Smith et al., 2017b). Furthermore, continuous lines of buildings can also act as a barrier to sand transport and cause fetch segmentation by detaching dunes from their beach or foredune sources (Jackson & Nordstrom, 2011; Smith et al., 2017b). As a result of these effects, patterns of erosion and sedimentation arise around buildings.

3

Buildings in the beach-dune interface cause erosion and sedimentation, so they can steer dune development and affect dune development rates in their surroundings. Smith et al. (2017b) and García Romero et al. (2016) found that cities at the Canary Islands have both stabilizing and destabilizing effects on adjacent dune fields. Nordstrom and McCluskey (1984) observed that houses actually built in the dunes can modify the dune form and cause depressions around the houses. Furthermore, the analysis of field measurements and aerial photos of dunes around Dutch beach buildings showed that buildings can have a significant effect on the long-term duneward sand transport (Hoonhout & Van Thiel de Vries, 2013; Reinders et al., 2014).

These morphological effects of buildings near the beach-dune interface can pose a safety risk to buildings themselves but also to hinterlands that depend on dunes for flood protection. Local deposition around buildings temporarily decreases the amount of landward sediment transport that remains available to be blown further into the dunes. In the long term, this can have detrimental effects on dune growth and hence on safety in a larger area. In addition, erosion around buildings can create weak spots in the dune line (Nordstrom & McCluskey, 1984, 1985). Furthermore, at the level of shorter term sediment dynamics, deposition induced

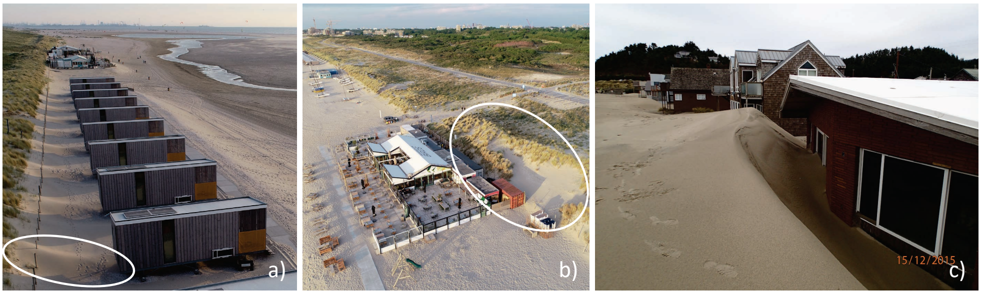

Figure 3.1: Buildings on the beach. a) A row of holiday houses with some deposition behind the houses (e.g. the white oval), in Kijkduin, The Netherlands. b) A beach restaurant with a more bare dune behind it (the white oval) in Kijkduin, The Netherlands. c) Houses with substantial deposition built in Pacific City, USA (photo courtesy of Oregon Parks and Recreation Department).

by buildings can cause a considerable hindrance to beach users, especially when occurring on beach entrances, walkways and terraces (Jackson & Nordstrom, 2011). Furthermore, natural values can suffer when dune vegetation is affected by changes in the sediment dynamics around buildings (Hoonhout & Van Thiel de Vries, 2013).

The abovementioned effects can pose serious problems to building owners, but also raise challenges for regional authorities and coastal managers who have to balance the interests of recreation, flood safety and nature with regards to permission and regulations for the construction of these buildings (Nordstrom & McCluskey, 1984; Winckel et al., 2008). Therefore, quantitative knowledge is required on the effects of buildings, the spatial extent over which buildings affect their surroundings and how this depends on the building characteristics.

Previous research into the morphological effects of buildings mostly described the erosion and deposition around specific scale models of buildings in a wind tunnel (Iversen et al., 1990; McKenna Neuman & Bédard, 2015; Tominaga et al., 2018). Systematic and quantitative knowledge is lacking on how sedimentation and erosion patterns depend on building design (building size and shape, use of poles to allow airflow under buildings), building location (distance from dune and other buildings) and building orientation (Hoonhout & Van Thiel de Vries, 2013; Hoonhout & Waagmeester, 2014). This knowledge gap hampers knowledge-supported regulations for beach-side buildings and limits capabilities to design and position beach-side buildings in such a way to minimize impact and reduce the hindrance of sedimentation and the need for sediment removal.

As a first step, this research aims to determine how the location and horizontal size of initial aeolian deposition patterns around buildings on the beach depend on the building's dimensions. The dependencies have been determined based on field tests with 32 scale models. By focussing on the initial deposition patterns we highlight the direct effects of buildings before morphologic feedback starts to interact with these patterns. To ensure that deposition patterns can develop without topographic constraints and under uniform wind conditions, buildings are examined on an open beach. Derived relationships have been validated against results of one full-scale model test. Given the lack of knowledge of large-scale effects of buildings on the beach-dune system, this chapter focuses on the larger scale deposition patterns around buildings, rather than on the local erosion features directly at the corners of the buildings.

In this chapter, we first present an overview of the expected effects of building dimensions on airflow and sedimentation patterns based on literature (section 3.2), followed by a description of the experimental set-up, the data collection and analysis methods (section 3.3). In section 3.4 we present the results of the experiments and predictive relationships between building dimensions and size of initial deposition patterns. Finally, the chapter ends with a discussion and conclusion.

3.2 Theory on airflow and sediment dynamics around buildings

Aeolian deposition and erosion patterns around buildings are the direct effect of airflow around buildings. Therefore, existing studies on airflow patterns around buildings (e.g. Hunt, 1971; Martinuzzi & Tropea, 1993; Peterka et al., 1985) can be used to hypothesize how building size and shape quantitatively depend on the size of sedimentation and erosion patterns. However, the step from flow structures to sand transport and to sedimentation and erosion patterns is far from straightforward (Kok et al., 2012), so the effect of building properties on sand transport and morphology have to be studied explicitly.

3.2.1 Airflow around buildings

The airflow pattern around bluff objects like buildings differs markedly from the airflow over natural bedforms and dunes. In both cases, flow is diverted over and around an object. However, over streamlined bedforms, flow more or less follows the topography, whereas at sharp building edges (additional) flow separation, recirculation and turbulence occur. As a result, the wind around buildings forms a horseshoe vortex and creates a highly turbulent wake behind the building (see Fig. 11 of Martinuzzi & Tropea, 1993; Fackrell, 1984; Hunt, 1971; Peterka et al., 1985).

The formation of this horseshoe vortex (Fig. 3.2) can be explained by the wind profile approaching the building. Wind approaching a building causes increased pressure at the upwind building face. Part of the wind is directly diverted over the building and to the sides. However, as wind velocity and thereby pressure increase with elevation, a downward flow is also formed. The upward and downward flows are separated by a stagnation zone at around 2/3 to 3/4 of the building height (Peterka et al., 1985). Above this zone, the wind is diverted

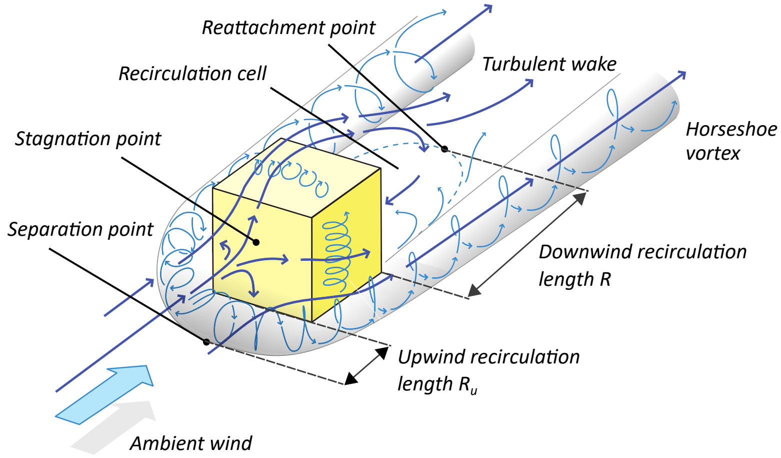

Figure 3.2: The airflow patterns around a building oriented perpendicular to the wind (adapted from Oke et al., 2017).

upwards and to the sides. Below this zone, the wind is diverted downwards and to the sides. This downward flow creates a reverse flow close to the ground, upwind of the building, which leads to a rotating vortex in front of the building. This vortex is wrapped around the building by the wind, thereby obtaining the horseshoe shape (Hunt, 1971; Martinuzzi & Tropea, 1993; Peterka et al., 1985).

The size of the vortex upwind of the building and hence the upwind recirculation length R_u (i.e. the distance between the flow separation point and the upwind building edge) depend on the building width (w) and height (h) (Beranek, 1984; Martinuzzi & Tropea, 1993; Peterka et al., 1985) and on the turbulent intensity (Peterka et al., 1985). With increasing building width or height, more wind is diverted, increasing the vortex size. Beranek (1984) approximated this effect with $R_u = 0.7\sqrt{wh}$ for aspect ratios (w/h ratios) between 0.8 and 3. However, for increasing building width, the effect is partially counteracted by more wind being diverted over the building instead of to the sides, causing a lowering of the stagnation point (Martinuzzi & Tropea, 1993). Consequently, in the experiments of Martinuzzi and Tropea (1993), $R_u = 0.8w^{0.4}h^{0.6}$ matched the results better for similar aspect ratios. Furthermore, they noted that the separation length becomes almost width-independent for wide buildings, between aspect ratios of 4 and 6.

The separated flow over the building edges can reattach at the top and sides of the building. Whether it reattaches before reaching the back of the building depends on the building's length-to-width and length-to height ratio and on the turbulent intensity (Fackrell, 1984; Hunt, 1971; Peterka et al., 1985). This reattachment roughly occurs if building length l is larger than $\frac{1}{2}\sqrt{h}$ (Fackrell, 1984). If flow reattaches on the building, a separate recirculation cell, also called a separation cavity, is formed downwind of the building. If flow reattachment does not occur, the flow at the side and top of the building forms one joint recirculation cell with the flow behind the building (Martinuzzi & Tropea, 1993; Peterka et al., 1985). In this case, the downwind recirculation length, so the distance between the downwind building edge and the flow reattachment point behind the building (see Fig. 3.2) becomes larger (Fackrell, 1984).

The downwind recirculation length R can be described with Eq. 3.1 (ASHRAE., 2005; Wilson, 1979).

$$R = \min(w,h)^{2/3} \cdot \max(w,h)^{1/3}, \qquad 1/8 < w/h < 8 \tag{3.1}$$

Alternative relationships between building dimensions and recirculation length can be found in e.g. Fackrell (1984) and Martinuzzi and Tropea (1993). Downwind of the recirculation cell, the airflow in the building wake still differs from the undisturbed wind field by having, along the centreline behind the building, a lower mean velocity and a higher turbulent intensity. For building aspect ratios between 1 and 4, this wake extends behind the building up to a distance of 10 to 30 times the building height (Peterka et al., 1985). Taking x as the distance behind the building, the velocity deficit decays with $x^{-1.3}$ behind approximately cubical buildings (Hunt, 1971; Peterka et al., 1985) and with x^{-1} behind really wide buildings (Hunt, 1971). With wind being diverted to the sides, wind in the horseshoe vortex behind a building (i.e. more to the sides) has both a higher velocity and a higher turbulent intensity.

3

3.2.2 Deposition and erosion patterns around buildings

The airflow around buildings affects windblown sediment transport, giving rise to deposition and erosion patterns. Wind tunnel experiments on erosion and deposition around buildings (Iversen et al., 1991; Iversen et al., 1990; Tominaga et al., 2018) reported strong erosion at the upwind building edge and especially the upwind corners. Deposition occurred some distance upwind of the building and downwind in the lee of the building, with the latter also being referred to as a shadow dune or sand shadow (Bagnold, 1941; Luo et al., 2012). A phenomenological examination of sand deposition and erosion around our scale models at the beach (Chapter 2) agreed with the erosion at the upwind building edge and the upwind deposition area a small distance upwind of the building. In addition, strong deposition tails were found downwind of the building and occasionally along the building, approximately at the location of the horseshoe vortex tails in Fig. 3.2. Similar deposition features were reported in several experiments on snow accumulation around buildings (Liu et al., 2018; Thiis, 2003; Thiis & Gjessing, 1999; for an overview see Poppema, 2020), that were performed both in wind tunnels and in the field.

The next step is quantitatively linking the size of this deposition to building dimensions. As quantitative knowledge on the location of sedimentation and erosion is poorly developed, related processes can be used to improve understanding of these deposition and erosion patterns. For example, deposition upwind of beach buildings can be compared to echo dunes in front of natural vertical cliffs as found in deserts and at beaches (Tsoar & Blumberg, 1991; Tsoar, 1983). Tsoar (1983) examined echo dune formation upwind of such cliffs using a wind tunnel. He observed that dunes formed a small distance upwind of the cliffs. Using cliff height h and a cliff over the full wind tunnel width, the initial separation distance was $0.3h$ to $0.4h$, while the dune crest was located at $0.5h$ to $0.6h$ upwind of the cliff. As echo dunes grew higher, their crest remained at the same location, but the edge grew toward the cliff.

The scaling of airflow structures around buildings with building dimensions may be used as a basis to predict the size of deposition patterns. However, airflow and sand transport around buildings differ in how they depend on building height. Wind speed increases away from the bed. Hence, the amount of wind blocked or diverted by buildings increases more than linearly with building height. Sand transport, to the contrary, is mainly concentrated in a saltation layer close to the bed. Common saltation layer heights are less than 0.5 m (Dong et al., 2003; Rotnicka, 2013), so lower than any building height. Hence, the amount of blocked or diverted sand transport is expected to increase little with building height. The downwind recirculation length R for airflow behind buildings as described in Eq. 3.1 also functions as a general *scaling length* for airflow around buildings (Wilson, 1979). The length and height of the recirculation cells on top of the building and behind the building scale linearly with R (i.e. their size is proportional to R). Likewise, R is used to describe the width of the recirculation cell and of the building wake (see Fig. 3.2), airflow streamlines and diffusion around buildings (Schulman et al., 2000). Given that R is used as a scaling length for the airflow and diffusion near buildings, it might also serve as a scaling length to predict the size of aeolian deposition.

However, with building height having less effect on sediment transport than on airflow patterns, the scaling length R as used for airflow patterns likely has to be adapted to be applicable for deposition patterns. Therefore, we introduce B, a new scaling length for deposition around buildings (Eq. 3.2), in which the powers of $\frac{2}{3}$ and $\frac{1}{3}$ are kept the same as in R, but the building width is consistently given the larger power to reflect its importance for sand transport. We expect that deposition patterns scale better with scaling length B than with R.

$$B = w^{2/3} h^{1/3} \tag{3.2}$$

3.2.3 Development rate of deposition patterns

Airflow patterns around buildings are generally independent of the wind speed, in the sense that the spatial pattern, expressed as a local wind speed U divided by the undisturbed wind speed U_0, does not depend on U_0 (Fackrell, 1984; Peterka et al., 1985). However, this implies that the *absolute* value of the wind speed at a given location will scale linearly with the undisturbed wind speed. This absolute wind speed is important for the creation of deposition patterns, because it determines the aeolian sediment transport capacity. This in turn affects deposition length, as further described below.

For the wind speed in the far wake of the building (downwind of the recirculation cell), there are some general expressions (Kothari et al., 1986; Peterka et al., 1985) for the dependence of U on the distance downwind of the building, x, allowing us to quantify the effect of wind speed on deposition rate. In the horseshoe vortex, which approximately coincides with the main deposition areas (Thiis & Gjessing, 1999), the wind speed is higher than the undisturbed wind speed. The wind speed excess ($\Delta U/U_0$) decays with the distance downwind of the building. This can be described by Eq. 3.3, in which the wind speed excess decays inversely proportional to x^β and α is a constant smaller than 1 (Hansen & Cermak, 1975; Peterka et al., 1985). Such a decreasing wind speed would mean a decreasing sediment transport rate, hence explaining the deposition areas behind a building. Assuming that deposition is dominantly determined by downwind gradients in the wind speed (i.e. neglecting the contribution from local changes in the wind direction) and that the sediment transport rate is proportional to the wind speed to the power n, then Eq. 3.4 describes the sediment transport rate Q_s and Eq. 3.5 the deposition rate $\frac{-dQs}{dx}$. For large x (more than a few times the recirculation length R), the deposition rate is then approximately proportional to $\frac{U_0^n}{x^{1+\beta}}$.

$$U = U_0\left(1 + \frac{\alpha}{x^\beta}\right) \tag{3.3}$$

$$Q_s \propto U^n = U_0^n \cdot \left(1 + \frac{\alpha}{x^\beta}\right)^n \tag{3.4}$$

$$-\frac{dQ_s}{dx} \propto U_0^n \cdot \alpha\beta n \cdot \left(1 + \frac{\alpha}{x^\beta}\right)^{n-1} \cdot \frac{1}{x^{1+\beta}} \tag{3.5}$$

Eq.3.5 shows that the deposition rate increases with wind speed, so deposition patterns around a building will develop faster at higher wind speeds. We can now also quantify how this affects the observed deposition length over a given timespan, if we assume that a certain minimum elevation change is needed to be detectable in the field as deposition (such as during our experiments).

For a given timespan, the minimum elevation change that defines the edge of the deposition pattern will now occur at a distance x where $dh = \frac{dQ}{dx}dt$ has a certain value. So for this given timespan, the deposition rate at the detectable edge of the deposition pattern is fixed. Hence, at the deposition edge, $\frac{U_0^n}{x^{1+\beta}}$ is a constant, such that with an increase in $U0$, the x-coordinate of the deposition edge will increase proportional to $U_0^{n/(1+\beta)}$. In other words, the deposition length that can develop within a given timespan scales with $U_0^{n/(1+\beta)}$.

It is known that the aeolian sediment transport rate scales approximately quadratically with the wind speed (Kok et al., 2012; Ungar & Haff, 1987), so n is approximately 2. Based on a perturbation analysis, Hunt (as cited by Hansen & Cermak, 1975; Kothari et al., 1979) expected the downwind vortex strength and wind speed excess to scale inversely proportional to $\sqrt{x}$ for a downwind distance x larger than $5h$. It follows that β is likely close to 0.5. This would make the downwind deposition length proportional to $U_0^{1.33}$. However, this value of β is still uncertain. A decay as quick as $x^-1.3$, like Peterka et al. (1985) measured for the velocity deficit at the centreline behind a building, is unlikely due to (extra building-induced) turbulence and vortices that convect air with higher velocities down from higher elevations, thereby delaying the wind speed decay (Kothari et al., 1986). An intermediate value of for instance $\beta = 1$ would result in a deposition length that is exactly linear with U_0. This is quite similar to the result of $U_0^{1.33}$, so even though the exact scaling is still unknown, the initial downwind deposition length that can develop within a given timespan scales close to linearly with wind speed.

For deposition sizes other than the downwind length, the effect of wind speed is more difficult to predict. The analysis for the initial downwind deposition length is based on explicit relations for the downwind gradient in windspeed magnitude. Without explicit descriptions of the lateral gradient and the upwind wind field, the effect of wind speed on the downwind deposition width and upwind width and length cannot be quantified. However, the general principle still holds that at higher wind speeds, a similar gradient in the sediment transport rate (i.e. a similar deposition rate) can be reached at a smaller gradient in the wind speed magnitude, so further from the building. Besides, lateral variations in wind speed are probably more local than downwind variations because advection dominantly works in x-direction. If the lateral decay of wind speed disturbances is faster (if β in Eq. 3.5 is larger), then deposition width is less affected by wind speed than deposition length.

3.3 Methodology

3.3.1 Set-up experiments at the beach

A field experiment with scale models of buildings at the beach was used to examine aeolian deposition and erosion patterns around beach buildings (see Fig. 3.3, 3.4). The scale models consisted of cuboid stacks of cardboard boxes. To examine the effect that building size and shape have on the size of deposition patterns, the scale models size and shape were varied. The model length, width, and height ranged between 1 and 4 boxes, with individual boxes being 33×50×3 cm (w×l×h). Boxes were filled with a sandbag to prevent them from being blown away.

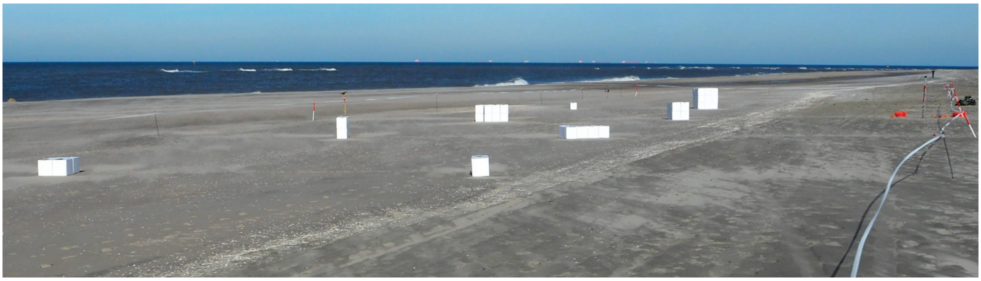

Figure 3.3: The set-up at one of the days (12-10-2018), testing the effect of building width and height. Note: scale model configuration, orientation and location changed between all experiments.

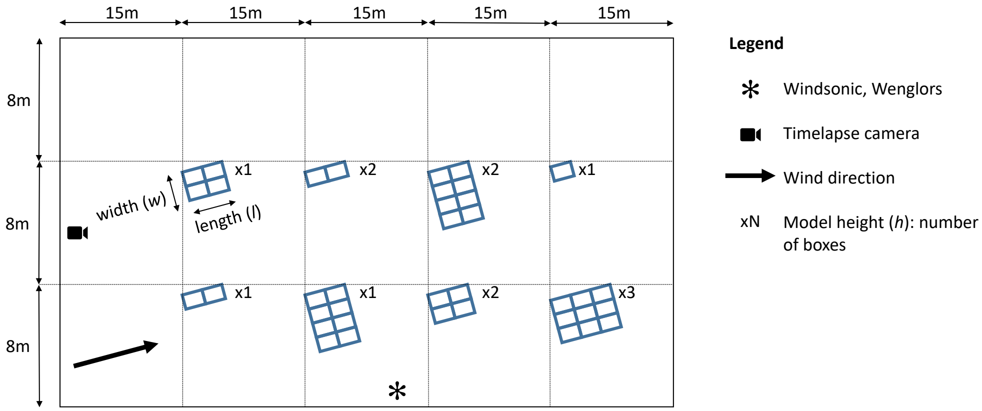

Figure 3.4: A sketch of the set-up shown in Fig. 3.3. Distance between scale models not to scale.

The experiment was conducted at the beach instead of in a wind tunnel, to allow testing under natural conditions and at a natural scale. While wind tunnels are commonly used to model airflow around buildings, modelling sediment transport as well is more problematic as it involves the scaling of additional processes (creep, saltation), quantities (grain density, fall velocity, sediment flux) and length and time scales (grain size, saltation layer height, saturation length). Unfortunately, these cannot be properly scaled due to irreconcilable processes and dimensionless numbers (Duthinh & Simiu, 2011; White, 1996). Furthermore, turbulent field conditions are notoriously difficult to simulate in wind tunnels (Duthinh & Simiu, 2011) but indispensable for the flow structures around buildings (Peterka et al., 1985; Smith et al., 2017b). By placing models at the beach, the models could be larger than what is possible in a wind tunnel for sand transport, thereby alleviating the scaling issues. Nevertheless, some degree of scaling was still applied in the field experiments – approximately a 1:10 to 1:3 scale for a typical Dutch beach hut of 3×6×3 m – to make the set-up more flexible and manageable.

Scale models were placed at the beach in the morning, and the resulting deposition patterns were recorded at the end of the day, so that patterns could develop for one day. For each experiment, the orientation of the boxes was tuned to the dominant wind direction during placement of the scale models (cf. Fig. 3.4). For the analysis, we regard the orientation of the boxes as completely perpendicular to the wind, without taking variations in wind direction ($<15^\circ$ over a day, see Table 3.1) into account. In total there were four days during which sedimentation and erosion patterns around models were successfully recorded. Six to ten models (i.e. six to ten stacks of different dimensions) were placed on the beach every day (see Fig. 3.3, 3.4), making for a total of 32 observations.

The experiments were mainly conducted at the Sand Motor in the Netherlands (Fig. 3.5). The beach is more than 500 metres wide at this mega beach nourishment. Exact locations on the Sand Motor were chosen based on the prevailing wind conditions of a day to ensure large fetch lengths (more than 400 m): close to the sea for offshore wind directions (11-10-2018; 12-10-2018) and vice versa (23-10-2018). The median grain size at the Sand Motor is 335 µm (Hoonhout & De Vries, 2019). One experiment took place at the beach near Formerum, Terschelling. Here the beach is approximately 300 metres wide, so in combination with the almost shore-parallel wind that occurred, aeolian sand transport was well developed. The median grain size here is approximately 200 µm (Guillén & Hoekstra, 1997). Table 3.1 shows an overview of the conducted experiments.

During the experiment, the wind speed and direction were measured using a 2D Windsonic ultrasonic anemometer, at 1.8 m high and with a 1 s interval. The height of the saltation layer was measured with a vertical array of 10 Wenglor laser particle counters (see Goossens et al., 2018; Hugenholtz & Barchyn, 2011). The Wenglors were placed between 5 cm and approximately 1 m above the bed, with the height of the highest sensors varying slightly to

Figure 3.5: A map with the locations of the experiments, indicated by X on the local maps. A and B indicate locations of one-day experiments. C indicates the location of the 5-week experiment.

Table 3.1: An overview of the conducted one-day experiments. Scale model size is indicated in boxes. Each box is 33×50×35 cm ($w \times l \times h$). The indicated wind speed is the average measured during the experiments. The wind direction variation is the difference between the dominant wind direction at the start and end of the experiment.

Date	Location	Wind speed [m/s]	Wind direction variation [°]	Variables tested	Configurations $w \times l \times h$ [boxes]	Bed moisture
29-05-2018	Terschelling	6.9	15	l; h	3×1,2,4×1,2	High: close to groundwater table
11-10-2018	Sand Motor	5.9	10	w; h	1,2,2,4×1×1; 2,4×1×2; 1,2×1×4	High: on intertidal beach
12-10-2018	Sand Motor	7.3	10	w; h	2×1,2,4×1,2; 1×1×1; 3×3×3	High: on intertidal beach
23-10-2018	Sand Motor	9.5	15	w; h; l	1,2,4×1,2×1; 2×1,2×1,2	Low

3

Table 3.2: An overview of the measurements taken at the 5-week experiment conducted at Noordwijk. Indicated wind speeds are the average of all wind speeds higher than 6 m/s.

Date	Period	Wind speed [m/s]	Remarks
09-02-2020	1 storm day	10	Only upwind deposition measurable at the full-scale model
11-02-2020	3 storm days	17	Tails of full-scale model end up in dune
11-03-2020	5 weeks	13	Small scale model located in tail of full-scale model

ensure the highest Wenglor was placed higher than the scale model height. The saltation layer height varied between 15 and 25 cm, so in all cases lower than the lowest scale models. Furthermore, a time-lapse with a 10 s interval was made with a camera from a height of 5 metres, to be able to later identify interesting events, such as streamers or natural bedforms migrating trough the experiment area.

Additionally, a longer-term experiment was conducted, where two scale models were placed on the beach for multiple weeks: a small scale model and a full-scale model. The small scale model was a box of 0.5×2×0.5 m, so comparable in size to the one-day experiments, but more elongated in shape. The full-scale model, consisting of two shipping containers, measured 2.5×12×2.5 m, so with comparable proportions as the small scale model, but in size comparable to a real beach hut. The goals of this experiment were to determine whether the results from the small-scale one-day experiments also apply on the scale of a beach hut, and to examine morphological development over a longer period. This experiment took place in Noordwijk, The Netherlands, at a beach of approximately 150 m wide, with a measured median grain size of 300 μm (C. van IJzendoorn, pers. comm., June 8, 2020). Both scale models were placed parallel to the coast, 20 m from each other and the dune foot. The dominant wind direction was alongshore to slightly onshore, so approximately facing the short side of the scale models. Multiple storms occurred, including a heavy storm 2 days after the experiment started (Fig. 3.6). Results were measured at three different days (Table 3.2): after 1 and 3 storms days to examine the initial development, and after 5 weeks to examine the longer-term effects. Within this thesis, this experiment is referred to as the 5-week experiment.

Wind speed data for the 5-week experiment was derived from a WindGuru measurement station at approximately 100 metres from the experiment, that measures the 10-minute average wind speed at 10 m above the bed. Measurements were converted to a height of 1.8 m, as measured by the WindSonic anemometer in the one-day experiments, using a constant factor of 1.7, derived from a 3 day period for which WindSonic and WindGuru

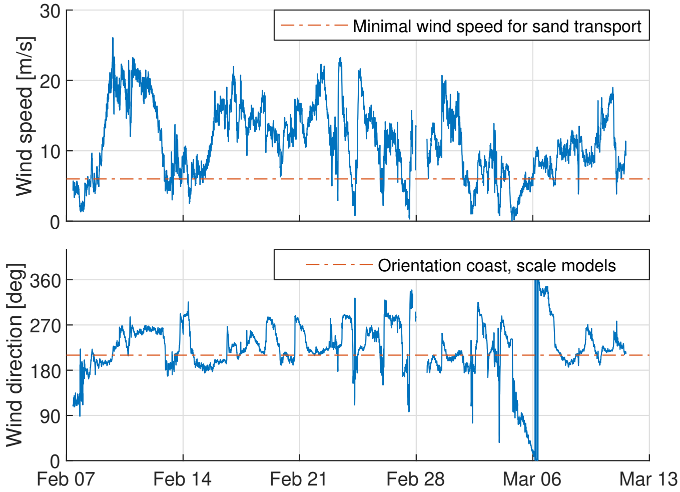

Figure 3.6: Wind speed and wind direction during the 5-week experiment at Noordwijk. For comparison, wind speeds are converted to of height of 1.8 m as measured during the one-day experiments. The dashed orange line in the lower panel indicates the orientation of the coast and of the long axis of the scale models, with values above the orange line being landward blowing wind.

measurements at the test site were compared.

The sedimentation and erosion patterns were measured using structure-from-motion photogrammetry (Fonstad et al., 2013), a technique that has been used extensively in recent years for high-resolution geomorphic surveys of beaches and dunes (e.g. Scarelli et al., 2017; Sturdivant et al., 2017; Van Puijenbroek et al., 2017). For the 1-day experiments, photos of the experimental area were taken from a height of 5 metres using a camera on a telescopic stick. Photos were only taken at the end of each experiment to avoid the extra disturbance a pre-experiment survey would have created in the form of additional footsteps in the area. Given that the deposition detection method was primarily based on orthophotos rather than elevation data (see section 3.3.3), having a pre-experiment survey was also of lesser importance. For the 5-week experiment in Noordwijk photos were also collected with the camera on the telescopic stick, except for the last survey (11-03-2020), when wind conditions were sufficiently mild to fly a Phantom 4 Pro drone. In all cases automatic white balance settings were used. Scale bars were dispersed throughout the experimental area for referencing. Additionally, for the measurement on 11-03-2020, markers were placed as ground control points and their position was measured by RTK GPS, with a vertical and horizontal accuracy of approximately 2 cm. Further details of the camera set-up, photos, and weather conditions affecting the photos can be found in Table 3.3.

Table 3.3: Camera and photo properties and weather conditions during surveying.

Date	Experiment	Camera	Number of photos	Weather conditions
29-05-2018	1-day experiments	[1]	469	Sunny, dry
11-10-2018		[2]	356	Sunny, dry
12-10-2018		[2]	416	Mostly sunny, dry
23-10-2018		[2]	459	Mostly cloudy, dry
09-02-2020	5-week experiment	[2]	742	Cloudy, dry
11-02-2020		[2]	1501	Mostly cloudy, dry but recent rain
11-03-2020		[3]	1836	Mostly sunny, dry

[1]Canon EOS 450D with 20 mm lens (58° horizontal angle of view), 12 Mpix jpeg photos
[2]Olympus E-PL7 with 20 mm lens (47° AoV), 16 Mpix raw photos
[3]Phantom 4 Pro drone with 8.8 mm lens (74° AoV), 20 Mpix jpeg photos

3

3.3.2 Structure-from-motion photogrammetry

Agisoft Metashape (previously named Agisoft Photoscan) was used for the structure-from-motion (SfM) photogrammetry. Within Metashape, a 3D point cloud was calculated from overlap between photos. Based on interpolation of the point cloud, a digital elevation model (DEM) was constructed. Projecting the photos onto the DEM resulted in an orthophoto (i.e. an ortho-rectified or distortion-free top view) of the experimental area. In Metashape the accuracy was set to high for photo alignment and dense cloud generation, resulting in a horizontal resolution of approximately 2 mm for the DEM and orthophoto.

For the one-day experiments, a subset of the scale bars (between 4 and 10) was used as a reference to set the scale and improve the camera alignment in Metashape. The RMS error of these scale bars was generally below 2 mm, and 3 mm for 23-10-2018. The horizontal accuracy was additionally assessed using another subset of the scale bars (at least 12), that was not used in the referencing procedure. The RMS error of this new subset of scale bars ranged between 2 and 7 mm for the different surveys, which, given the 60 cm scalebar length, amounts to a relative error of 1.2 percent or less. For the 5-week experiment, we assessed the horizontal accuracy by comparing the length and width of the scale models, as measured on the orthophotos of the three measurement days. These measurements, that should all have a fixed size, differed less than 2 mm for the small scale model and less than 25 mm for the large scale model, which amounts to errors of less than 0.6 percent.

With this accuracy and resolution, the structure-from-motion photogrammetry managed to capture the results well. The orthophoto was successful and sharp in all cases. The digital

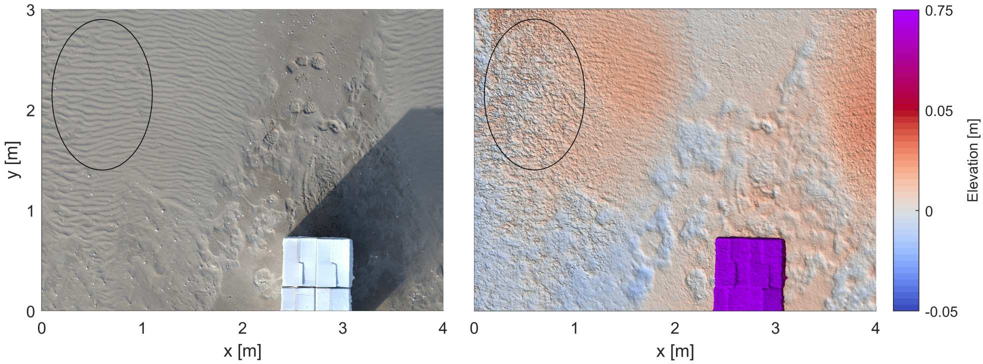

Figure 3.7: Detail of the photogrammetry results, with the circle indicating an area locally disturbed by noise on the DEM (right), but still sharp on the orthophoto (left). Elevations are relative to a fitted quadratic surface of the experimental area, to highlight local differences caused by erosion and deposition (12-10-2018, scale model of $0.66 \times 1 \times 0.7$ m).

3

elevation models showed more variation in quality, with some completely successful, while others were locally disturbed by noise (see Fig. 3.7), or in case of the results of 23-10-2018, strongly disturbed by noise. This difference between DEM quality and orthophoto quality is caused by DEMs being more sensitive to projection errors than orthophotos: a difference in the vertical position of a few cm by definition changes the DEM, but it does not really affect the projection of a photo as needed for the orthophoto.

3.3.3 Methodology of data analysis

To determine the location and size of the deposition patterns both the orthophoto and the DEM were used, but primarily the orthophoto. Section 3.3.3.1 defines the types of deposition features that were measured. For these measurements, scale-model-induced deposition had to be distinguished from the unaffected beach surface. Hereto a semi-automated method was used. The edges of the deposition areas were first detected using an image recognition algorithm based on orthophoto brightness and smoothness (section 3.3.3.2). Next, deposition size was measured based on the detected edges and, as a quality control, these values were compared to a visual assessment of the deposition size (section 3.3.3.3). Finally, the measured deposition sizes were analysed to determine how they correlated with building dimensions and wind speed (section 3.3.3.4).

The semi-automated method for deposition detection was chosen to combine the strong points of both automated detection and detection by eye. Deposition around scale models can be recognized from a number of properties. In the first place, the deposition areas in our experiments were generally lighter than their surroundings and showed less variation in colour, because of freshly deposited sand covering shells and other surface irregularities (see also Fig. 3.8 and Chapter 2). Image brightness and smoothness can easily be quantified with an algorithm from an orthophoto, and offer a consistent and repeatable criterion for identifying the edge of deposition across all set-ups and orthophotos. The human eye can more easily combine more qualitative indicators to recognize scale-model-induced deposition such as its position relative to the scale models, the presence and orientation of ripples, the degree to which shells and other large particles were covered, shadows and colour differences, as well as combine it with height information from the DEM. These additional indicators were used to check the algorithmic results, to combine the consistent and repeatable results of an image recognition algorithm with the human ability to recognize patterns under changing circumstances and from multiple information sources.

3.3.3.1 Deposition features of interest

To determine the location and size of the deposition patterns, several deposition features were measured (see Fig. 3.8). Upwind of the scale models, a deposition area generally developed a small distance from the building, with a steep slope - close to the angle of repose - facing the scale model. Of this upwind deposition, the upwind length (L_u) was measured from the upwind building edge and the upwind width (W_u) at the widest point. The upwind separation distance (L_u), so the distance between the model and deposition, was measured both at the crest of the steep slope and at the very edge of the upwind deposition (closest to the building), in both cases measured at the centreline of the scale model. Downwind, buildings generally developed two deposition tails. For each tail, the downwind length (L_d) was measured from the downwind building edge and the downwind width (W_d) at its widest location. Furthermore, the downwind spread (S), so the largest distance between the outer edges of both tails, was measured.

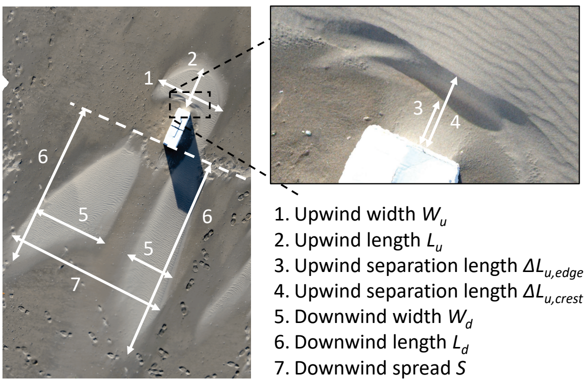

Figure 3.8: The definition of the deposition size features

Height information from the digital elevation models was only used in the manual estimate of the horizontal deposition extent and not for quantifying vertical deposition size and deposition volume. Because of our focus on initial deposition size (so deposition dominated by the scale model effect on airflow) the precise height of deposition was of lesser importance, as vertical build-up in initial deposition areas continues with time, where transport rate and duration will influence how fast this vertical build-up occurs. Indeed, deposition heights varied between experiments, ranging from only being visible as a colour difference without measurable vertical elevation change, to occasionally more than 10 cm. As argued in section 3.2.3, the effect of wind speed (as proxy for transport rate) on horizontal size of initial deposition areas is expected to be approximately linear, and such effects of wind speed are examined in the Results section.

3.3.3.2 Edge detection algorithm

To distinguish the deposition patterns in the one-day experiments, an edge detection algorithm was used. This algorithm is based on the orthophotos, because deposition varied greatly in height, and occasionally consisted of a very thin layer that was only visible on the orthophotos and not on elevation maps. Thresholding is applied to the orthophotos to distinguish the lighter and smoother deposition areas from the undisturbed bed. The workflow to detect these areas consists of three steps: image preparation, binarization and edge detection (Fig. 3.9). For the 5-week experiment, with larger deposition heights and lower contrast due to drier background surfaces, this algorithm was not used, and measurements were primarily based on the elevation map.

As image preparation, the orthophoto of the area was downscaled to a 1 cm resolution and then converted to greyscale. Next, the image intensity was normalized. The area (pixels) with boxes was filtered out, to only look at the sandy areas. The remaining image intensity was normalized, by assigning pixels that were 3 standard deviations darker/brighter than the mean as black resp. white (value 0 resp. 255).

This grayscale image was binarized, to divide the area in 'deposition areas' and 'rest'. Deposition areas were generally lighter than their surroundings, so pixels were classified as deposition if they were lighter than some threshold T. To take the lower variation of deposition areas into account, the value of T was increased in areas with large variation. This was implemented using an adapted version of the Sauvola algorithm (Sauvola & Pietikäinen, 2000; Shafait et al., 2008). Further details can be found in Appendix 3A.

Finally, edge detection was used to focus on the largest detected areas. Hereto all areas with a surface area of less than 0.25 m^2 (2500 pixels) were removed. Next, the remaining areas were merged if they were less than 4 pixels (4 cm) apart and the outer edges of these areas were plotted.

3.3.3.3 Deposition measurement and correction

From the detected deposition edges (Fig. 3.9), the areas of interest were selected, so the upwind deposition and the downwind deposition areas. Then these areas were measured: the width, length and separation distance of the upwind deposition, and the width, length

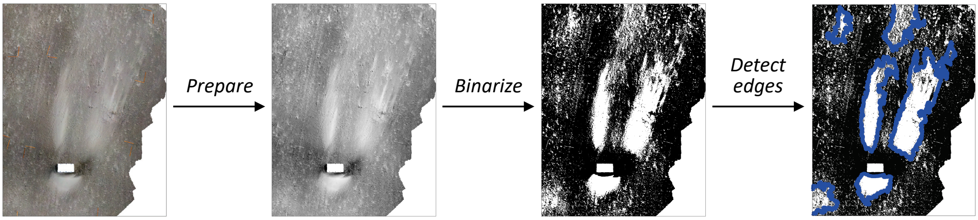

Figure 3.9: The edge detection algorithm. NB: The original orthophoto (left image) is in colour, there is just very little colour visible. After preparation it converted to grayscale.

and spread of the downwind deposition areas, as described in section 3.3.3.1. This is sketched in Fig. 3.10a.

Next, as a control, the extent of the deposition was also manually estimated based on visual identification of the deposition area (Fig. 3.10b, c). This visual identification was based on the degree to which shells and other large particles were covered by sand, shadows and colour differences in the orthophoto, the location with respect to the scale models, the presence and orientation of ripples, and height information from the DEM. Fig. 3.11 shows a more detailed example, to illustrate how shells, ripples and colour differences were used to estimate deposition dimensions.

The measurements of the automatically detected deposition areas were compared to the manually derived estimate (Fig. 3.10d, e). If the results of the manual estimate was significantly different (more than 10%), automatically detected edges were further examined. Automatic dimensions were kept in case they were plausible: deposition could be quite diffuse, so sometimes the edge of the detection could be quite different, but still realistic. The manual measurement was used in case the automatic edge detection was clearly incorrect.

For the upwind separation distance at the crest, the edge detection algorithm was never used. This was always measured by hand based on the DEM, as the algorithm did not include height information. For the upwind separation distance at the edge (see Fig. 3.8) manual correction was needed in nearly all the cases: due to the smaller feature size and reflections and shadows from the scale models, the edge detection algorithm did not perform well here. For the other features, this correction was needed in 25 percent of the cases.

3.3.3.4 Relating deposition size to building dimensions and wind speed

After determining the deposition size, the effect of separate building dimensions (w, h and l) and compound scaling lengths (R and B, see Eq. 3.1 and 3.2) on the horizontal deposition size was examined. For the downwind length and width, the deposition size was based on the average value of both tails. In case only one tail has been measured, that value was used. The strength of these effects was determined using linear regression, based only on the one-day experiments with boxes. Results of the 5-week experiment were compared to the

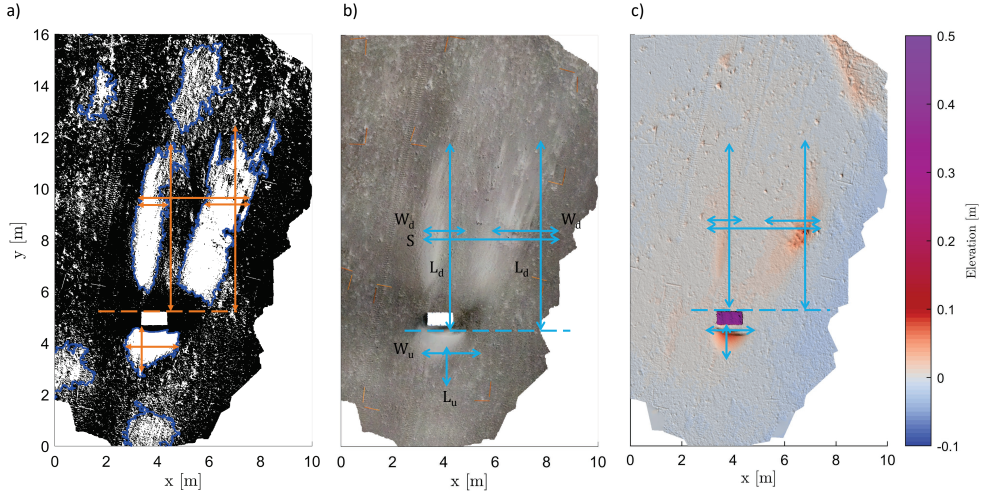

d)

Compare measurements

Less than 10% difference between algorithmic and manual measurement? → *Yes* → Keep algorithmic measurement

↓ *No*

Algorithmic measurement plausible? → *Yes* → Keep algorithmic measurement

↓ *No*

Use manual measurement

e)

Dimension		**Measurement [m]**		**Value used**
		Algorithm	Manual	
W_u		2.1	2	Algorithm: values similar
L_u		1.8	1.4	Manual measurement of orthophoto
Δl_u	edge		0.17	Manual measurement of orthophoto
	crest		0.4	Manual measurement of DEM & orthophoto
W_d	left	1.2	1.4	Algorithm: value plausible
	right	1.8	2.2	Algorithm: value plausible
L_d	left	6.5	6.5	Algorithm: values similar
	right	7.2	6.6	Algorithm: values similar
S		4.35	4.45	Algorithm: values similar

Figure 3.10: The measurement of deposition size, indicated by arrows on the orthophotos and DEM for one scale model (29-05-2018, model of 1×0.5×0.35 m). a) Measurement of the algorithmically detected edges, here plotted in blue on the binarized orthophoto. b) Manual measurements on the orthophoto, based on visual inspection. c) Manual measurements on an elevation map. Elevations are relative to a fitted quadratic surface, to highlight local differences caused by erosion and deposition. d) The workflow for comparing algorithmic and manual measurements. e) Example of the determination of deposition size from algorithmic and manual measurements.

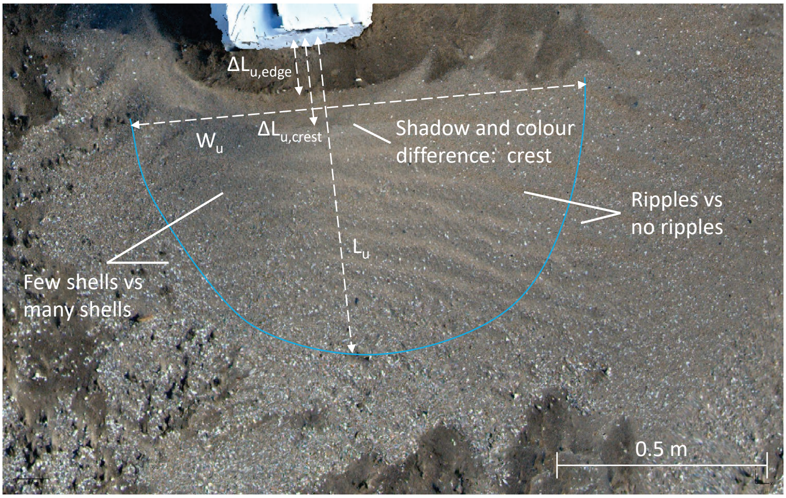

Figure 3.11: Detail of an orthophoto of upwind deposition, showing how shells, ripples and colour differences were used to distinguish and measure the deposition size (23-10-2018, model of 0.33×0.5×0.35 m). The blue line indicates the best manual estimate of the deposition edge.

one-day experiment results, but both small-scale and full-scale results were excluded from the regression to serve as first validation for how well the derived relationships perform for longer periods and full-scale buildings.

The effect of wind speed was examined next. From the theory, measured downwind deposition length is expected to increases linearly with wind speed – if the measurement duration and other conditions are similar and the bed remains flat enough that initial conditions still apply. For the other measures of deposition size, the effect of wind speed is not known yet. To determine which deposition dimensions were affected by the wind speed, the effect of building dimensions on deposition was first removed by dividing the deposition dimensions by B. Then the residual variation was examined: we assessed for which deposition dimensions a significant linear correlation ($\alpha = 0.01$) existed between wind speed and the deposition dimension divided by B. For the deposition dimensions with significant wind speed effects, a new trend for B was calculated, compensated for the effect of wind speed. Hereto correlation was examined between B and the deposition dimensions divided by the relative wind speed $U/\bar{U}$ (so the wind speed divided by the average wind speed of the four days).

3.4 Results

The deposition patterns of the one-day experiments (Fig. 3.12 a-d) and of the 5-week experiment at Noordwijk (Fig. 3.12e, f) were measured to determine how deposition size depends on the building dimensions. The deposition patterns around the scale models were substantial in size: the total deposition length (from upwind to downwind edge) and width could be an order of magnitude larger than the horizontal scale model dimensions (see e.g. Fig. 3.12d). Next, the effect of the building dimensions on the horizontal deposition dimensions was examined in more detail. Table 3.4 shows how the dimensions of the one-day scale models correlate with the deposition dimensions. The scale model width had far more effect on the deposition dimensions than the model height and length. Although model height has little predictive value on its own, using both width and height information – by means of R or B – substantially improves the correlation. Of the two, B (Eq. 3.2) scores better than R (Eq. 3.1). This effect of B, based on only the one-day experiments, is also plotted as a trend line in Fig. 3.13.

Figure 3.13 also shows the measurements of the 5-week experiment, including both a full-scale model (Fig. 3.12e) and a small scale model (Fig. 3.12f). Three measurements were taken during the 5-week experiment: after 1 storm day, 3 storms days and 5 weeks. For the full-scale model, deposition developed more slowly: after 1 storm day, it exhibited no measurable downwind deposition, so only the upwind deposition dimensions were measured and plotted in Fig. 3.13. Notable for the result after 3 days is that the wind direction was at an angle of about 45 degrees with respect to the scale models (Fig. 3.6), affecting the deposition development (see Fig. 3.14a). Deposition dimensions have been measured in the direction of the container in this case, so at an angle to the wind. The deposition tails extended up to the dune toe, making tail lengths difficult to measure. Therefore the measured lengths up to the dune foot are indicated as a lower limit. Notable for the result after 5 weeks is that the small scale model is situated exactly in the deposition tail of the container due to the wind direction, causing it to become partially buried (Fig. 3.12f, Fig. 3.14).

Comparing the 5-week experiment to the 1-day experiment, measurements from the first days of the 5-week experiment exhibit the best agreement with the 1-day experiments. Of the measurements taken after one storm day, 5 fall within the confidence interval of the 1-day experiment, while two are just outside the interval. After three storm days, mostly with wind at an angle to the scale models, 5 measurements are within the confidence interval, and 5 above the interval. After 5 weeks, 2 measurements are within the interval, 2 below the interval and 5 above it. Especially measured lengths are larger than expected: the downwind length after 3 storm days and the upwind and downwind length after 5 weeks are all well outside the confidence interval. This is likely due to the combination of strong wind (see Table 3.2 and Fig. 3.6) and a longer period compared to the one-day experiments.

Therefore, the effect of wind speed was examined next. Within the one-day experiments, the deposition size, scaled (divided) by B, generally increased with wind speed (not shown). For the downwind length and downwind spread, this effect was significant at $\alpha = 0.01$. Therefore, we made new plots for the effect of B on deposition size, in which we aimed

Figure 3.12: Examples of deposition around scale models, with arrows indicating the (dominant) wind direction. a) Small scale models of different length, with upwind deposition and deposition tails visible as lighter areas (29-05-2018). b) The nearest small scale model of photo *a* from another angle. c) Deposition with a considerable elevation difference (23-10-2018). d) An orthophoto of deposition (12-10-2018). e) The full-scale model of the 5-week experiment, showing deposition, erosion and undercutting under the upwind side of the container (11-03-2020). f) The small scale model of the 5-week experiment, half-buried and with a deposition tail downwind of the model (11-02-2020).

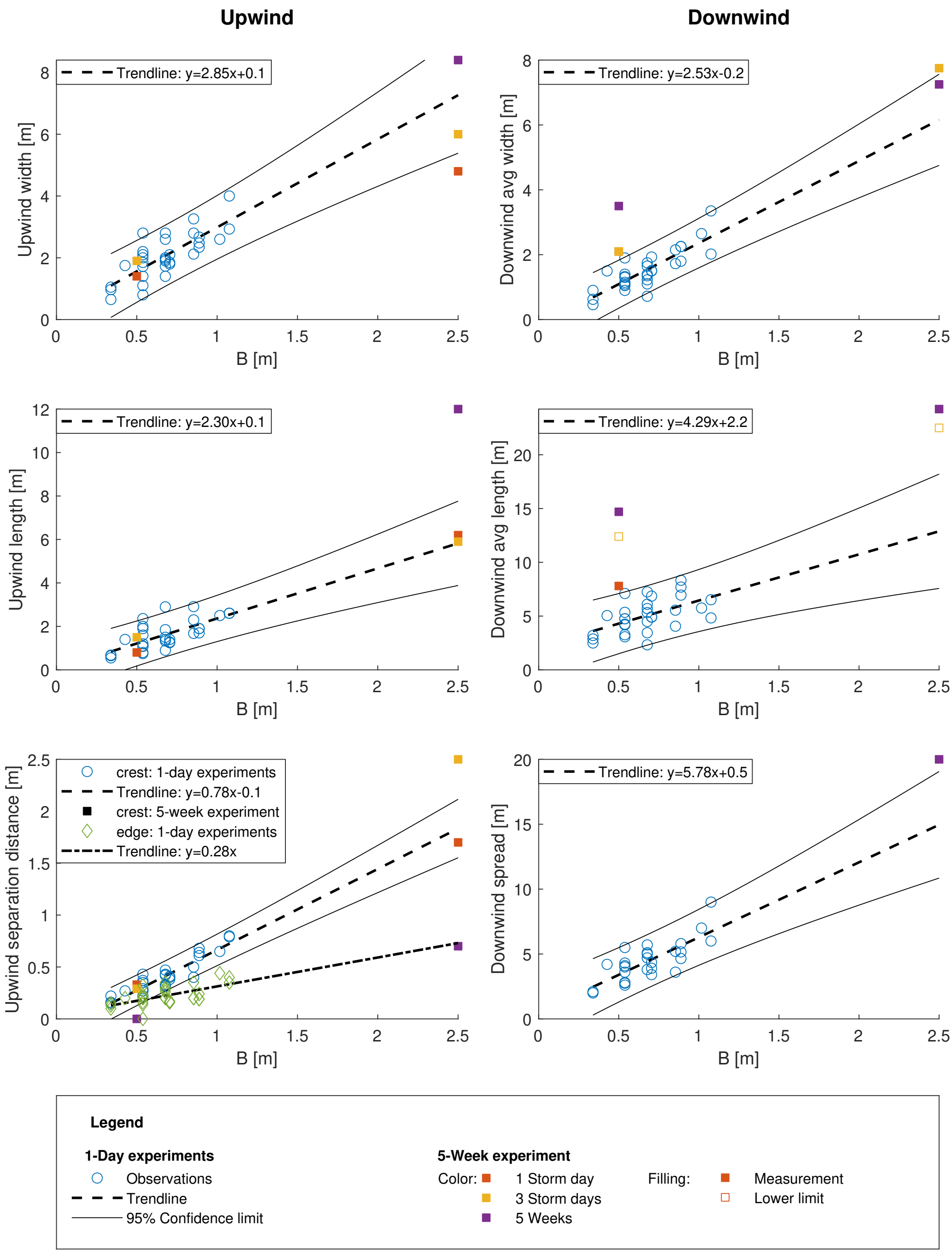

Figure 3.13: Experimental results showing the effect of the building scaling length B on deposition size. Plotted trendlines are only based on the one-day experiments, squares indicate results of the 5-week experiment with the small scale model (at $B = 0.5$ m) and full-scale model (at $B = 2.5$ m) in Noordwijk.

Table 3.4: Determination coefficients (R^2 values) for the best linear fit between building dimensions and deposition dimensions of the one-day experiments. For B^* the deposition dimensions have been divided by the relative daily wind speed $U/\bar{U}$. Individual R^2 values that are not significant at an α=0.01 level are indicated between brackets.

	w	h	l	R	B	B^*
Upwind width (W_u)	0.51	(0.03)	(0.02)	0.44	0.60	0.54
Upwind length (L_u)	0.38	(0.05)	(0.08)	0.38	0.48	0.54
Upwind separation distance edge ($\Delta L_{u,edge}$)	(0.12)	0.29	(0.03)	0.51	0.38	0.17
Upwind separation distance crest ($\Delta L_{u,crest}$)	0.62	0.28	(0.01)	0.77	0.85	0.64
Avg downwind width (W_d)	0.59	(0.05)	(0.07)	0.51	0.68	0.66
Avg downwind length (L_d)	(0.20)	(0.05)	(0.09)	0.29	0.30	0.47
Downwind spread (S)	0.32	0.44	(0.06)	0.64	0.60	0.73
Average R^2 value	0.39	0.17	0.05	0.51	0.56	0.54

to compensate for these wind speed effects. Dividing the deposition sizes by the relative wind speed (so $U/\bar{U}$ of the four days) improves the correlation of only the upwind length, downwind length and downwind spread (Fig. 3.15 and the last column of Table 3.4). In addition, this scaling improves the match between the container results and the empirical trendlines.

To test to what extent the power of ⅓ and ⅔ in B (Eq. 3.2) actually match the data, we also fitted Eq. 3.6 to the data, with x denoting any of the deposition dimensions, and power γ and $1-\gamma$ to have powers with a summed value of 1 (Wilson, 1979). Averaged over all the deposition dimensions, the maximum determination coefficient (R^2) was obtained with a value of $\gamma = 0.63$, so very close to the ⅔ used in B. The R^2 value increases with less than 0.01 and the adjusted R^2 value – where the value of R^2 is adjusted for the number of terms in a model to prevent overfitting (Theil, 1961) – actually decreases, further supporting the original powers in B.

$$x = \alpha + \beta\, w^{\gamma} h^{(1-\gamma)} \tag{3.6}$$

3.5 Discussion

3.5.1 Experimental set-up: scaling and uncertainties

In this experiment, scale models were placed at the beach in order to examine aeolian deposition around buildings. Using scale models, only the building size was scaled and all

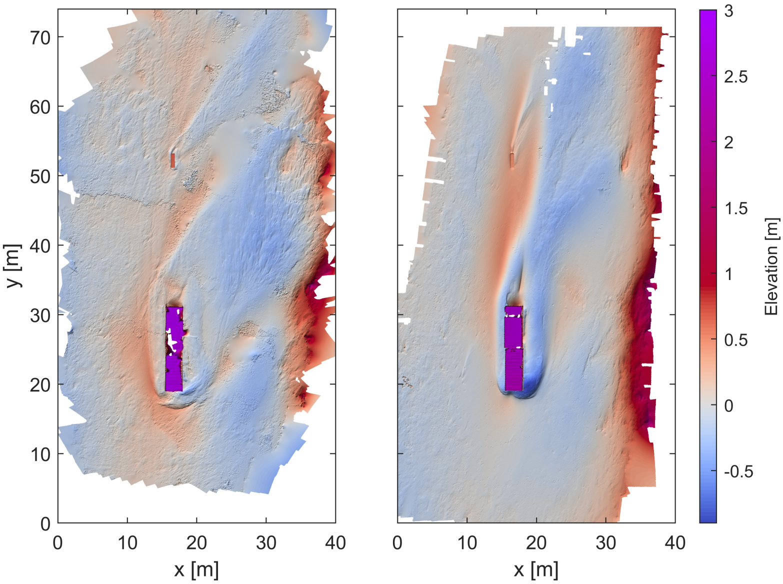

Figure 3.14: Elevation maps of the deposition around the 5-week scale models at Noordwijk. The small scale model is located around $x = 15$, $y = 50$. The elevation is relative to a fitted quadratic surface to highlight local disturbances. Higher elevations at the righthand edge are the toe of the dune. Left: elevation map after 3 storm days. Right: elevation map after 5 weeks.

other conditions (wind speed, grain size, saltation height, etc.) were not. The downside of this approach is that it can introduce scaling issues. Due to the high density of sand compared to air, grains do not instantaneously follow airflow but take some time and distance to adapt. Relative to the size of buildings and airflow patterns, this adaptation length becomes larger. Furthermore, sand transport occurs mostly in the saltation layer near the bed and decreases with elevation, so sand transport over small scale models may be larger than sand transport over actual buildings. This implies that deposition behind a small scale model might over-estimate deposition behind a full-scale building. However, measurements with a vertical array of Wenglor sensors showed that our smallest scale models were already higher than the saltation layer, hence this is assumed to have very little effect in our experiments.

In experiments similar to ours, on the deposition of snow around scaled buildings in a natural environment, scaling issues only played a small role (Liu et al., 2018; Oikawa & Tomabechi, 2000). In addition, strong scaling issues within our experiments would likely be visible as discontinuities in the relations found, or relations breaking down at smaller scales. Our relations fit the entire range of the one-day experiments and also match the results obtained around the full-scale model after the first days of the 5-week experiment quite well. Furthermore, if results from the 5-week experiment deviated from the relations, same-day

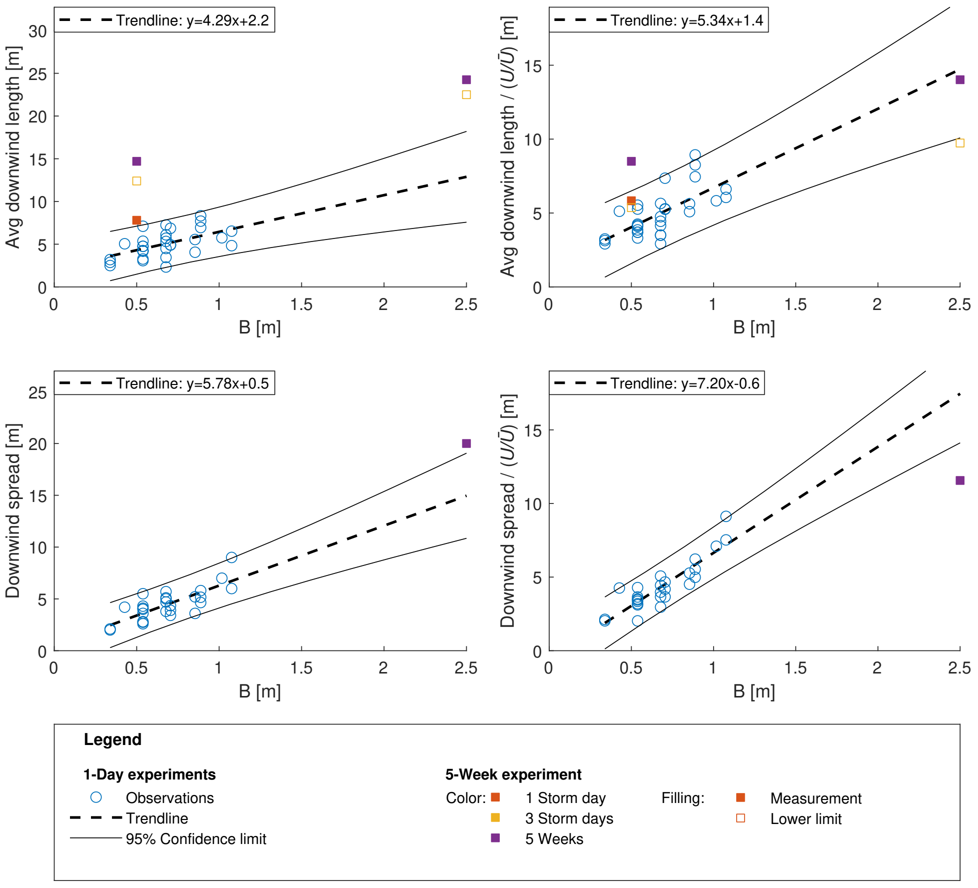

Figure 3.15: The effect of building scaling length B on deposition size, compensated for wind speed. Trendlines are only based on the one-day experiments, squares indicate results of the 5-week experiment with the small scale model and full-scale model in Noordwijk. Subplots on the left are equal to Fig. 3.13.

measurements around the full-scale model and the small scale model usually deviated in a similar manner (see in Fig. 3.13 the upwind separation distance after 5 weeks, and the downwind deposition length and width). Together, this suggests that the importance of scaling issues for our experiment is limited, with likely sand transport following the same paths, predominantly around (not over) buildings, similar airflow around scale models and buildings and these airflow patterns similarly controlling the deposition size and location.

The morphological development was further affected by variations in transport conditions. As expected, deposition patterns developed more quickly on days with larger wind speeds, resulting in somewhat larger horizontal deposition dimensions. This is especially visible for the downwind deposition length and spread in the one-day experiments (Table 3.4), fitting the hypothesis that the initial downwind length scales linearly with wind speed. For the downwind spread, the increasing deposition length is likely the underlying cause: for diverging tails, downwind spread increases automatically with length. For the other horizontal deposition sizes, there was no significant effect from wind speed.

For the 5-week experiment, the wind speed effect largely explains the deviations of the measured deposition dimension from the empirical relations, especially for the downwind deposition length and spread (see also Fig. 3.15). Moreover, the measurements were taken after multiple days to a month, thereby giving the morphology a long time to develop, further explaining the larger deposition. The exceptional weather conditions during the 5 weeks – multiple storms in a month with an almost constant wind direction, dominantly alongshore directed and hardly any rain – resulted in abundant aeolian transport that created deposition patterns that are most likely exceptionally well developed in terms of deposition size. Normally, frequent changes in wind direction lead to a reshaping of morphological patterns, thereby limiting the maximum deposition development.

The separation distance of the upwind deposition observed in the full-scale test after 3 days of storm conditions was also larger than predicted by the empirical relation. This could be related to the oblique wind angle and very elongated scale model shape: this increased the effective wind-facing surface, possibly creating a larger recirculation vortex (see Fig. 3.2) and thereby increasing the separation distance. This also indicates that wind at oblique angles to a building causes different deposition patterns than perpendicular winds (see also the results in Fig. 3.14), so this should be examined further. Conversely, the upwind separation distance of the crest after a month was considerably smaller than predicted. This may be explained by the strong topographic change that occurred on the upwind side of the full-scale model. Erosion undercutted the front of the model, causing the model to tilt down, while simultaneously strong deposition occurred upwind of the model. Together, this decreased the model height relative to the surrounding bed level. This would decrease the size of the recirculation vortex upwind of the model, over time allowing the upwind deposition to extend further toward the full-scale model.

The 5-week experiment further demonstrated that the physical size of scale models influences the time it takes for erosion and deposition to develop. The small scale model showed clear deposition after one storm day, while the full-scale model showed only starting upwind deposition (lower than in front of the small scale model, and no crest visible), and no visible downwind deposition yet. This implies that the results of the small-scale one-day experiments may be interpreted as more or less representative of the state around full-scale buildings after a somewhat longer period.

The comparison of deposition patterns of the 5-week experiment to those predicted by the empirical relations for *initial* deposition size also revealed the extent to which these relations are meaningful for longer-term morphological development. Here *initial* refers to the situation in which the building is situated on a generally flat bed, so that the building itself dominates the airflow patterns and sediment dynamics. The 5-week experiment examined deposition development around a small and a full-scale model and for a longer period, which resulted in substantial deposition also in the vertical dimension (up to 0.5 m). The horizontal size of deposition patterns after 1 and 3 days of the 5-week experiment, matched the empirical relations reasonably well, although better for the small scale model than for the full-scale model (Fig. 3.13). The deposition areas observed after 5 weeks were generally larger than predicted by the relations. The larger deposition area could be partially attributed to the high wind speeds (Table 3.2), but given the considerable bed level change at this point (Fig. 3.14), the situation after 5 weeks could likely no longer be characterized as initial deposition

Although initial deposition areas grow with wind speed and with time, this growth will not continue indefinitely. Over time, as the deposition height increases, the topography itself starts to affect airflow, partially cancelling out airflow effects induced by the building (McKenna Neuman & Bédard, 2015; McKenna Neuman et al., 2013). From the reasonable match between the results of the 5-week experiment and the windspeed-corrected empirical relations for initial deposition size, it seems that horizontal deposition growth after the formation of initial deposition is relatively limited. Hence, the empirical relationships of this study, with the exception of the upwind separation distance, can reasonably be applied to approximate longer-term deposition size.

Finally, in the correction for wind speed effects, wind speed is used as a proxy for sediment transport rate, as patterns develop more quickly with larger transport rates. However, also other factors determine the transport rate, such as fetch length, soil moisture and grain size (e.g. Bauer et al., 2009; Delgado-Fernandez, 2010; Kok et al., 2012). With experiments on different days and different locations this is considered a source of the scatter around the derived relations. Similarly, variation in wind speed or direction during a day and differences in the transport duration between days may have caused some further scatter.

Apart from variation in these environmental conditions, the measurement accuracy also has some contribution to the scatter. As illustrated by Fig. 3.10, there is uncertainty in identifying the edges of deposition patterns, and sometimes there could be quite a wide range of plausible locations for the border between deposition and undisturbed beach (decimetres up to occasionally metres). To limit the subjectivity in edge detection, an algorithm was applied to detect the edge, and visual identification was only applied in case of clearly erroneous edge detection.

3.5.2 Effect building dimensions on deposition size

In the observed patterns of erosion and deposition around the small-scale and full-scale models, deposition dominated and occurred in a large area around the models, while erosion seemed to be restricted to the area directly around the models in most cases (with erosion areas judged from darker areas, areas with more shells or elevation data for the one-day scale experiments (see Chapter 2) and from elevation data for the 5-week experiments). There are several reasons for this. The strong acceleration of wind forced by a building only takes place directly around a building, leading to a local increase of sediment transport rates and erosion. The downwind deceleration and decrease of sediment transport rates toward undisturbed equilibrium conditions is a more gradual process, thereby taking place over a longer distance. However, the amount of deposition and erosion also varied between the cases. For instance, on day 2 and 3 of the small-scale experiments, erosion was further limited by soil moisture. Conversely, the small-scale experiments of day 4 (23-10-2018), conducted during high wind speeds, and the 5-week experiment, experienced strong erosion at the upwind building edges, resulting in undercutting of the scale models (Fig. 3.12e). Overall, the observed dominance of deposition over erosion shows that the buildings do not only redistribute sand locally (i.e. from erosive to accreting areas), but that they can also capture sand that would otherwise be transported further downwind.

In the experiment, the upwind separation distance of the crest showed exceptionally good correlation with B, while the upwind separation distance of the edge showed more variation. This fits the results of Tsoar (1983), who found that in a wind tunnel the crest position of echo dunes in front of a cliff was relatively fixed, while the edge position grew toward a cliff with dune height. Together, these results imply that the location of the crest of the upwind deposition is determined by the building and by the airflow structures, while the edge depends also on the deposition height and angle of repose and hence on a range of other factors (most notably the experimental duration and sediment transport rate). This is further supported by the fact that the relationship we found for the morphological upwind separation distance of the crest ($0.1 + 0.8B$) is similar to the relations from earlier experiments on the aerodynamic upwind separation distance: $R_u = 0.7\sqrt{wh}$ and $R_u = 0.8w^{0.4}h^{0.6}$ (Beranek, 1984; Martinuzzi & Tropea, 1993).

The length of deposition features showed the lowest correlations with building dimensions,

3

both for the upwind and downwind deposition – although still clearly statistically significant at $\alpha = 0.01$. A part of this can be contributed to the wind speed: as demonstrated in the theory-section, wind speed affects deposition length more strongly than deposition width. With deposition length depending more strongly on local conditions, the correlation with building properties becomes lower.

Overall, the new scaling length B for the deposition around buildings (Eq. 3.2) correlates well with the measured deposition dimensions. In earlier literature (Schulman et al., 2000; Wilson, 1979), length scale R (Eq. 3.1) was used as a scaling factor for aerodynamic flow structures around buildings. For B, the contribution of building width is set larger, because building width is more important than building height for the disruption of sediment transport: sediment transport occurs mostly close to the bed. This physical reasoning, in combination with the fact that B is a simpler equation than R, yet correlates stronger with the one-day experiments, and the very close fit for B with the powers as calibration parameters (Eq. 3.6) as well as the good match with 5-week and larger-scale container results, instils confidence that B is an improvement over R for describing the dependence of deposition patterns on building dimensions.

The small scale models, on which the empirical relations between deposition size and building scaling length B are based, had aspect ratios (w/h) between 0.2 and 3.4. Because the *type* of airflow pattern developing around a building also depends on the aspect ratio, these relations should not be used for any arbitrary building aspect ratio. When the aspect ratio of a building increases, relatively more wind will be diverted over the building instead of along its sides, causing a lowering of the stagnation point at the upwind building face (see Fig. 3.2). Eventually, for very wide buildings ($w/h > 10$), flow patterns change completely, with also longitudinal vortices developing over the building (Martinuzzi & Tropea, 1993). As a result, the scaling of the upwind and downwind separation length with building width as reported by Martinuzzi and Tropea (1993) changes around $w/h = 4$, and especially the upwind separation length subsequently becomes almost width-independent for $w/h > 6$. Given these results and the range of aspect ratios tested in our scale experiments, we suggest limiting the application of our empirical relations for predicting deposition dimensions to buildings with aspect ratios between 0.2 and 4.

The new quantitative knowledge on the horizontal size of deposition around a building can be used to indicate the local area of influence of a beach building. As a next step, the long-term implications of these effects for the larger beach-dune area should be determined, by examining the interaction between local deposition and beach-dune dynamics. Furthermore, building-induced deposition on walkways, terraces and beach entrances often forms a hindrance to the public or building owners (Jackson & Nordstrom, 2011). The empirical relations on deposition size can be used as a guideline to place buildings or beach infrastructure in such a way that the hindrance from deposition and the need for sediment removal is minimized, for instance as a minimum required distance between a building and a beach entrance.

3.6 Conclusions

Block-shaped scale models of buildings were placed at the beach to study how the size of initial aeolian deposition patterns around buildings depends on building dimensions. These deposition patterns are of considerable size: their length and width are up to an order of magnitude larger than the horizontal building dimensions. The deposition patterns are caused by the airflow patterns around buildings, which form a horseshoe vortex. While the size of building-induced airflow patterns scales with both building width (w, measured perpendicular to the wind direction) and building height (h), related sedimentation patterns scale more strongly with the width of the building. This is explained by sand transport mostly occurring close to the bed, so little sand is blown over buildings irrespective of building height. This difference is reflected by the new scaling length B for deposition around buildings, with $B = w^{2/3}h^{1/3}$ to combine the effects of building width and building height.

In scale experiments with scale models of buildings placed at the beach for a single day, B scaled linearly with the horizontal dimensions of upwind and downwind deposition patterns, while building length had very little effect. Fitted relations between B and the horizontal deposition dimensions were statistically significant and showed good correlation. The good match between these relations and the deposition development around a full-scale model that was tested for 5 weeks, supports the use of B and these relations for predicting the horizontal deposition size around buildings at the beach. The w/h ratios of the tested scale models and the behaviour of airflow around buildings suggest these relations are applicable for buildings with a w/h ratio between approximately 0.2 and 4.

3.7 Acknowledgements

This research forms part of the ShoreScape project. The 5-week experiment at Noordwijk forms part of the larger Scanex experiment, organized by the CoastScan project. ShoreScape is funded by the Netherlands Organization for Scientific Research (NWO), contract number ALWTW.2016.036, co-funded by Hoogheemraadschap Hollands Noorderkwartier and Rijkswaterstaat, and in kind supported by Deltares, Witteveen&Bos, and H+N+S. CoastScan is also funded by NWO under project number 2018/STW/00505023 and focuses on coastal variability and resilience and the influence of natural and anthropogenic factors on these properties. We also want to thank Rijkswaterstaat for the logistic support during the experiment at the Sand Motor, the municipality of Noordwijk for their support on the Scanex experiment, Vaclav Hornik of Windguru.cz for sharing wind data from Noordwijk and Christa van IJzendoorn for sharing grain size data from Noordwijk. Furthermore, we thank Jan Willem van Dokkum and Mieke Kuschnerus for their excellent help during the preparation and execution of the experiments. In addition, we are grateful to Janneke van Bergen, Paran Pourteimouri, Geert Campmans, Sara Dionísio António, Weiqiu Chen, Joost Kranenborg, Mariëlle Rotteveel, Sam de Roover, Ton van der Heide and the Oerol festival organization for their assistance with the experiments.

Appendix 3A Orthophoto binarizing algorithm

The Sauvola algorithm (Eq. 3.7) is a local thresholding technique, with the local threshold T depending on the mean m and standard deviation σ of the intensity in a window centred around the pixel. R is the dynamic range of the standard deviation, so the highest value of σ for the entire image; k is a calibration parameter. This algorithm was originally developed for text recognition (Sauvola & Pietikäinen, 2000), but has also been used in a range of medical and engineering applications (e.g. Kim et al., 2017; Senthilkumaran & Vaithegi, 2016).

In its original application, the features of interest (letters) are darker and exhibit more variation than the background. In our case the opposite applies: deposition areas are lighter and exhibit less variation. Therefore, Eq. 3.8 is used instead. Conceptually this results in the same behaviour: the threshold is equal to m in the most promising area and stricter by a factor k in the least promising area. For parameter k, a value of 0.8 is used. The mean and standard deviation are calculated in a neighbourhood around the pixel of interest. Here, two different window sizes are used. For the mean a window of 4×4 m is used, to ensure that the window is larger than deposition features (otherwise deposition could not be distinguished by being lighter than the mean). For the standard deviation, a window of 30×30 cm is used, so this is really the variation of the area directly around the pixel itself.

$$T = m\left(1 + k\left[\frac{\sigma}{R} - 1\right]\right) \tag{3.7}$$

$$T = m\left(1 + k\frac{\sigma}{R}\right) \tag{3.8}$$


shorescape

4

Effects of building spacing and orientation on morphological patterns

4

Effects of building spacing and orientation on morphological patterns

Abstract: Airflow at the beach creates sand deposition patterns around buildings. To assess how initial deposition patterns depend on the orientation of a building relative to the wind direction and on the spacing between buildings, a series of one-day field experiments was conducted with cuboid scale models, in which 34 configurations were tested. Scale models placed further apart than 2 to 3 times the building width created deposition patterns that were similar to those for stand-alone buildings, where downwind deposition tails were the sum of the individual buildings' effects where these overlapped. For smaller spacings, between 0.5 and 2 times the building width, deposition patterns fundamentally differed from those for individual buildings, indicating a different type of airflow developed between the buildings. This created more complex depositional patterns that depended on the gap width. Rotation of an individual building relative to the wind direction induced an asymmetry in the downwind deposition patterns. A new rule of thumb quantitatively relates the asymmetry in the length of the deposition tails behind a building to the angle of the wind relative to the building and the length:width ratio of the building.

Figure previous page: Photo of scale models at various building spacings, of experiment C in this chapter.

This chapter is published as Poppema, D.W., Wijnberg, K.M., Mulder, J.P.M., & Hulscher, S.J.M.H. (2022). Deposition patterns around buildings at the beach: Effects of building spacing and orientation. *Geomorphology*, Volume 401, 108114. DOI: 10.1016/j.geomorph.2022.108114. Data available at https://doi.org/10.4121/16860145.v3.

4.1 Introduction

ALTHOUGH PEOPLE MIGHT REGARD buildings as passive structures, simply standing in their environment, buildings can actually affect and shape their surroundings profoundly. Buildings act as obstacles to the wind, thereby changing the wind field and creating complicated airflow patterns (Hunt, 1971; Peterka et al., 1985). In sandy environments, such as deserts, beaches and dunes, these airflow patterns affect aeolian sediment transport, creating patterns of deposition and erosion (see Chapter 2 and Nordstrom & McCluskey, 1984). This can pose problems, if for instance walkways or buildings entrances get blocked by building-induced deposition (Jackson & Nordstrom, 2011; Nordstrom & Jackson, 1998). It can even have repercussions for flood safety, if local scour around buildings creates a weak spot in the dunes (Nordstrom & McCluskey, 1984).

With coastal tourism and the demand for buildings at the beach increasing (Hall, 2001; Malavasi et al., 2013), knowledge about these deposition and erosion patterns is useful for coastal managers and local authorities who have to decide if, or under which restrictions, buildings are permitted along the coast. Quantitative understanding of building-induced erosion-deposition patterns can provide scientific support for regulation on the placement of buildings: for instance on the allowed size, location and orientation of buildings (Nordstrom & McCluskey, 1984). In addition, this knowledge helps to design and place buildings in such a way that unwanted deposition effects and the need for frequent sediment removal are minimized. Moreover, spatial designers have recently started explicitly utilizing building-induced effects to steer sediment to desired locations (e.g. for dune widening) (Van Bergen et al., 2021). Such designs need rules of thumb on how deposition and erosion depend on building placement and characteristics (Wijnberg et al., 2021).

Extensive research exists on airflow around bluff bodies such as buildings, often idealized as cuboid objects and also referred to as square cylinders (Bai & Alam, 2018; Baskaran & Kashef, 1996; Hunt, 1971; Martinuzzi & Tropea, 1993; Peterka et al., 1985). Wind approaching a building creates a downward flow at the upwind building face, creating a recirculation vortex directly upwind of the building. When this vortex is deflected downwind, a horseshoe vortex arises (Fig. 3.2). Flow separation at the top and sides of a building creates a recirculation zone behind the building. Some distance downwind, flow reattaches to the surface, with the downwind recirculation length generally less 1.5 building heights for approximately cubical buildings (Fackrell, 1984; Luo et al., 2012; Wilson, 1979). However, the horseshoe vortex remains present far longer, and turbulence and wind speed can remain affected at a downwind distance of 10 to 30 times the building height (Peterka et al., 1985).

For beach buildings placed directly at the surface, so not on stilts, deposition patterns generally follow this airflow pattern. (Nordstrom & McCluskey, 1984). This creates deposition a small distance upwind of the building (see Chapter 2), similar to echo dunes upwind of natural cliffs (Tsoar & Blumberg, 1991; Tsoar, 1983). Downwind deposition occurs in two tails, following the shape of the horseshoe vortex. In the building lee or wind shadow, centrally behind a building, deposition can also occur (Bagnold, 1941; Luo et al., 2012). Similar patterns can be found in snow accumulation around buildings (Liu et al., 2018; Thiis, 2003; Tominaga, 2017).

Although these morphological effects have long been recognized, systematic research into the deposition around buildings and how this depends on building characteristics is still in its infancy. In a recent study, we placed cuboid scale models at the beach to study how building geometry affects the size of aeolian deposition areas (Chapter 3). The deposition areas that developed were up to an order of magnitude larger than the horizontal building dimensions, and deposition size was found to depend on a building's width perpendicular to the wind and its height. However, in that study all scale models were placed perpendicular to the wind, while actual buildings also experience oblique wind directions. In addition, real-world buildings near the sea are often placed close together due to high demand and limited space. This affects the airflow, with e.g. a building's orientation to the wind changing flow topology and airflow separation and reattachment points (Becker et al., 2002; Luo et al., 2012) or building groups accelerating airflow between buildings (Baskaran & Kashef, 1996; Luo et al., 2014). Luo et al. performed a series of systematic wind tunnel experiments on how building orientation (Luo et al., 2012) and spacing (Luo et al., 2014; Luo et al., 2016) affect sediment deposition and erosion. However, they mainly measured airflow in order to predict expected effects for sediment transport and morphology; only their last study contained some experiments with actual sediment transport and deposition. To fill in the step from airflow to sediment transport and morphology and test under natural conditions, field experiments are needed (Luo et al., 2012; Luo et al., 2016).

Therefore, this chapter aims to determine how initial morphological patterns around buildings at a sandy beach are affected by building spacing and by a building's orientation relative to the wind. Hereto, as follow-up to Chapter 3, a new series of three experiments was performed, in which scale models of buildings were placed at the beach surface for a day and resulting deposition patterns were measured. The focus of this study is on deposition rather than erosion, because previous experiments showed deposition as the dominant building effect (Chapter 2 and 3). The area and volume of deposition are usually larger than that of erosion, with deposition occurring over a larger area, both upwind and downwind of a building, while erosion is mostly limited to the area directly along the building front and sides, where local wind acceleration scours the bed.

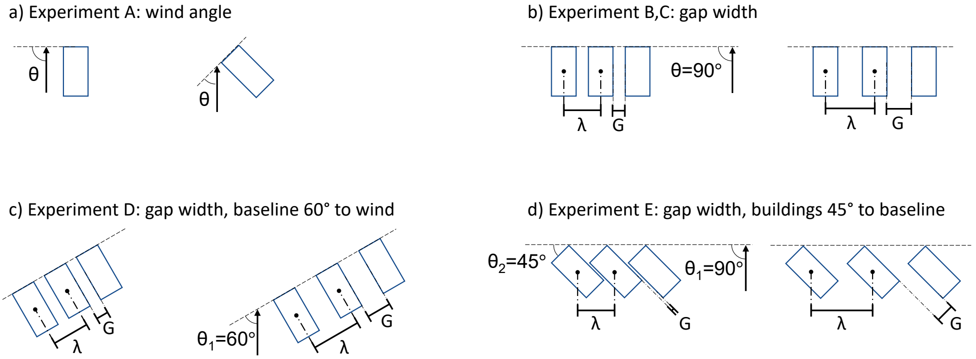

Figure 4.1: Overview of the variables tested in the experiment. In experiment A (subplot a) building orientation θ relative to the wind direction was varied, in experiments B-E (subplot b-d) gap width G was varied. Arrows indicate wind direction, dashed lines indicate the baseline, θ_1 (subplot c and d) indicates the angle of the base line to the wind, θ_2 (subplot d) the angle of the building to the base line. Note that the centre-to-centre distance λ was the same for experiment E and experiments B-D, but the resulting gap width differed between experiments due to staggered positioning of the buildings.

4.2 Methodology

4.2.1 Set-up experiments at the beach

Five experiments were conducted at a wide, flat part of the beach, each with different configurations of scale models to examine the effect of building orientation and the distance between buildings (experiment A-E, Fig. 4.1). The scale models, consisting of cuboid wooden boxes of 0.5×1×0.5 m ($w \times l \times h$), were placed at the beach surface when the wind was sufficiently strong for sand transport to occur (more than approximately 6 m/s). The resulting deposition patterns were recorded the next day, so deposition patterns had one day to develop. Depending on the wind conditions, this entailed 4 to 15 hours of wind stronger than 6 m/s (Fig. 4.4). For experiment A, deposition was measured three days after placing the models instead of one day, but during the last two days there was no sediment transport due to low wind speeds (2-5 m/s).

Deposition patterns were measured after one day, to focus on the direct effect of buildings. Over time, as deposition and erosion depth increase, morphological feedback would interact with the deposition patterns, as the topography will (under fixed wind conditions) start sheltering the bed and partly cancel out the airflow effects induced by a building (McKenna Neuman & Bédard, 2015; McKenna Neuman et al., 2013). The scale model size was chosen to be large enough to represent sedimentation effects around full scale buildings. This has been shown in Chapter 3, in which deposition patterns around small scale models and a full-scale model compared quite well. For these smaller scale models, the most important scaling effect is that deposition develops more quickly than around real buildings. The effect

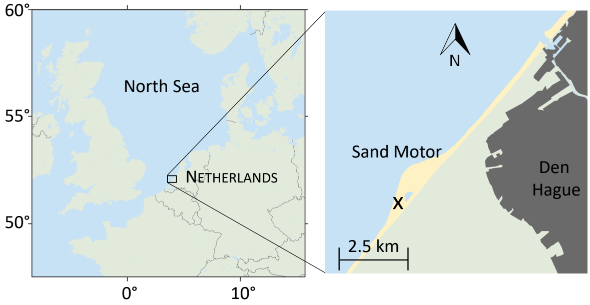

Figure 4.2: The location of the experiments, indicated by the X on the local map.

of other scaling issues is most likely limited, based on the limited importance of scaling effects in Chapter 3 and in similar experiments on the accumulation of snow around scaled buildings in a natural environment (Liu et al., 2018; Oikawa & Tomabechi, 2000).

All experiments were conducted at the south side of the Sand Motor in the Netherlands (Fig. 4.2), on the newly accreted beach area. The beach at this location is very flat with a 1:500 slope, and approximately 400 m wide, ensuring large fetch lengths (200 m for the offshore wind of experiment C, more than 500 m for the obliquely onshore winds of the other experiments). The median grain size at the Sand Motor is 335 µm (Hoonhout & De Vries, 2019).

To determine the effect of the orientation of an individual building relative to the wind, experiment A consisted of 9 scale models placed at the beach simultaneously, each with a different orientation to the wind (Fig. 4.1a, Table 4.1). A windvane was used to achieve the desired angles between scale models and wind direction, as prevailing during the set-up of each experiment.

To determine the effect of building spacing, experiment B consisted of six groups of three scale models (Fig. 4.1b, Fig. 4.3), with gap width G varying between 0 and 2 m (Table 4.1). Scale models were placed with the short axis parallel to a base line, and the base line perpendicular to the wind. For experiment C this was extended with a seventh group, with a gap width of 3 m. Resulting gap ratios g^* range between 0 and 0.86, where $g^* = G/\lambda$ and λ is the centre-to-centre distance of the scale models (Luo et al., 2014; Luo et al., 2016). This gap ratio can be regarded as the porosity of a configuration to wind and sand transport, varying by definition between 0 and 1.

In experiment D and E, the combined effect of building spacing and orientation was examined. Experiment D was a repetition of experiment B, but with the baseline at 60° to the wind (Fig. 4.1c). In experiment E, the baseline was perpendicular to the wind and scale models were oriented at 45° to the baseline, with building faces forming a staggered line (Fig. 4.1d). Here, centre-to-centre distances of scale models were kept the same as in previous experiments.

4

Table 4.1: An overview of the conducted experiments. Wind conditions characterize only the period during which sediment transport occurred (wind speed over 6 m/s). Orientations of experiment A are as measured, relative to the dominant wind direction, hence the irregular interval between tested orientations.

Experiment	Survey date	Variables tested	Gap width G [cm]	Gap ratio g^* [-]	Orientation baseline to wind [°]	Orientation object to baseline [°]	Wind speed [m/s]	Wind direction	St. dev. of wind dir. [°]
A	15-4-2019	Object orientation	-	-	21; 32; 35; 51; 70; 81; 93; 112; 173	0	7.3	NNE	6
B	12-4-2019	Gap width	0; 25; 50; 100; 150; 200	0; 0.33; 0.5; 0.67; 0.75; 0.8	90	0	8.3	NNE	13
C	25-4-2019	Gap width	0; 25; 50; 100; 150; 200; 300	0; 0.33; 0.5; 0.67; 0.75; 0.8; 0.86	90	0	8.3	SSE	16
D	14-5-2019	Gap width, group orientation	0; 25; 50; 100; 150; 200	0; 0.33; 0.5; 0.67; 0.75; 0.8	60	0	8.1	N	12
E	15-5-2019	Gap width, object orientation	0; 3; 21; 56; 91; 127	0; 0.06; 0.29; 0.53; 0.65; 0.72	90	45	7.8	NNE	7

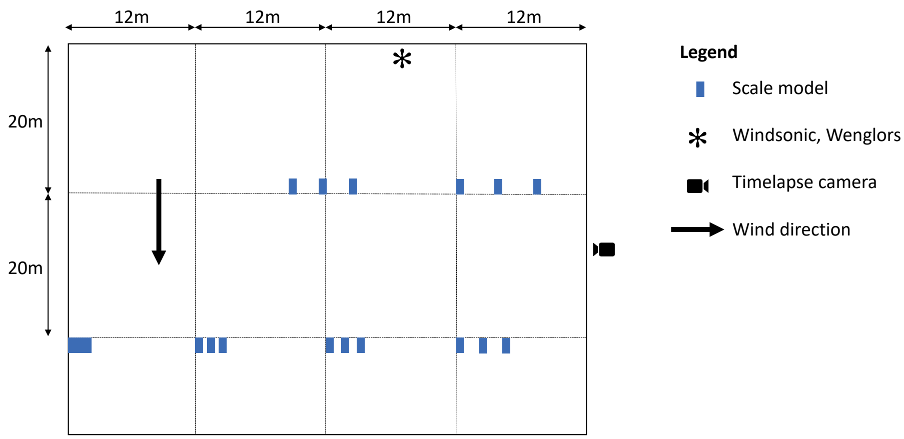

Figure 4.3: A sketch of the set-up of experiment B (scale models not drawn to scale).

The wind speed and direction, shown in Fig. 4.4 and Table 4.1, were measured using a 2D Windsonic ultrasonic anemometer, at 1.8 m high and using a sampling frequency of 0.2 to 0.6 Hz. In experiment A, the WindSonic was likely not properly aligned to the north, given that the direction of sand ripples in areas without scale models was consistent with a wind direction from a somewhat more northerly direction than derived from the Windsonic data. The average direction of the deposition tails downwind of the scale models was also in line with this more northerly wind direction, which deviated by 12° from the Sonic-derived wind direction. In the analysis of experiment A, we therefore used a corrected wind direction.

On the last day of experiment A, the WindSonic and Wenglors stopped recording due to an empty battery. For experiment C, they were not employed because of a thunderstorm. In both cases, wind data were retrieved from a public KNMI weather station at Hoek van Holland (KNMI, 2020), at 9 km distance. This station measured the hourly averaged windspeed and direction at 15 m above the ground. Windspeed measurements were converted to a height of 1.8 m, as measured by the WindSonic anemometer in the other experiments, using a constant difference of 2 m/s, based on a comparison of WindSonic and KNMI measurements for the other experiments.

The height of the saltation layer was measured by a vertical array of 10 Wenglor laser particle counters (see Duarte-Campos et al., 2021; Hugenholtz & Barchyn, 2011). The Wenglors were positioned between 0.05 and 1 m above the bed. The saltation layer height varied between 0.2 and 0.3 m, so in all cases lower than the scale models. Furthermore, for experiment B and C a time-lapse video with a 10 s sampling interval was recorded by a camera mounted 5 metres above the beach.

The sedimentation patterns around the scale models were measured using structure-from-motion photogrammetry (Fonstad et al., 2013; Westoby et al., 2012). Photos were taken

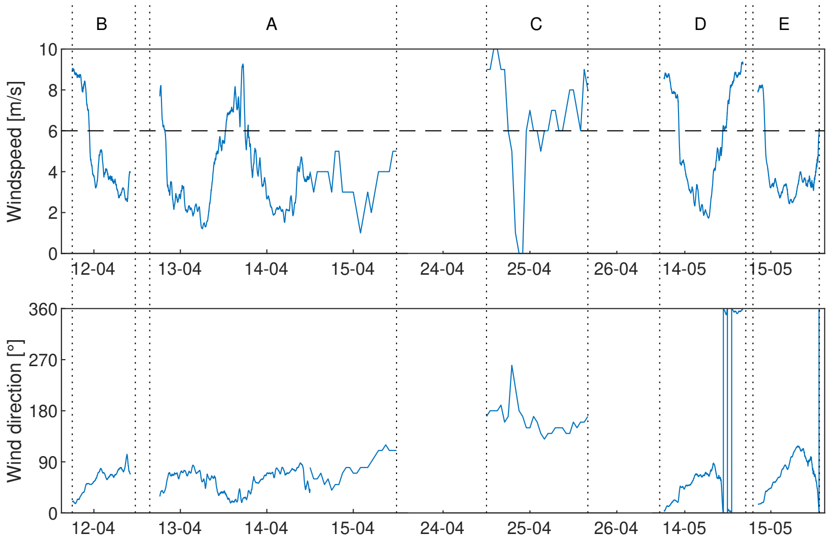

Figure 4.4: The wind conditions during the experiments. The horizontal dashed line indicates the critical wind speed for sediment transport to occur, vertical dotted lines indicate the start and end of each experiment (i.e. the moment scale models were placed and that deposition patterns were surveyed).

from a height of 5 m, using either a Phantom 4 Pro drone or an Olympus E-PL7 camera on a telescopic stick). Drone photos are of a 20 megapixel resolution, taken with a fixed 8.8 mm lens (74° horizontal angle of view). Photos taken with the Olympus camera are of 16 megapixel resolution, with a 20 mm lens (47° horizontal angle of view). With these camera properties and image shooting distance, the typical pixel footprint size of individual photos was approximately 1 mm. Scale bars were dispersed throughout the experimental area for referencing. In addition, ground control points were measured using a Leica GS14 RTK GPS, with an accuracy of approximately 2 cm. Further details of the camera set-up, photos, and weather conditions affecting the photos can be found in Table 4.2.

4.2.2 Structure from motion photogrammetry

Agisoft Metascan was used for the structure-from-motion (SfM) photogrammetry, following the same workflow as in Chapter 3. The horizontal resolution of the constructed DEMs and orthophotos was approximately 2 mm. Ground control point accuracy was generally at least 2.5 cm and scale bar accuracy at least 1 mm. Light conditions (Table 4.2) affect photogrammetry (Brunier et al., 2016; Chiba & Thiis, 2016), with e.g. sunny conditions creating contrast-rich photos, but also sharp shadows around scale models (Fig. 4.8). Nevertheless, this did not cause noticeable differences in accuracy, with especially the DEMs also showing clear details in shadowed regions.

Table 4.2: Camera and photo properties and weather conditions during surveying

Experiment	Camera	Number of photos	Weather conditions
A	Olympus E-PL7	1026	Mostly sunny
B	Olympus E-PL7	953	Mostly cloudy
C	Olympus E-PL7 + Phantom 4 Pro	139 + 968	Cloudy, occasional rain
D	Phantom 4 Pro	2181	Sunny
E	Phantom 4 Pro	2428	Sunny

4.2.3 Methodology of data analysis

4.2.3.1 Measuring deposition patterns

4

The DEM and orthophoto were first assessed visually, to qualitatively describe the nature of deposition patterns and identify the differences between different configurations. For the experiments on gap width, elevation profiles were additionally extracted from the DEM to quantitatively compare the deposition height and length around scale models. For the experiments on building orientation, the length of the downwind deposition tails was measured to quantitatively analyse their asymmetry. These tails were measured using the methodology described in section 3.3.3. A tailored image thresholding algorithm (Fig. 4.5) was applied to the orthophoto to distinguish deposition areas, based on their lighter colour and more uniform appearance. Then, as a control, these lengths were compared to a manual estimate based on visual inspection of the orthophoto and the DEM. In cases where both lengths differed significantly ($> 10\%$), algorithmically detected edges where checked, and incorrectly or unlikely drawn edges were corrected.

4.2.3.2 Linking building orientation to deposition length

The effect of a rectangular building's orientation to the wind was examined based on the length of the downwind deposition tails. The length of the left and right deposition tail depends on the amount of sand transport around each building side toward that tail. We will now develop a rule of thumb on how the fraction of sediment steered to the left and right of a building (α_L and α_R in Fig. 7) depends on the building orientation and building shape. Fraction α_L and α_R are defined relative to the total sediment transport downwind, so excluding the upwind deposition volume (i.e. $\alpha_L + \alpha_R = 100\%$).

To quantify the sediment partitioning to the downwind deposition tails, we examine the contribution of each wind-facing wall separately, under the premise that the contribution of each wall can be determined independently (Fig. 4.6). For each wind-facing wall, its orientation and length determine (1) its effective width projected perpendicular to the overall

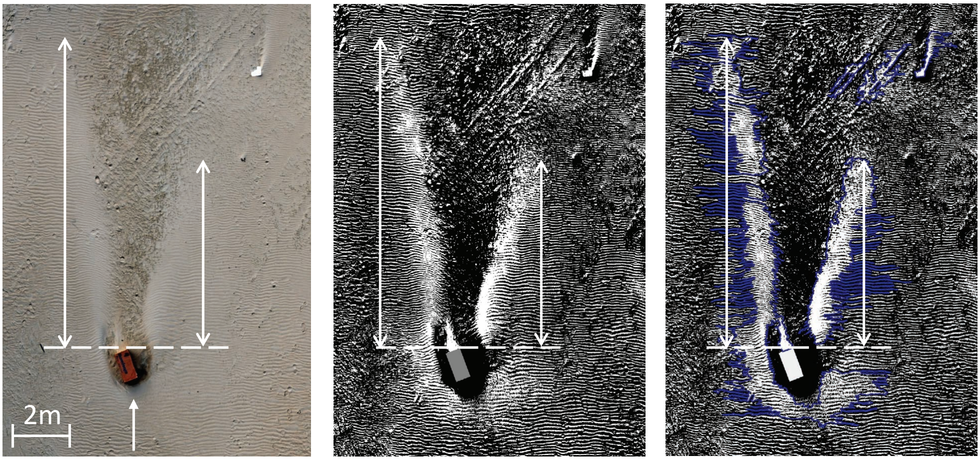

Figure 4.5: Example of the determination of the tail length, for the scale model at a 70° angle to the wind. The orthophoto (left) was binarized (middle), with white pixels indicating bright areas and hence (likely) deposition. Then the edges of the largest deposition areas were detected (right, with blue lines for the edges) and the length from the scale model to the downwind end of the deposition areas was measured.

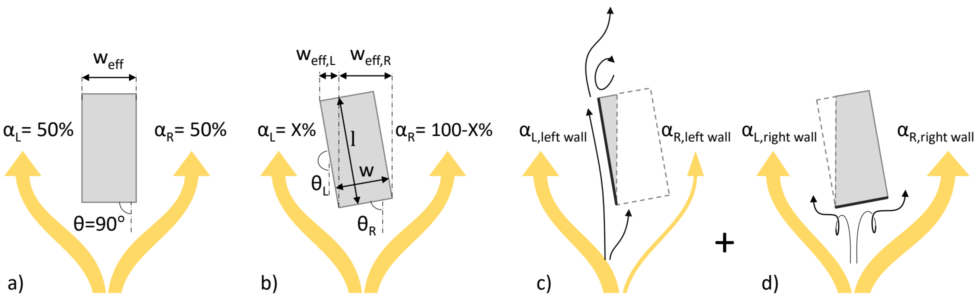

Figure 4.6: The partitioning of sediment transport towards the downwind deposition tails by both building sides. For a building oriented perpendicular to the wind (a), the percentages of sediment steered to the left (α_L) and the right (α_R) are equal. For a building oriented at an oblique angle to the wind (b), the division of sediment depends on the effective width (w_{eff}) and orientation (θ) of each wall. This division can be regarded as the summation of the independent contribution of both walls (c+d). The right-hand wall, which is oriented almost perpendicular to the wind, steers slightly more sediment to the right than to the left. The left-hand wall, which is oriented almost parallel to the wind direction, steers sediment almost fully to the left. Black arrows indicate important airflow patterns for the considered wall.

4

wind direction (e.g. in Fig. 4.6b $w_{eff,L} = L \sin \theta_L$) and (2) to what degree it steers sediment to either side ($\alpha_{L,\ wall}$ and $\alpha_{R,\ wall}$ in Fig. 4.6c, d). The effect of both wind-facing walls is then combined to determine what fraction of the sediment transport the entire building steers to either side (α_L and α_R in Fig. 4.6b), using the effective width of the walls to take into account the amount of sand approaching each individual wall.

In case of a rectangular object oriented perpendicular to the wind (Fig. 4.6a), there is only a single wind-facing wall, with flow separation in front of this wall creating a recirculation vortex that is wrapped around the building (Fig. 3.2) and transports sand equally to both sides. For an object at an oblique angle to the wind, there are two wind-facing walls, and the orientation of each individual wall determines how that wall divides sediment between both sides: a more wind-perpendicular wall will divide sand more evenly, while a wall more parallel to the wind will steer sand mostly to one side. For instance, the wall in Fig. 4.6d – which is almost wind-perpendicular – steers slightly more sediment to the right than to the left. Because this wall acts as a strong obstacle to the wind, a recirculation vortex forms, which also creates substantial sediment transport to the left. For the left wind-facing wall – which is almost parallel to the wind (Fig. 4.6c) – wind and sand can easily flow along the wall without being blocked, so the vast majority of sand transport toward this wall is steered to the left.

Changes in a wall's orientation have a *gradual* effect on the division of sediment to both sides. As a wall's orientation becomes more aligned with the dominant wind direction, wind increasingly follows the wall instead of being blocked and diverted to two sides. Consequently, a larger fraction of the sediment transport approaching this individual wall is steered parallel to the orientation of the wall, and a smaller portion is recirculated to the other side. However, even walls almost parallel to the wind can still steer sediment to both sides. For example, at the wall of Fig. 4.6c, a small fraction of the sediment transport towards this wall will still flow towards the right-hand tail (the yellow arrows in Fig. 4.6c). This is due to a small rightward airflow upwind of the building, and due to the rightward airflow found downwind of the recirculation cell that develops directly behind the building. This is indicated by the black arrows in Fig. 4.6c (c.f. Luo et al., 2012, especially the streamlines in their Fig. 5).

As a first approximation of this process, we propose to describe the division of sediment by a wall to its left and right side using linear interpolation between the two extremes, i.e. interpolation between the (almost) wind-parallel walls fully steering sediment to the left or right. For a single wall, this can mathematically be described as a fraction $\alpha_L = \theta/180$ of the sediment being steered to the left, and a fraction $\alpha_R = 1 - \alpha_L$ to the right, where the angle θ is defined according to Fig. 4.6. For a wall perpendicular to the wind ($\theta = 90°$), this indeed amounts to $\alpha_L = \alpha_R = \frac{1}{2}$, so half the sediment being steered to either side.

For a building with an obliquely approaching wind, the contribution of both wind-facing

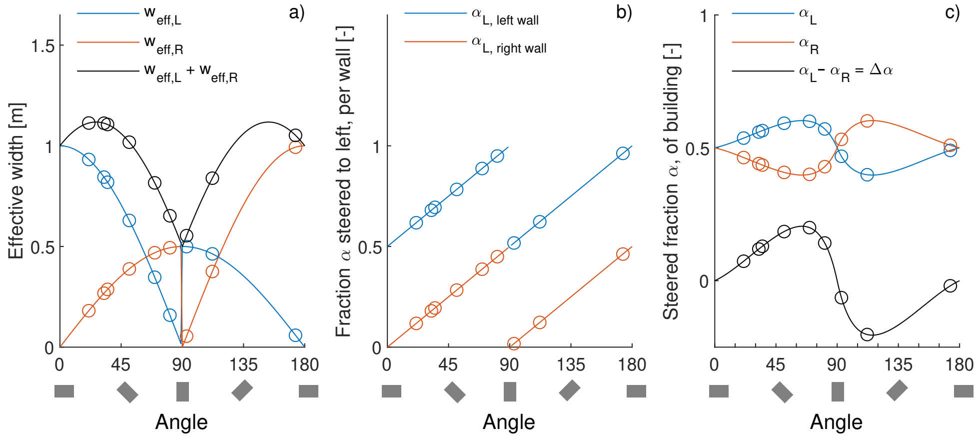

Figure 4.7: Theoretical sediment partitioning for a scale model of 0.5×1×0.5 m. Circles indicate angles tested in the experiments. Angles refer to the angle of the wind with the short face of the scale model , corresponding building orientations are sketched in grey for a wind coming from below. a) The effective width of the scale model sides at either side of the of the upwind corner. b) Theoretical fraction of sediment steered to the left by each building wall. c) The resulting sediment partitioning for a building, to either side, and its asymmetry.

walls has to be combined, taking into account the effective wind-facing width of both walls. Hence, the total fraction of the sediment steered to the left can be calculated as the weighted average of the fractions steered to the left by each wall ($\alpha_{L,\ left\ wall} = \theta_L/180$ and $\alpha_{L,\ right\ wall} = \theta_R/180$):

$$\alpha_L = \frac{\alpha_{L,left\ wall} \cdot w_{eff,L} + \alpha_{L,right\ wall} \cdot w_{eff,R}}{w_{eff,L} + w_{eff,R}} \tag{4.1}$$

The rightward steered fraction of the building is then simply equal to $1 - \alpha_L$, just as for a single wall. Alternatively, for rectangular buildings Eq. 4.1 can be rewritten in terms of only angle θ_R and the width:length ratio of a building, by directly calculating the steered fractions and effective widths and using $\theta_L = \theta_R + 90\circ$. This results in Eq. 4.2, with building width w measured at the right wind-facing wall, and length l at the left wall (Fig. 4.6b).

$$\alpha_L = \frac{\theta_R}{180} + \frac{0.5}{\tan(\theta) \cdot \frac{w}{\ell} + 1} \tag{4.2}$$

Figure 4.7 sketches how the orientation of the scale models in the experiments affects their effective width and expected partitioning of sediment transport. This will be used to correlate the asymmetry in the expected sediment partitioning to the asymmetry in the measured lengths of deposition tails.

4.3 Results

4.3.1 Effect of building orientation

Deposition patterns around individual scale models placed at various angles to the wind revealed the effect of building orientation (Experiment A). In general, the patterns were similar for all orientations, with deposition upwind of the scale models and downwind deposition in two tails (Fig. 4.8a, b). The orientation of the upwind deposition ridge was oriented somewhere between perpendicular to the main wind direction and parallel to the upwind building face, but closer to the former. This is illustrated in Fig. 4.8b. Along the front of the scale model erosion generally occurred, especially at corners. There was little deposition next to the building, so upwind deposition and downwind deposition tails were mostly separated, rather than forming a continuous horseshoe shape.

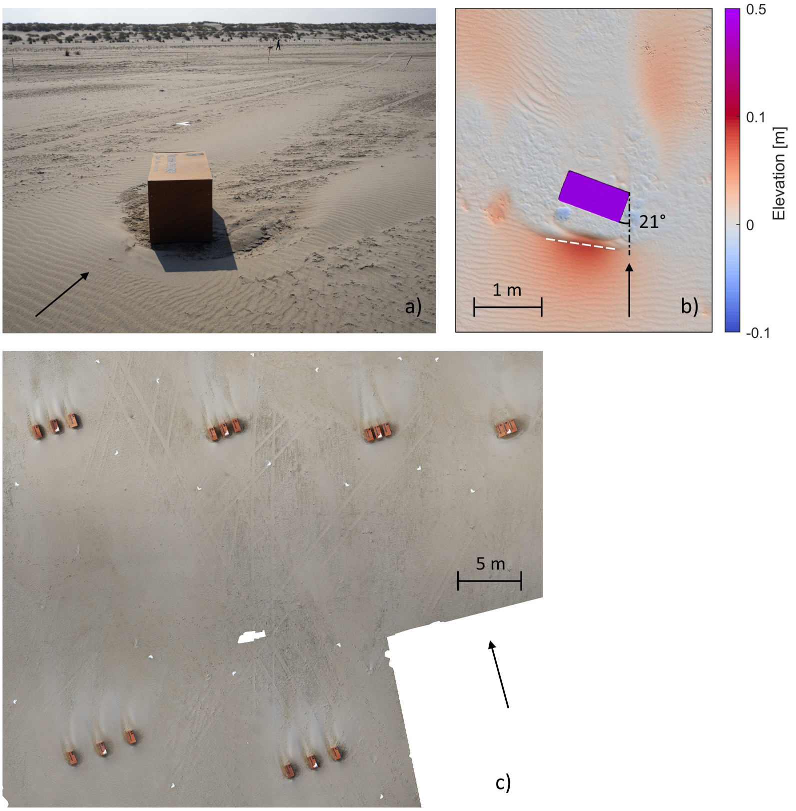

Figure 4.8: Examples of deposition around scale models, with wind direction indicated by arrows. a) A scale model at a 51° wind angle. b) A DEM of a scale model at a 21° wind angle, with the white dashed line illustrating the orientation of the upwind deposition zone. c) An orthophoto of experiment B for the effect of gap width.

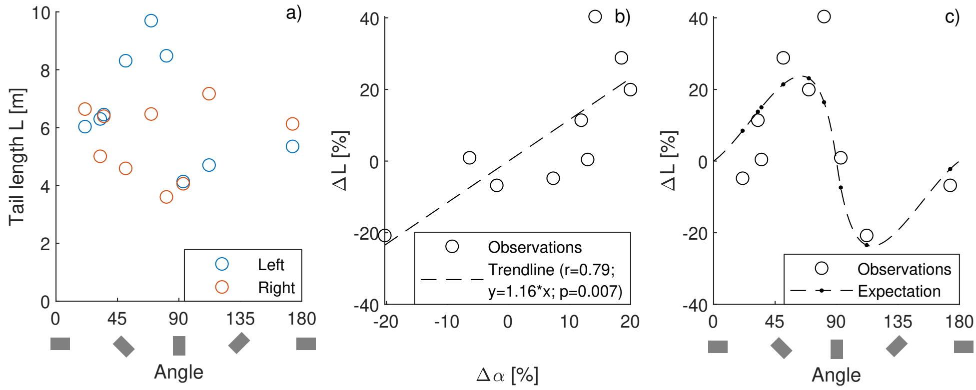

Figure 4.9: a) Observed deposition tail length L as a factor of the building angle. b) The correlation between the predicted asymmetry in the flow partitioning and the observed asymmetry in the tail length. c) Expectation of the tail asymmetry at arbitrary building angles, based on the trendline determined in subplot b.

Another observation is that the two deposition tails downwind of a scale model often differed in length (Fig. 4.9a). This asymmetry also shows in the deposition pattern of Fig. 4.5. The expected *asymmetry* in the fraction of sediment steered to the left and right ($\Delta\alpha$) and the observed *asymmetry* in the tail lengths (ΔL) show a quite strong linear correlation ($r = 0.79$, Fig. 4.9b). ($\Delta\alpha = \alpha_L - \alpha_R$ and $\Delta_L = \frac{L_{left} - L_{right}}{L_{left} + L_{right}}$). The slope of the trendline between $\Delta\alpha$ and ΔL is 1.16, with a 95% confidence interval of 1.16 ± 0.65. Note that a trendline without intercept is used in this case to ensure tails are of equal length for wind perpendicular to the building. Based on this linear relation, it is shown in Fig. 4.9c that the proposed sediment flow partitioning concept, based on wind angle and building length and width (Eq. 4.2), is consistent with the observed asymmetry in tail lengths.

4.3.2 Effect of building spacing

For experiment B, on the effect of building spacing (Fig. 4.8c), scale model groups with no gap or very small gaps showed a single upwind deposition area, with maximum deposition height in front of the middle scale model. This was the case for gap ratios ($g^* = G/\lambda$) of 0 and 0.33 (Fig. 4.10). For wider gaps, the deposition height directly upwind of the gaps decreased, so local maxima were formed in front of the individual scale models. As a result, one can recognize the individual upwind deposition areas of the three scale models for the configurations with $g^* \geq 0.67$. For the first two set-ups, the upwind deposition was generally higher and continued further upwind than for the larger gap widths, as visible in the centreline cross sections in Fig. 4.11a. Also the peak in the upwind deposition height of these two set-ups was higher and located further upwind from the building edge, especially for the continuous scale model (no gaps, $g^* = 0$).

4

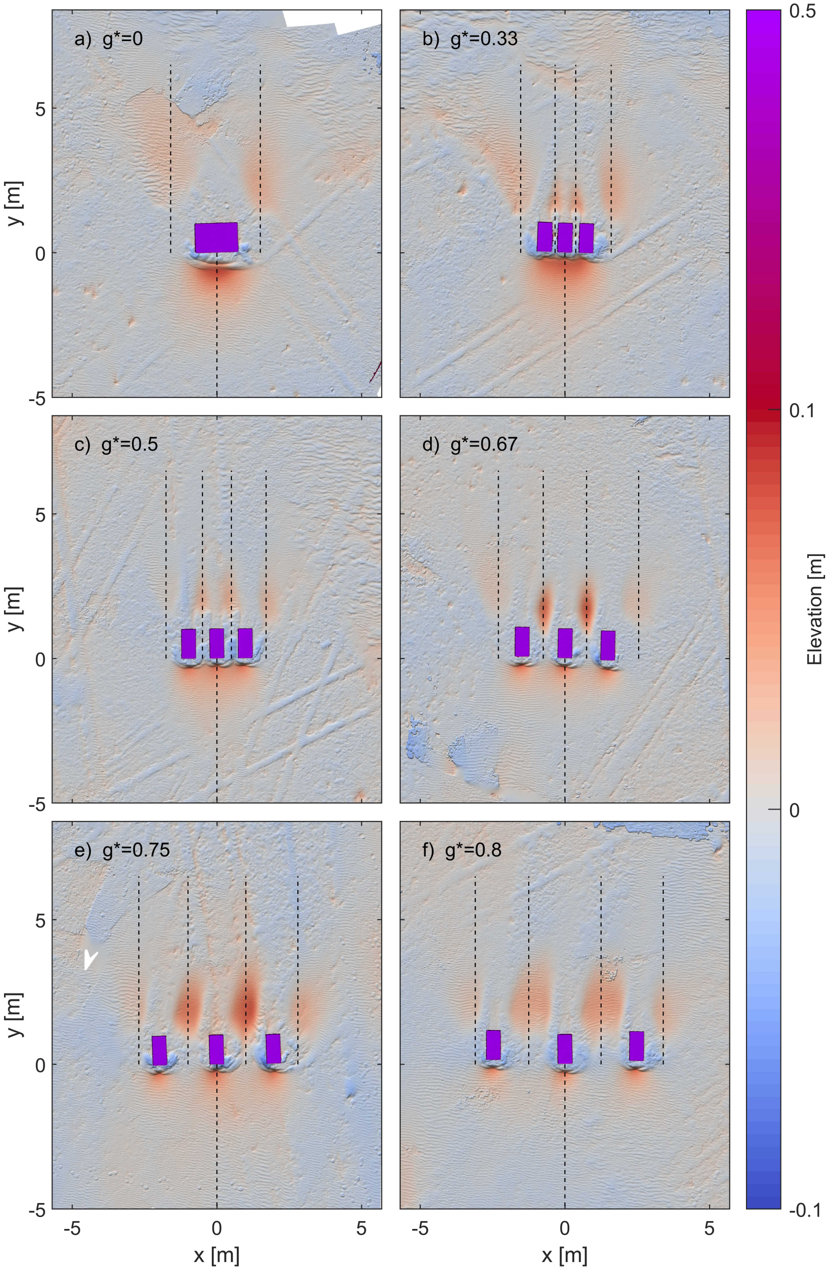

Figure 4.10: Digital elevation models around scale models with various gap widths (experiment B), with wind coming from below. Black dashed lines indicate the location of the cross sections plotted in Fig. 4.11. Elevations are relative to a linear surface fitted per subplot, to highlight local differences caused by erosion and deposition. Wind is coming from below.

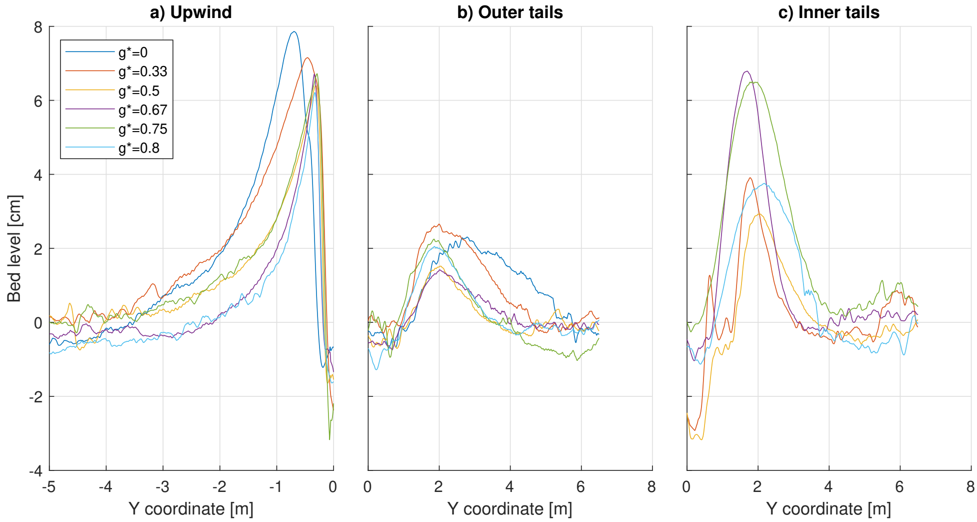

Figure 4.11: Cross sections of the digital elevation models (Fig. 4.10) to highlight erosion and deposition, with the scale models located from $y = 0$ to $y = 1$. Bed levels of the outer tails and inner tails are the average of the left and right tail. All cross sections are smoothed using a 10 cm moving average, to filter out ripples and focus on the larger structures.

Downwind of the scale models, deposition behind the gaps – which we call the inner tails – developed differently from the outer tails at the outside of a building group. The set-up without gaps showed only outer deposition tails. For small gap widths ($g^* = 0.33$ and $g^* = 0.5$), inner tails formed as well, but the outer deposition tails remained wider and longer than the inner tails (Fig. 4.10). In the gap between the scale models and directly downwind of the gaps, erosion occurred, as also visible in Fig. 4.11c from the negative bed levels between y=0 and y=1.5 m. Some distance downwind of the gap this changed into deposition, forming the inner tails. When gap widths increase further, the erosion in and directly behind the gap disappeared. Consequently, inner tails started just in between the scale models for a gap ratio of 0.67. They were still smaller in length and width compared to the outer tails, but larger in height. For gap ratios of 0.75 and 0.8, the inner tails were similar in length compared to the outer tails, with inner tails at $g^* = 0.8$ wider and lower than at $g^* = 0.75$. Overall, this amounts to inner tails being higher than outer tails, and to a trend of outer tails becoming smaller with increasing gap widths, while inner tails become larger.

The gap width affected not only the size of the deposition tails, but also their planform shape. At the larger gap ratios, both the inner and outer tails were roughly oval in shape. However, at the smaller gap ratios of $g^* = 0.33$ and 0.5, the inner tails instead had a more triangular shape, while the outside tails remained roughly oval. Additionally, a smaller difference could be found in the presence of sand ripples. Ripples were largely absent from the inner tails at $g^* = 0.33$, while all the other inner and outer tails of other set-ups showed

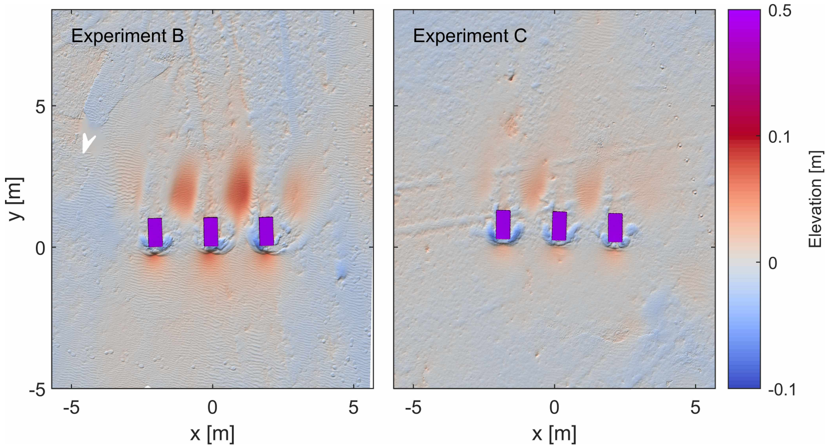

Figure 4.12: Comparison of the results from experiment B and C, for a gap ratio of $g^* = 0.75$. General patterns are comparable, but deposition was lower in experiment C.

4

ripples.

Comparing the two experiments on gap width (B and C), the patterns in the repeat experiment (C) are consistent with the general deposition patterns described above (B). However, patterns developed at a slightly oblique angle to the building ($10°$ to $15°$) in experiment C, caused by a change in wind direction during the experiment (Fig. 4.4). Also, the morphological patterns in experiment C were about half as high as in experiment B, likely as the result of rain during the experiment having decreased sediment transport rates. The lower deposition height made it more difficult to distinguish scale-model-induced deposition on DEMs from bed level variation already present in the undisturbed beach. Nonetheless, overall deposition patterns were quite comparable, as shown in Fig. 4.12 for one of the set-ups. For a complete overview with all gap ratios, see Appendix 4A.

4.3.3 Results complex configurations

For complex configurations, with groups of three buildings placed at an oblique angle to the wind, buildings were placed in two different configurations (Fig. 4.1c, d). For experiment D, the baselines of the entire scale models groups were oriented at a $60°$ angle to the wind. Here, inner and outer tails obtained a similar size for gap ratios of 0.75 and larger (Fig. 4.13). This gap ratio amounts to a gap width of 1.5 m perpendicular to the building, which effectively results in a gap of 0.8 m perpendicular to the wind (Fig. 4.13c). For smaller gap ratios, the inner tails were clearly shorter than the outer tails. Compared to experiment B and C, which had the scale model groups oriented perpendicular to the wind, more deposition occurred in the lee directly behind the scale models, occasionally forming a sharp ridge. For the smallest gap widths ($g^* = 0.33$ and $g^* = 0.5$), deposition from the inner tail and the lee of

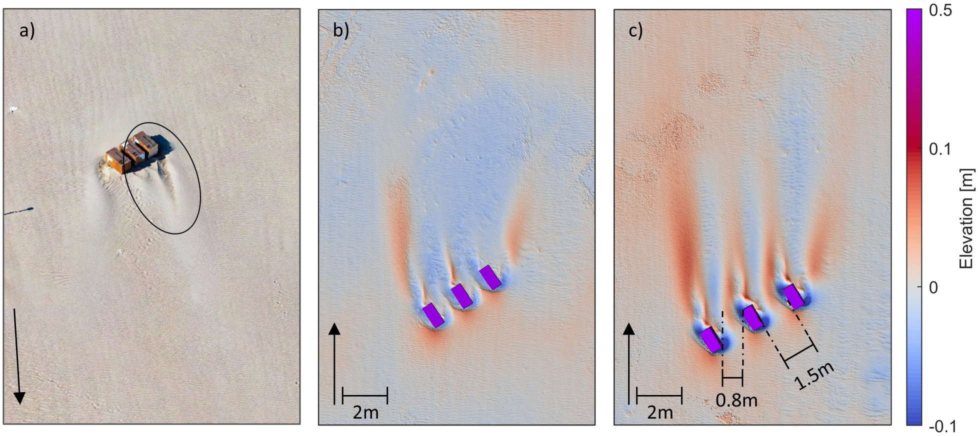

Figure 4.13: Building groups at a 60° orientation to the wind. Arrows indicate wind direction. a) set-up of $g^* = 0.33$, the oval line indicates where the inner and outer tail merge. b) $g^* = 0.67$. c): $g^* = 0.75$, with gap width indicated perpendicular to the building group and perpendicular to the wind. Elevations in b) and c) are relative to a fitted linear surface, to highlight local differences caused by erosion and deposition.

the scale models in addition partially merged with the outer tail (Fig. 4.13a). Lastly, viewing in the downwind direction, the left-hand outer tail was generally slightly higher than the right-hand tail.

For the second configuration (experiment E), where the baseline of objects was kept perpendicular to the wind and scale models were rotated individually at a 45° angle to the wind, similar results were observed. Also here a minimum gap ratio of 0.75 was required for inner tails to be comparable in length to the outer tails. This amounts to a gap of 0.9 m perpendicular to the wind direction. Deposition directly in the lee of scale models was again larger than for experiment B and C, but slightly less pronounced than for experiment D.

4.4 Discussion

4.4.1 Building orientation

The tails of the obliquely oriented individual scale models were asymmetrical: the left and right tails often had different lengths. Our sediment partitioning theory, which we developed to predict which fraction of the sediment flow passes along the left or right side of a building, showed significant correlation with the *asymmetry* in the tail lengths. The slope of the linear fit between sediment partitioning asymmetry and tail length asymmetry was 1.16, with a 95% confidence interval from 0.51 to 1.81.

To estimate tail asymmetry for buildings of arbitrary length:width ratio, we simplify the

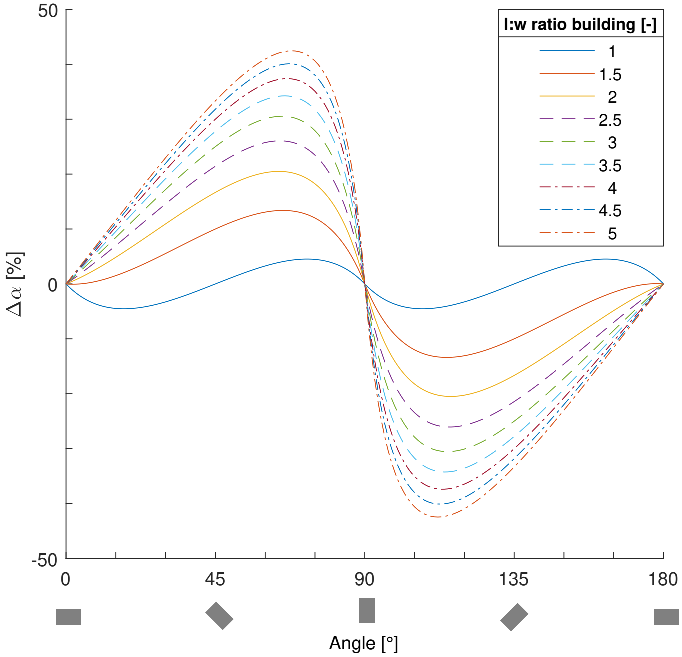

Figure 4.14: Asymmetry in sediment partitioning ($\Delta\alpha$) for buildings of several length:width ratios and arbitrary orientations. Corresponding building orientations are sketched underneath the x-axis, assuming wind coming from below. Following the rule of thumb, the asymmetry of the deposition tail length is equal to $\Delta\alpha$.

result to tail length asymmetry being equal to the expected sediment partitioning asymmetry, based on the large confidence interval around the 1.16 slope. This assumes that the sediment transport volume steered to each side is proportional to both the volume and length of each deposition tail; and thus that the left and right tail only differ in length, but have the same width and height. Hereby, the sediment partitioning method (section 4.2.3.2) can be used as a rule of thumb to estimate how the asymmetry in deposition patterns for individual buildings, of arbitrary cuboid geometry, depends on the building shape and orientation (Fig. 4.14). It follows that maximum tail asymmetry develops when the angle (θ) between the wind and the shortest side of the building is about 65° to 70○. In addition, the physical reasoning behind the rule does not depend on buildings having right-angled corners, so the rule can also be applied for buildings consisting of straight walls at angles other than 90°, as long as they are mostly uniform in height.

The proposed flow partitioning theory manages to predict asymmetry in the length of the deposition tails, without explicitly including complicated 3D flow patterns and changes in the airflow topology (Luo et al., 2012; Yen & Liu, 2011). This makes it simple enough to use in rule-based morphological computer models such as Dubeveg (Keijsers et al., 2016) or for design exercises where building-induced deposition is important (Van Bergen et al., 2021). However, the rule of thumb is still based on a very limited amount of observations. Furthermore, only morphological effects (i.e. deposition) were measured, without measurements of airflow or sediment transport around the building and over this topography. Therefore, further research by additional field experiments, controlled wind tunnel experiments, or CFD modelling of airflow around buildings (e.g. Pourteimouri et al., 2022), would be very valuable to further test and develop the theory. For instance, experiments with more repetitions or buildings with various length:width ratios would help to determine if other fractions than the so far used linearly interpolated steered fractions (i.e. the formula $\alpha_L = \theta/180$) describe the effect of building orientation on sediment partitioning better.

With the focus so far on tail length *asymmetry*, the question remains how large *absolute* tail length is. Absolute tail length depends strongly on the effective wind-facing surface of a building and hence on building size (Chapter 3). In addition, tail length depends on the sediment flux, and thereby on the wind speed, on local conditions as grain size, surface moisture and armouring and on the time available for deposition to develop. The effect of wind speed and duration also appeared in another experiment for the effect of building orientation, where 10 hours of strong winds of 10.5 m/s created deposition tails that had such lengths ($\pm$15 m), that tails of simultaneously placed scale model set-ups mixed and fused together[1]. This also fits the results in Chapter 3, which show that especially the downwind length of deposition patterns increases with wind speed, with approximately linear scaling between wind speed and tail length. However, all these factors mainly affect the total sediment flux, rather than the airflow patterns or the division of sediment between both building sides. Hence, they should have little effect on the tail length asymmetry as predicted by the rule of thumb.

In addition, the building orientation to the wind itself might affect absolute tail lengths, not only by determining the wind-facing surface and the division of flow over both sides, but also by creating fundamentally different airflow patterns behind the building. Luo et al. (2012) found that the shape and size of the recirculation cells behind a building (see Fig. 4.15) depend on the wind angle, and that for sufficiently oblique winds only a single recirculation cell is formed. Although this proves that the type of airflow pattern changes, such changes cannot be linked directly to the deposition length, especially as our experiment showed deposition in two tails stretching out far behind the building (on average 6 m, so 12 times building height h), while recirculation cells are shorter (2.5 h to 3.5 h for Luo et al., 2012) and located more centrally behind the building.

Lastly, the deposition patterns observed in the experiment are the *initial* deposition patterns that developed after a day at the beach. This short timespan is chosen to examine the effect

[1]This experiment was not analysed quantitatively, because tail ends were undefined due to tails merging with other deposition features. Appendix 4B shows an impression, in which the morphology also illustrates how sediment is diverted around buildings.

4

of a building on a flat beach, without morphological feedback interacting with building effects. The short time span also assured that the wind direction remained reasonably constant during the experiment (the standard deviation was 6° for experiment A). Although variations in the wind direction have had no visible effect, they could have slightly altered the deposition size or shape. Around real buildings at the beach, with continuously changing wind conditions, more complex deposition patterns can develop over time as the cumulative result of multiple independent wind events.

4.4.2 Gap width between buildings

By varying the gap width between scale models, we observed changes in shape and location of deposition patterns that suggest differences in the nature of the airflow. Upwind of the building groups, the configuration with three continuous scale models without gaps (gap ratio $g^* = 0.33$) developed a deposition area that extended further upwind, had a larger deposition height and had the crest located further from the building edge than the other set-ups (Fig. 4.11). This fits the results of Chapter 3, that upwind deposition length and upwind separation distance scale with building width and height. Likewise, the upwind separation distance for snow accumulation is also found to increase with building height (Thiis & Gjessing, 1999). The observations from $g^* = 0.33$ applied – to a lesser degree – to the configuration with narrow gaps ($g^* = 0.33$), showing that at $g^* = 0.33$ the upwind deposition height and location depend directly on the gap width. At gaps of $g^* = 0.5$ and larger, the height and location of the crest of the upwind deposition appeared constant, independent of the gap width. Physically, the larger separation distance between the upwind deposition and the building and the larger downwind deposition length at $g^* = 0.33$ can be explained by most of the wind still being diverted around the building, with limited airflow through the gaps, hence creating a larger rolling vortex upwind of the row of scale models. For gaps even smaller than $g^* = 0.33$, buildings will likely increasingly act as a single building, with barely any airflow or sediment transport in between buildings, but such small gaps were not examined in the experiments.

Downwind of the building groups, the overall trend observed was that inner deposition tails become larger with increasing gap width, while outer tails become smaller. Similar to the upwind results, this can be explained by the increasing airflow and sediment transport through the gaps. For narrow gaps, building groups act almost as a large building, with little transport through the gaps and airflow tending towards a shared horse vortex system (Luo et al., 2014; Yen & Liu, 2011). Consequently, most of the sand is transported around the building group, creating large outer tails. As the gap width increases, transport increasingly occurs through the gaps instead of around the building group, so inner tails grow larger, while outer tails become smaller. This is similar to how inner tails increased with gap width in a series of experiments on gap width and snow accumulation (Thiis & Jaedicke, 2000, with $g^* = 0.4$, 0.66 and 0.7), although there the inner tail was completely absent at the smallest tested gap width, possibly as the result of the oblique wind angle (64°).

Our more detailed observations on deposition behind the gaps can be compared to findings of Luo et al. (2014), who examined the airflow patterns downwind of two adjacent buildings in a wind tunnel, in order to better understand the formation of aeolian deposition and erosion patterns. Although we mostly examined larger gap widths than Luo et al. (2014) (g*=0.33-0.86 compared to g*=0.09-0.44), their airflow measurements help to understand the deposition and erosion patterns we observed. Our set-ups with the smallest gaps ($g^* = 0.33$ and $g^* = 0.5$) showed erosion in between the buildings and directly downwind of the gaps, followed by deposition. For $g^* = 0.09$ (so smaller than the smallest gap we tested), Luo et al. (2014) observed very limited airflow through the gap, creating a pair of counter-rotating recirculation cells behind the entire building group, with flow reversal behind the gap. For larger gap widths, the funnelling effect of the buildings created flow acceleration in and directly behind the gap. Upon leaving the gap, wind had space to expand, leading to deceleration at a distance of 0.5 to 1 building heights downwind of the gap. This fits well with our observed erosion in and directly behind the gaps at $g^* = 0.33$ and 0.5, where airflow accelerates, closely followed by deposition where the wind decelerates.

These airflow patterns can also explain why our inner deposition tails at $g^* = 0.33$ barely displayed any ripples. For relatively small gap widths, the outer recirculation cells are larger than the inner cells (see Fig. 4.15A) because more airflow is flowing around the building group than through the gap. These outer recirculation cells can wrap around the inner cells, meeting in the centre (Luo et al., 2014). This causes flow reversal where they meet, if the outer recirculation cells are dominant enough (see the flow reversal between point $S1$ and $S2$ in Fig. 4.15a and the red line in Fig. 4.15c). For slightly larger gaps, and less difference between inner and outer cells, flow is decelerated instead of reversed (see the blue line in Fig. 4.15c). Given that ripple formation requires saltating grains and sufficient wind speed (Anderson, 1987; Nishimori & Ouchi, 1993), such flow deceleration or reversal likely explains why the inner deposition tails barely displayed any ripples in our results of $g^* = 0.33$.

However, our results differ from those of Luo et al. (2014) with respect to the minimum gap width at which flow patterns become similar to those of individual buildings. For Luo et al. (2014), their largest gap width of $g^* = 0.44$ created balanced recirculation cells behind both buildings, seemingly unaffected by the neighbouring building. So inner and outer recirculation cells were of a similar size, preventing the outer cells from meeting in the centre and hence creating strictly downwind streamlines through the gap (see Fig. 4.15b). In our result at $g^* = 0.5$, the inner and outer deposition tails were still clearly different (Fig. 4.10), suggesting fundamentally different flow behind the gaps due to the combined effect of closely-spaced scale models. At $g^* = 0.67$ our set-up still exhibited inner tails that were narrower and shorter than the outer tails. Only at $g^* = 0.75$, inner and outer tails were of a

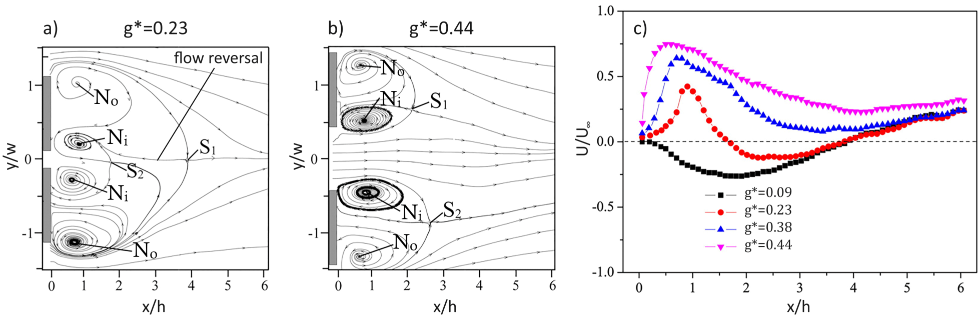

Figure 4.15: a) and b) Airflow patterns around pairs of buildings with varying gap widths for the experiments of Luo et al. (2014), with wind coming from the left. N_o and N_i indicate the nodes of the inner and outer recirculation cells. c) The horizontal wind velocity at the centreline near the bed. X and y-coordinates are scaled by h and w, the scale model height and width. Figure adapted from Luo et al. (2014). ©Elsevier, with permission.

similar shape and size, as would be expected when flow behind the gaps is similar to the flow at the outside of the group.

4

This difference is likely partly caused by different scale model shapes: our scale models had a square wind-facing surface of 50×50 cm, while Luo et al. (2014) tested with wider scale models, with a width and height of 5×2.5 cm. Given that the size of the recirculation vortex in front of the building (see Fig. 3.2) increases with both building height and building width (Martinuzzi & Tropea, 1993; Peterka et al., 1985), a relatively taller building creates a larger vortex in front and next to the building (larger relative to the building width). Hence, a larger gap ratio is required for neighbouring buildings to allow these vortices to develop independently of any adjacent buildings. This is consistent with wind tunnel experiments of two adjacent buildings (Stathopoulos et al., 1992), which found that building width w and height h together determine the ratio of the airflow acceleration in the gap between buildings to the acceleration at the outside building corners (K_{gap}/K_{corner}). More precisely, the ratio K_{gap}/K_{corner} depended on the relative gap width G/R, in which gap width G is divided by the scaling length R for airflow around buildings. Here, $R = \min(w, h)^{2/3} \cdot \max(w, h)^{1/3}$, valid for building aspect ratios (w/h) between 1/8 and 8 (Wilson, 1979).

The gap ratio as used to describe deposition patterns for different building configurations is hence only valid for buildings of equal width and height: it describes the porosity of a configuration to wind and sand transport, but does not take into account the aspect ratio (w/h) of the buildings. If building height increases, a larger horseshoe vortex is formed, so a larger gap ratio would be needed to form typologically similar deposition patterns. When interested in buildings with arbitrary aspect ratios, the expected deposition around building groups can therefore best be described using our observations for a configuration with a similar relative gap width (similar G/R ratio), instead of the configuration with a similar gap ratio. In the future, experiments on deposition around building groups with various aspect ratios would be valuable to verify if this scaling using scaling length R indeed holds true.

Overall, these results show that at small to intermediate gap widths, scale models created a shared complex flow and deposition pattern per building group, while for larger gap widths individual scale models acted mostly independently, with deposition similar to the summation of the expected effects of the individual scale models. This transition occurred at a gap width of two to three building widths ($g^* = 0.67$ to 0.75). Especially the inner tails of $g^* = 0.75$ and $g^* = 0.8$ could be recognized as being the summed results of the scale models at either side of the gap. For $g^* = 0.75$ inner tails were clearly higher than the outer tails, as they are formed by the deposition of two scale models, that occurred at almost the same place, leading to a single tail (per gap) of increased height. For $g^* = 0.8$, the tails of the two scale models at either side of the gap were created mostly next to each other, hence forming a deposition area that is wider and lower than for $g^* = 0.75$.

In addition, our results show that deposition behind gaps in between building (i.e. inner tails) can occur at any gap width. Previous studies searched for a critical gap width above which accelerated airflow through the gaps precludes inner deposition tail formation. From flow velocity, bed shear stress and deposition measurements in a wind tunnel, Luo et al. (2014), Luo et al. (2016) concluded that inner tail deposition may disappear for gaps wider than $g^* = 0.44$, which was their largest tested gap width. However, at $g^* = 0.5$, so our value closest to 0.44, we still observed inner tail formation, and actually inner tails were even larger at larger gap widths (Fig. 4.10). Given that deposition occurred, upwind of the buildings and behind the gaps, at all tested gap widths, the more important question is *where* deposition occurs and how much, rather than *whether* deposition occurs. For example, the experiments showed stronger upwind deposition for scale models with $g^* = 0.33$ compared to $g^* \geq 0.5$. So for buildings with a similar aspect ratio, coastal managers that want to augment sediment transport past a building group to a hinterlying dune, should ensure a gap ratio of at least 0.5.

4.4.3 Complex configurations

Deposition patterns observed around the configurations in which gap width and building and baseline orientation where varied in combination (experiments D, E), where largely consistent with those observed for the simpler wind-perpendicular set-ups (experiment B, C), albeit that larger gap ratios were needed before substantial inner tails could form. However, the necessary gap widths become more comparable when using the *effective* gap width, measured perpendicular to the wind instead of perpendicular to the building (Fig. 4.13c), which may better characterize the corridor actually open to the wind. In real situations, where buildings experience various wind directions over time, this implies that the effective gap width for the wind will depend on the wind direction. Hence, if a certain gap width is desired, for instance to limit upwind deposition as described above, the dominant wind direction must be taken into account, and possibly the distance between buildings should be increased, to ensure a sufficiently open profile under various wind directions.

A notable difference between the complex configuration results and those of experiment B and C, was the stronger deposition in the lee directly behind scale models. Directly behind a building is a sheltered area with low wind speeds (Luo et al., 2012, 2014), where wind recirculates. Earlier wind tunnel research predicted (Luo et al., 2012) or observed (McKenna Neuman et al., 2013) the lee behind buildings to be a major deposition area, with low wind speeds favouring deposition over erosion. The lack of initial deposition in this area in experiment B and C might be explained by airflow into this area containing little sand. But if the more complicated and messy airflow created by multiple oblique buildings blows sand into the area, the low wind speed in this area will result in deposition.

4.5 Conclusion

This chapter aimed to determine how the initial aeolian deposition patterns around buildings at a sandy beach are affected by building spacing and by the orientation of a building and building group relative to the wind. Building spacing determines whether wind and sediment can flow through the gaps between the buildings, thereby determining whether a building group acts as a single large building to the wind, as fully separated buildings, or something in between. Upwind, buildings placed close together (with a gap ratio g^* of 0.33 for the studied building shape where building height and width are equal) create a single large deposition area of a similar shape as a single large building, but in size falling between that of a single large building and that of wider spaced buildings. Buildings placed further apart ($g^* \geq 0.5$) create deposition with local crests in front of the individual buildings, with deposition slightly lower and shorter in length, but also spread over a wider area. Downwind, the experiments showed little deposition in the lee directly behind the buildings: main downwind deposition was in tails more to the sides, on the outside of the group and behind the gaps. For gap ratios of at least 0.67 to 0.75, the deposition tails behind the gaps (inner tails) and the tails at the outside of a building group (outer tails) were similar in size and shape. For smaller gaps, they differed significantly: a small erosion area formed directly behind the gap caused by accelerated airflow through the gap, followed by a shorter inner deposition tail. These differences show that deposition patterns behind buildings placed close together are formed by a shared complex airflow pattern. For buildings far enough apart – with a gap ratio larger than 0.67 to 0.75 for the studied square wind-facing wall – airflow patterns and deposition effects of a building can be regarded independently of effects by neighbouring buildings. For buildings for which the wind-facing wall is not square, these transitions in deposition and flow typology occur would occur at smaller gap ratios for relatively wide building (w>h) and v.v.

The orientation of a building determines how airflow and sediment transport are divided along both sides of a building, which affects the length of the deposition tails behind a building. Based on observed asymmetry in the tail lengths, a new rule-of-thumb was developed, where the sediment partitioning to the left and right depends linearly on the wind angle. This rule can be used to estimate the asymmetry of deposition tails behind buildings. By focusing on the morphological result of deposition, rather than on complex airflow patterns and sediment transport processes, this rule is simple enough to be used in rule-based morphological computer modelling and in spatial designs aiming to explicitly manage or utilize deposition caused by buildings.

For the spatial design and management of buildings at the beach, these results can be used to minimize the need for sediment removal by optimizing the locations of roads, walkways and buildings. In addition, they support regulation that stipulates a minimum distance between buildings to allow for sediment transport past buildings; and indicate that this distance should increase if the dominant wind direction is at an oblique angle to the buildings. Lastly, the practice of removing unwanted deposition around buildings inherently results in sediment displacement, so the substantial deposition observed highlights the importance of rules on where this sediment may be moved to, to prevent this 'human sediment transport' from counteracting other coastal management goals.

4

4.6 Acknowledgements

This research forms part of the ShoreScape project. ShoreScape is funded by the Dutch Research Council (NWO), contract number ALWTW.2016.036, co-funded by Hoogheemraadschap Hollands Noorderkwartier and Rijkswaterstaat, and in kind supported by Deltares, Witteveen&Bos, and H+N+S. We are also grateful to all the people whose assistance made the experiments possible: Jan Willem van Dokkum, Janneke van Bergen, Paran Pourteimouri, Geert Campmans, Sara Dionísio António, Weiqiu Chen, Joost Kranenborg, Vera van Bergeijk, Wessel van der Sande and Andrea Flores Ramírez for their assistance with the experiments. In addition, we want to thank Janneke, Paran and Geert for valuable discussions on the paper. Finally, we thank Thomas Thiis and one anonymous reviewer for their constructive comments and suggestions.

Appendix 4A Digital elevation models experiment C

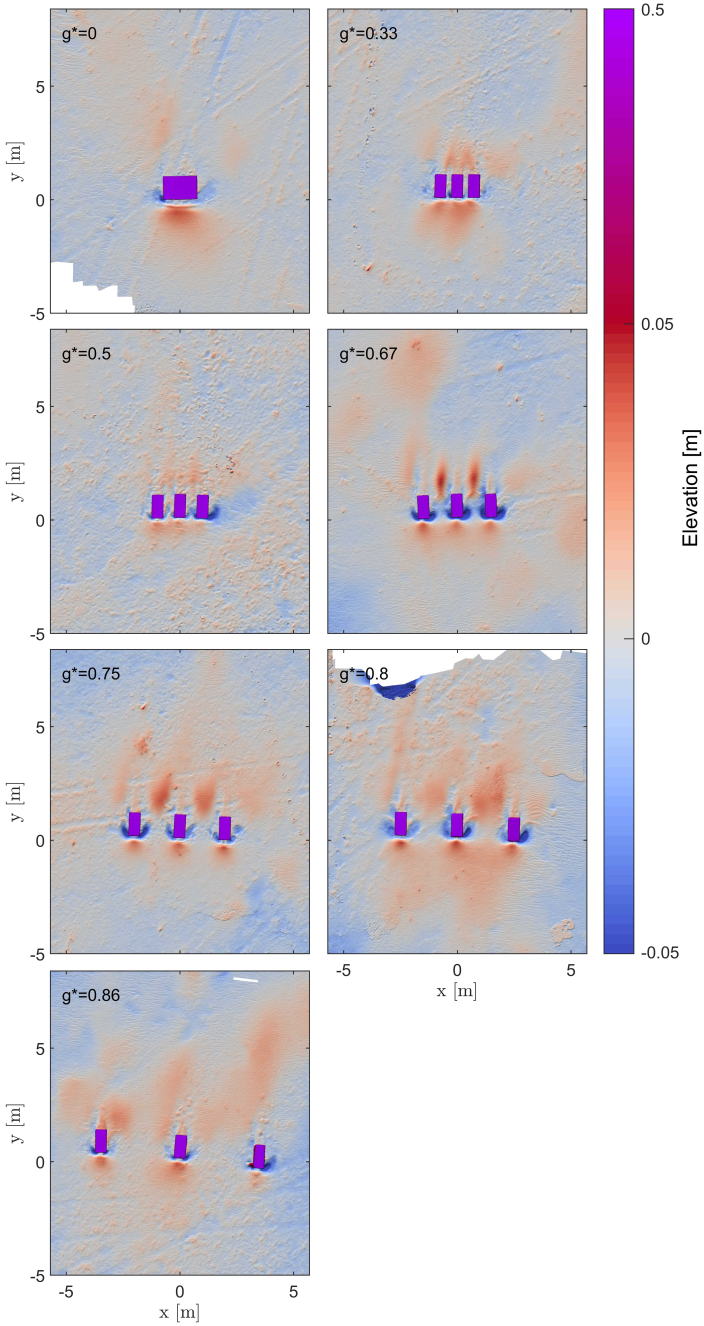

Figure 4.16: Digital elevation models of experiment C, with wind coming from below. Elevations are relative to a linear surface fitted per subplot. See Fig. 4.10 for the DEMs of experiment B.

Appendix 4B Orthophoto of unused experiment for the effect of building orientation

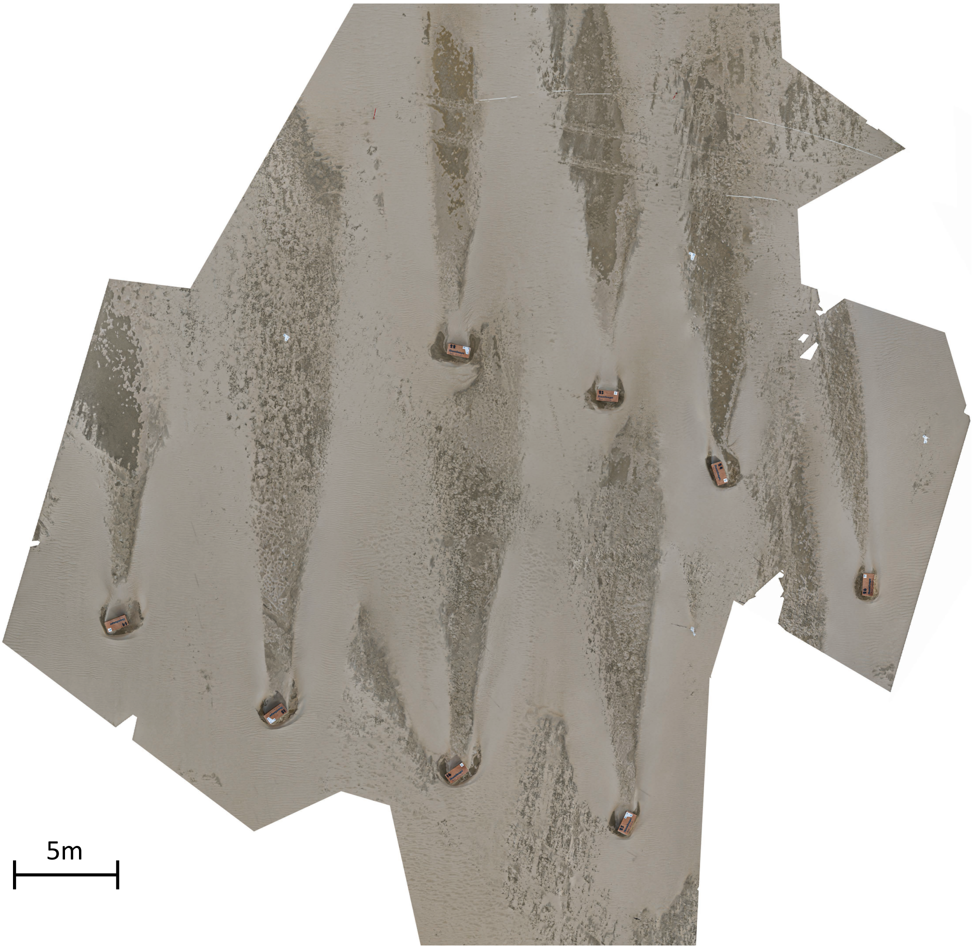

Figure 4.17: Orthophoto of an experiment for the effect of building orientation, performed at the Sand Motor at 27-04-2019, with wind coming from below. The morphology clearly shows how sand is blocked and diverted around scale models. Until far behind the scale models, this leads to erosion, or at least a lack of deposition. Due to the strong wind (10.5 m/s), deposition tails were so long that they mixed, making it impossible to distinguish the edges of individual tails.

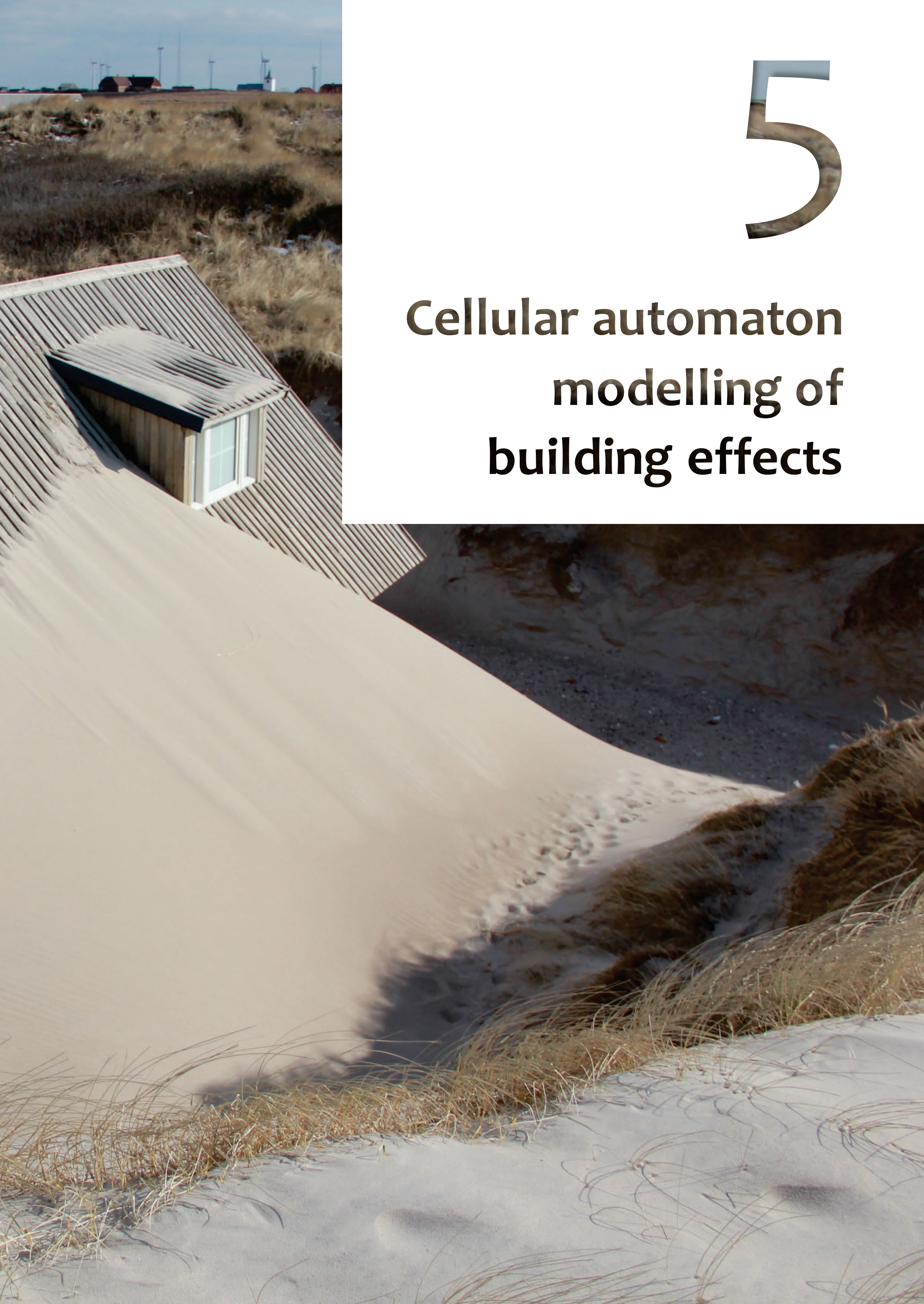

5

Cellular automaton modelling of building effects

5

Cellular automaton modelling of building effects

Abstract: Buildings affect aeolian sediment transport and bedform development in sandy environments. Cellular automaton (CA) models have, however, only been used to simulate natural bedform dynamics. This study extends a well-known aeolian CA model to include sediment dynamics around buildings, and uses this model to explore the interaction of building-induced deposition and erosion with natural bedform dynamics. New CA rules are introduced to represent acceleration, deceleration and sideward transport of sediment around obstacles. The simulated deposition and erosion patterns show good agreement with field experiments. The model reproduces the shape and location of the morphological pattern around a single building, and effects of building spacing on this pattern for building groups. Model results further demonstrate that building-induced effects interact with local bedform dynamics and can alter the shape, growth and migration of sand dunes.

Figure previous page: sand accumulation at a beach house near Fjaltring, Denmark. By Per Sørensen.

By Poppema, D.W., Baas, A.C.W., Hulscher, S.J.M.H. & Wijnberg, K.M. (2022). Submitted to *Aeolian Research*

5.1 Introduction

Buildings constructed in environments with active aeolian sediment transport, such as deserts or beaches, affect local morphodynamics. As unerodable, bluff objects, buildings change the wind field in their surroundings (Hunt, 1971; Nordstrom & McCluskey, 1985), create patterns of erosion and deposition (Chapter 2), and act as an obstacle to sediment transport (Jackson & Nordstrom, 2011). Cities neighbouring deserts and dune fields have been shown to alter wind speed, wind direction, sediment transport capacity, and vegetation cover in their surroundings, and can cut off dune fields from their sediment source (Hernández-Calvento et al., 2014; Malvárez et al., 2013; Smith et al., 2017b).

Deposition and erosion around buildings can have considerable consequences for surrounding infrastructure. Building entrances, walkways, and roads may be blocked by sand deposition (Jackson & Nordstrom, 2011) and in coastal settings there may be repercussions for flood safety, for instance with local scour around buildings creating a weak spot in the dunes (Nordstrom & McCluskey, 1984, 1985). In addition, locally increased deposition around buildings may intercept sediment transport into coastal dunes (Hoonhout & Van Thiel de Vries, 2013; Reinders et al., 2014), reducing dune growth and coastal safety in a larger area. Dune migration can also cause extensive damage to buildings in deserts (Abbasi et al., 2019; Lorenz et al., 2013) or coastal environments (Sherman & Nordstrom, 1994).

Existing studies on the morphological effects of buildings have focused on the local effects in a uniform flat environment, using scaled field experiments at the beach (Chapter 2-4) or in wind tunnel experiments (Iversen et al., 1990; Luo et al., 2012, 2014; Luo et al., 2016; McKenna Neuman & Bédard, 2015; McKenna Neuman et al., 2013). However, deserts and beach-dune systems are dynamic environments that exhibit strong bedform dynamics. Building-induced deposition and erosion features are not formed statically in a flat landscape, but they interact with self-organizing bedform dynamics and change under influence of fluctuating wind directions and conditions.

Aeolian bedform dynamics have been studied extensively using Cellular automaton (CA) models (Baas, 2002; Barchyn & Hugenholtz, 2012; Eastwood et al., 2011; Nield & Baas, 2008a; Werner, 1995; Zhang et al., 2012). These models describe aeolian sand transport using relatively simple rules, which through self-organization lead to remarkably complex bedform dynamics (Baas, 2002; Fonstad, 2013). The seminal Werner Algorithm (Werner, 1995) models sand transport as sand slabs moving over a grid with spatially varying probabilities of slab erosion and deposition. This algorithm successfully models the formation of barchan, linear and star dunes. The DECAL model (Discrete ECogeomorphic Aeolian Landscape model) adds vegetation dynamics, allowing for the formation of parabolic dunes (Baas, 2002, 2007; Nield & Baas, 2008a). The Dubeveg (Dune Beach Vegetation) model further adds hydrodynamic beach dynamics and implements groundwater as limiting factors for aeolian erosion, to model coastal beach-dune systems (De Groot et al., 2011; Keijsers et al., 2016). The feedbacks and interactions between all these processes allow for a wide range of applications, such as the effect of vegetation characteristics on dune dynamics (Nield & Baas, 2008a; Yan & Baas, 2017), of sea level rise on dune evolution (Keijsers et al., 2016) and of groundwater on coastal dune development (Galiforni Silva et al., 2018).

This model is used as basis for this study, because its performance in capturing the spatial interactions between processes make it suitable to study feedbacks between building-induced bed patterns and natural bedforms, and the resulting spatial distribution of sediment. Moreover, compared to process-based models such as the Coastal Dune Model (Duran & Moore, 2013), Aeolis (Hoonhout & De Vries, 2016) or Duna (Roelvink & Costas, 2019), the model has advantages in the model flexibility for adding building effects, the range of coastal processes that can be included, and the run-time for yearly to decadal simulations.

This study aims to: 1) extend these morphodynamic CA models with effects of buildings, and 2) use this to explore how building-induced morphological patterns interact with self-organized aeolian bedform dynamics. We develop new CA rules for the effects of buildings on local sediment transport. To test the performance of these rules, CA results of scenarios with buildings are compared to the field experiments of Chapter 3 and 4 in which individual scale models and scale model groups were placed on an open beach. Longer-term model scenarios (up to decadal time scale) are used to explore interactions between self-organized bedform dynamics and building-induced deposition and erosion.

5.2 Background: deposition and erosion around buildings

The morphological effect of a building on its surroundings starts with a building obstructing airflow and aeolian sediment transport. Upwind of a building, a portion of the airflow hitting the building is deflected downwards, creating a rolling vortex in front of the building. This rolling vortex is then wrapped around the building, forming a horseshoe vortex structure (Fig. 5.1). In sandy environments, the flow reversal in front of a building placed on the ground (i.e. not on stilts) creates deposition a small distance upwind of the building, similar to echo dunes in front of natural cliffs (Qian et al., 2011; Tsoar & Blumberg, 1991; Tsoar, 1983). In experiments with cliffs over the entire wind tunnel width, Tsoar (1983) found the distance from dune crest to cliff to be approximately 0.6 times the cliff height. However, the field experiments of Chapter 3 showed that the deposition size and location around buildings are also determined by building width, because wider buildings intercept more sand and create a larger vortex in front of the building.

Sand that is not deposited in front of the building is mainly blown around rather than over the building: most sand transport occurs close to the bed and follows the horseshoe vortex structure. This often creates downwind deposition near the horseshoe vortex tails. At the building sides, wind speed and sediment transport are increased due to sand and wind

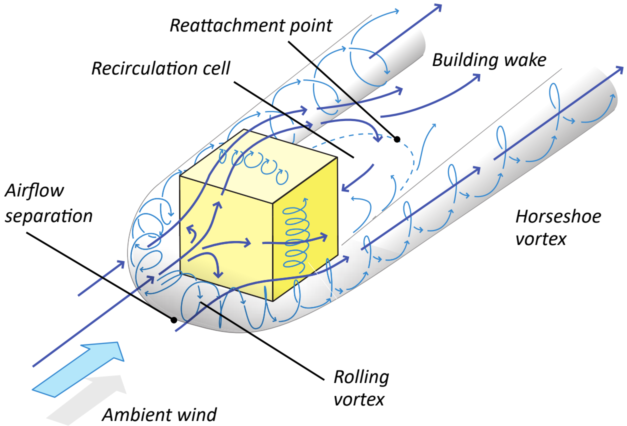

Figure 5.1: Idealized airflow patterns around a building oriented perpendicular to the wind (adapted from Oke et al., 2017).

diverted around the building. As wind speed slowly reverts to the undisturbed conditions, the sediment transport capacity decreases, explaining the downwind deposition. Apart from wind speed, the complex 3D flow field also plays a role here, with horizontal convergence promoting deposition in the horseshoe vortex tails (Pourteimouri et al., 2022). Directly adjacent to a building, the accelerated airflow can create scour. However, lateral deposition is also possible here, similar to the downwind deposition tails. Finally, in the lee behind the building, erosion can occur, due to sediment being diverted around the buildings leading to a lower sediment influx. However, the flow deceleration in this area also decreases the sediment transport capacity, so if sediment enters the area directly behind the building, this can create deposition (see Chapter 2 and Luo et al., 2012). This deposition in the lee of an object is alternatively referred to as a sand shadow (Bagnold, 1941; Luo et al., 2012); shadow dune or lee dune (Cooke et al., 1993; Hesp, 1981; Pye & Tsoar, 2008); or leeward drift (Beyers & Waechter, 2008).

When multiple buildings are placed close together, this changes the airflow pattern and thereby the morphological effect. For a row of adjacent buildings, the effect depends on the building spacing. At smaller building spacings, airflow and sediment transport through the gaps between buildings is limited, as wind and sand are predominantly diverted around the building group (Luo et al., 2014; Thiis & Jaedicke, 2000; Yen & Liu, 2011). As shown by the scale experiments of Chapter 4, this creates downwind deposition tails at the outside of the building group that are larger than the deposition tails behind the gaps. If building spacing increases, wind and sand increasingly flow through the gaps instead of around the building group. As a result, deposition outside of the building group decreases, while it increases behind the gaps. For large building spacing, airflow and sediment transport around each building are barely affected by the neighbouring building, and the morphological pattern is almost a superposition of the deposition and erosion expected around individual buildings. For buildings with an approximately square wind-facing surface, this occurs for a building spacing of more than approximately 2 buildings widths. Locally, erosion can occur in the gaps between buildings and directly behind gaps, due to the high velocity of wind funnelled through the gaps.

5.3 Methodology

5.3.1 Model description

The model used in this study is an extension of Werner (1995), where the domain consists of a cellular grid covered with stacks of slabs of a fixed thickness to represent topography. Sediment transport occurs stochastically by the movement of slabs in orthogonal directions, with periodic boundary conditions at the grid edges. Sediment transport starts by random selection of cells to be eroded, where the top slab of every cell has a probability p_e to be eroded. Eroded slabs are then moved one cell downwind, where they have a probability p_d to be deposited. If not, they are moved to the next cell and the process is repeated. When all eroded slabs are deposited, the angle of repose is enforced by avalanching: slabs are shifted in the direction of the steepest slope whenever the slope between cells is larger than 30°.

Shadow zones behind dunes are essential for dune formation in the model (Nield & Baas, 2008a). These shadow zones represent the sheltered area behind relief where flow deceleration or recirculation occurs, leading to accretion and dune growth behind a dune and thereby to dune migration. Originally, Werner (1995) implemented this as zones with a p_d value of 1 for cells behind relief that are enclosed by a line of 15° to horizontal. In nearly all following work (Baas, 2002; Eastwood et al., 2011; Galiforni Silva et al., 2018; Keijsers et al., 2016; Momiji et al., 2000; Nield & Baas, 2008a), the erosion probability was additionally set to zero, for shadow zones with immediate deposition and no erosion.

The model implementation of this study does not contain vegetation. This makes for a fairer comparison with the field experiments, which were performed on a sandy beach without vegetation. In this sense the model is more similar to the original Werner bare-sand model (Werner, 1995) than to the later DECAL (Baas, 2002) or Dubeveg (Keijsers et al., 2016) models.

Time evolution is represented through repeated iterations of erosion, deposition and avalanching. The time step and spatial scale follow from the combined parameter settings for the cell size (L), slab height (H_s), erosion and deposition probability and number of aeolian iterations per year (n), together setting the potential aeolian sediment transport rate Q (Keijsers et al., 2016; Nield & Baas, 2008a):

$$Q = H_s L \left(\frac{p_e}{p_d} \right) n \tag{5.1}$$

5.3.2 Model extension: buildings

Buildings differ in two key aspects from natural bedforms and dunes: they are static, in the sense that they have a fixed location and configuration, and they have a bluff shape. The fixed state of buildings is implemented in the model by setting bed elevation to the building height and turning off erosion, deposition and avalanching in grid cells with buildings ($p_e = 0$; $p_d = 0$; angle of repose of 90°). Deposition on top of buildings is theoretically possible, but is disregarded in the model, because sediment transport occurs predominantly close to the bed instead of at roof level (Dong et al., 2003; Rotnicka, 2013), and deposition is further impeded by accelerated airflow over buildings and, if present, gabled roofs. However, the bluff building shape requires larger changes to the model. It creates airflow separation, leading to sideward transport of sediment diverted around buildings and to bed level change upwind and next to buildings, in contrast with streamlined dunes whose morphological effects are mainly downwind.

Therefore, new rules are needed to describe sideward transport for sediment diverted around buildings (Fig. 5.2, area 2 and 3). In addition, rules are needed for the altered pickup and deposition of slabs in three regions around a building. For the deposition upwind of an obstacle (Fig. 5.2, area 1 and 2) and the scour next to obstacles (area 4), new rules are added. For the downwind effect of an obstacle, the shadow zone rules are adapted (area 5 and 6). In these three regions, p_e and p_d are altered through three spatially varying modifiers: the upwind deposition effectiveness, lateral scour effectiveness and downwind lee protection effectiveness (η_{upw}, η_{lat} and η_{downw}. η_{upw} and η_{downw} range between 0 and 1 (0% and 100%), while η_{lat} ranges between 0 and -1 (0% and -100%). Positive values increase deposition while decreasing erosion, and vice versa.

These three effectiveness values are summed to derive the cumulative effectiveness (η_{tot}, with values constrained to the range -1 to +1). η_{tot} modifies the local probabilities of erosion and deposition linearly from their base values. From $\eta_{tot} = 0$ to $\eta_{tot} = 1$, p_d increases linearly from its base value to 1 (immediate deposition) and p_e decreases from its base value to 0 (no erosion). This is identical to the rules for the combined vegetation effectiveness of multiple vegetation species in DECAL and Dubeveg (Keijsers et al., 2016; Nield & Baas, 2008a). From $\eta_{tot} = 0$ to $\eta_{tot} = -1$, the behaviour is reversed: p_d decreases linearly from its base value to 0 and p_e increases from its base value to 1.

Horizon angles

Larger buildings affect airflow and morphology in a larger area. We therefore introduce the *horizon angle* to express cell proximity to buildings, relative to the building size. The

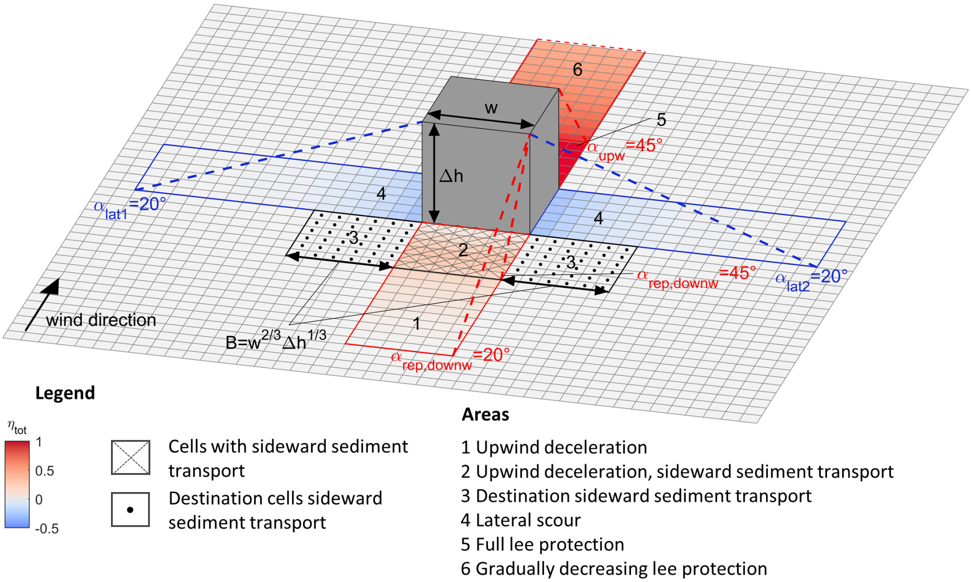

Figure 5.2: A sketch of the CA model, indicating in which areas a building affects the cumulative deposition effectiveness η_{tot}, and hence p_e and p_d.

horizon angle is the slope at which an imaginary line, starting from the current level of a cell, intersects exactly with the horizon, measured in the four cardinal directions (Fig. 5.3). In other words, it is the steepest slope at which the line still intersects with another cell. This other cell can either be a sandy cell (dune) or a building, making the horizon angle a general measure for the entire model domain: there is no distinction between sandy cells and building cells, only the elevation of a cell matters. If a cell is higher than all following cells in a direction, the horizon angle of that direction is set to zero.

The horizon angle only takes into account the height of an obstacle (i.e. dune or building). However, obstacle width also matters. Horizontal deposition size scales linearly with building factor B (Chapter 3), with $B = w^{2/3}h^{1/3}$, building width w measured perpendicular to the wind and building height h. Therefore, we additionally define a *representative downwind horizon angle* ($\alpha_{rep,\ downw}$), calculated using B instead of the height difference between cells. For the CA implementation, the downwind cell causing the horizon angle is determined first. Next, obstacle width is determined from the number of consecutive neighbouring cells perpendicular to the wind direction with at least the same elevation. For further details, see Appendix 5A on CA model rules.

The erosion and deposition probability around buildings

To model deposition upwind of a building, the representative downwind horizon angle at upwind cells affects the local erosion and deposition probabilities through the *upwind*

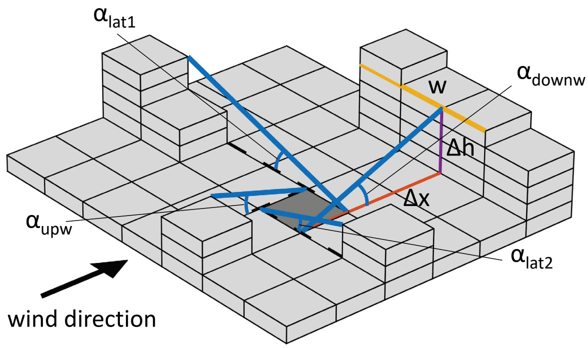

Figure 5.3: The horizon angles of a cell, determined in four directions, indicate the slope of the steepest line that still intersects with another cell. The representative downwind horizon angle ($\alpha_{rep,\ downw}$) of a cell is calculated using obstacle width w, combined with the height difference Δh and horizontal distance Δx with the cell intersected by the downwind horizon line (see also Appendix 5A.

deposition effectiveness (η_{upw}), defined by the curve shown in Fig. 5.4a. (Note: *upwind* deposition is linked to the *downwind* horizon angle: if you are located upwind of a building, you see the building by looking in the downwind direction). Next to a building, the strong airflow can scour the bed. Cells located between two obstacles can be subject to more scour than next to a single building, so in the CA model the lateral scour effectiveness α_{lat} depends on the sum of the lateral horizon angles in both directions ($\alpha_{lat} = \alpha_{lat,1} + \alpha_{lat,2}$). For $20° < \alpha_{lat} \leq 180°$, p_e and p_d depend quadratically on the horizon angle (Fig. 5.4b). In the lee behind buildings, the bed is sheltered, causing flow deceleration and recirculation and thereby deposition (Smith et al., 2017a). Previous CA models already included this effect for dunes, implemented as full deposition ($p_d = 1$) and no erosion ($p_e = 0$) in shadow zones, so in all cells with an upwind horizon angle of more than 15° (Baas, 2002). To represent buildings, which have a constant location and large elevation differences with surrounding cells, more nuance is added: a gradual *lee protection effectiveness* replaces the binary shadow zones, so that the effectiveness η_{downw} increases linearly with the horizon angle for $0° < \alpha_{upw} \leq 45°$ (Fig. 5.4c). For more details on the model rules and the reasoning behind them, see Appendix 5A.

Sideward sediment transport

Buildings do not only change the local deposition and erosion, they also divert sand around them. So the model needs to include some form of sideward sediment transport, i.e. transport perpendicular to the wind direction. Sediment is mainly blown to the side by the rolling vortex directly upwind of a building. This is represented in the model by slabs in transport just upwind of a building having a 50 percent probability of being transported to the side. This applies when $\alpha_{\mathrm{rep,downw}}$ is 45° or larger (so within a distance of one building factor B

5

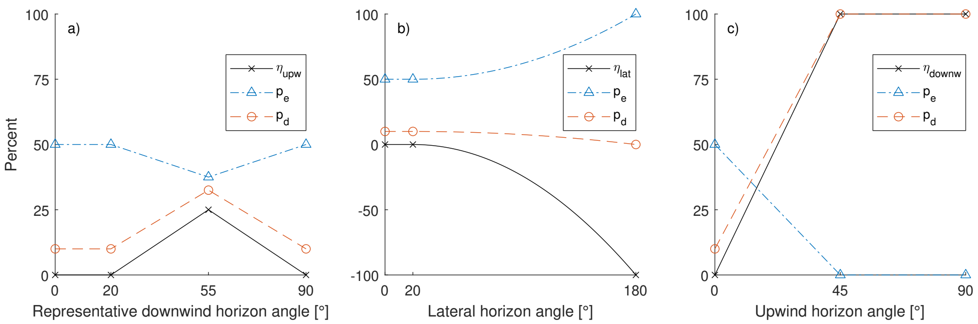

Figure 5.4: The horizon angles determine the (a) upwind deposition effectiveness (η_{upw}), (b) lateral scour effectiveness (η_{lat}) and (c) lee protection effectiveness (η_{downw}) and thereby p_e and p_d. The lines for p_e and p_d are based on base values of $p_e = 0.5$ and $p_d = 0.1$.

to the building). If moved sideward, slabs are shifted to a cell that is between 1 cell and a distance B at either side of the building. For further details, see Appendix 5A on sideward sediment transport.

Effect of CA rules on sediment flux

The model rules described above produce seemingly realistic sediment transport patterns around a building, with slabs being diverted around and deposition in front of the building (Fig. 5.5). In area 1 of Fig. 5.5, upwind deceleration causes the sediment flux to decrease. In area 2, slabs start being shifted to the side. This causes a sideward flux, stronger at the edge of the area (around x=0) than at the building's centreline. It also causes a further decrease in the y-component of the flux. Area 3 receives the slabs that were shifted to the side in area 2. This results in an increased sediment flux compared to the undisturbed upwind cells; and in a sideward sediment flux, especially in the grid columns close to the building. In area 4 lateral scour occurs, explaining why the flux is slightly larger in columns directly against the building edge than further away from the building. Although this zone theoretically extends up to a lateral horizon angle of 20°, the scour effectiveness is so weak at the edges of zone 4 that there is no noticeable effect. Area 5 is the zone behind the building where the horizon angle exceeds 45°, so the lee protection effectiveness is 100%. This means immediate deposition and no erosion, and hence no sediment flux. In area 6, the lee protection effectiveness slowly decreases, allowing for slabs to be picked up from the bed and resulting in an increasing sediment flux.

5.3.3 Model settings

All scenarios start with an initially flat bed and use an initial sand layer thickness of 1 metre (i.e. the maximum possible erosion is 1 m). The latter represents the supply limitation that was present in our field experiments due to ground water and, for the full-scale experiment,

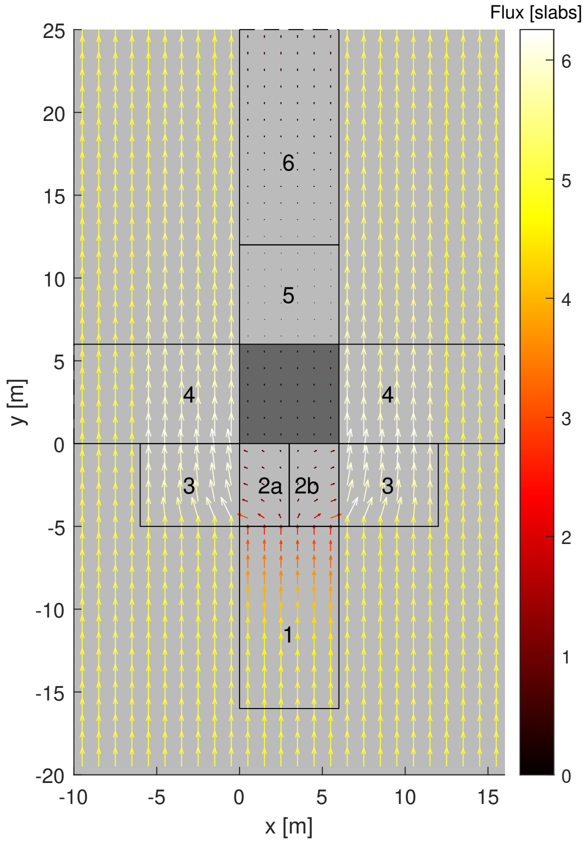

Figure 5.5: The average sediment flux pattern around a building of 6×6×6 m on a flat bed, based on 100 model repetitions of the first aeolian iteration on a flat bed. Arrow colours indicate the sediment flux magnitude, in slabs/cell/iteration. The base flux is 5 slabs/cell/iteration ($p_e/p_d = 0.5/0.1 = 5$). Dark grey cells indicate the building and numbered rectangles the location of the areas described in the text, following the same numbering as Fig. 5.2

the development of an armouring layer. Furthermore, all scenarios use base probabilities of p_e=0.5 and p_d=0.1, a year of 50 aeolian iterations, a cell size of 1×1 m, a slab thickness of 0.1 m and 30° for the angle of repose. These values are based on previous studies of Dutch dune dynamics with Dubeveg (Galiforni Silva et al., 2018, 2019; Keijsers et al., 2016) and result in a potential sediment flux of 25 m^3/m/year.

5.3.4 Model scenarios

Both short-term and long-term scenarios are examined with the model. For the short-term scenarios, the model is run for two years (100 aeolian iterations) to focus on the period in which the morphological effects from the building dominate local bedform dynamics. First the modelled morphological development under a unidirectional wind regime is compared to deposition and erosion patterns observed in field experiments with single buildings (section 5.4.1) and building groups (section 5.4.2). Next, the effect of a variable wind regime on short-term morphological development around buildings is examined (section 5.4.3). Finally, durations are extended to up to 15 years to examine interactions between natural bedform dynamics and building-induced deposition and erosion patterns (section 5.4.4).

Different building configurations and wind directions are examined in these scenarios (Table 5.1). To study the effect of building geometry, different building sizes are tested, with building widths (perpendicular to the wind) of 4, 8 and 12 m, and building lengths and heights of 4 and 8 m. To study the effect of building spacing, the set-up of the field experiment of Chapter 4 was implemented in the model. Triplets of buildings are placed in a row perpendicular to the wind and building spacing varied per triplet. Buildings are 4×8×4 m (w×l×h), which means that they have the same shape as the tested scale models (0.5×1×0.5 m), but have the size of actual beach cabins. This building size is chosen because it matches the cell size of the CA model: 1×1 m, based on the cell size for which CA model parameters have previously been calibrated (Keijsers et al., 2016; Nield & Baas, 2008a). Modelling on the scale of the field experiments would require a substantial decrease in the cell size and hence a recalibration of the model parameters. Conversely, applying the scale of real buildings only increases the expected size of the deposition and erosion patterns, but not their shape, as also shown in the 5-week field experiment of Chapter 3 in which deposition and erosion around a small scale model (0.5×2×0.5 m) and a similarly shaped building (2.5×12×2.5 m) were observed simultaneously.

For the scenario with different building spacings, six different building spacings are tested (Table 5.1). These are expressed as the gap ratio g^*: the gap width relative to the combined width of the gap and building, to indicate the porosity of the set-up (Luo et al., 2014). For the wind direction scenarios, wind direction alternates deterministically, so e.g. consistently 1 iteration from the south, then 1 iteration from the west.

For the long-term scenarios, scenarios of up to 15 years are examined, with various building

Table 5.1: Description of the model scenarios. Building width is measured in the x-direction, so perpendicular to the wind for unidirectional wind from the south.

Scenario	Duration (year)	Wind direction (%, south+west+east)	Building size (w×l×h, in m)	Group size (# of buildings)	Gap ratio g^* (-)
Short term, single building	2	100+0+0	4,8,12×4×4; 4,8,12×8×4; 4,8,12×4×8	-	-
Short term, multiple buildings	2	100+0+0	4×8×4	3	0; 0.33; 0.5; 0.67; 0.75 and 0.8
Short term, wind direction	2	100+0+0; 67+33+0; 50+50+0; 50+25+25	6×6×6; 12×6×6; 6×12×6	-	-
Long term, single building	15	100+0+0	10×12×3	-	-
Long term, wind direction	6	50+50+0	15×15×6	-	-
Long term, wind direction 2	15	50+50+0	25×25×15	-	-
Long term, building group	12	100+0+0	10×10×6	5	0.33
Long term, group + direction	12	67+33+0	10×10×6	5	0.33

5

sizes, wind directions and building group configurations. These scenarios include larger buildings, ranging up to 25×25×10 m, to include some buildings that are larger than the developing dunes.

5.4 Results

5.4.1 Single buildings

The general pattern that develops around a single building in the CA model (Fig. 5.6) qualitatively matches the results from the field experiments quite well (Fig. 5.7), with deposition upwind of the building, in tails behind the building, and often some deposition next to the buildings. This is especially visible in the right half of Fig. 5.6, where the average of 100 model repetitions is shown to focus on consistent building-induced effects and filter out spatial and temporal variations caused by natural bedform migration in the area. Upwind of the buildings, a deposition area develops. This deposition shows a steep slope toward the foot of the building, fitting field observations. The area directly against the upwind building edge initially erodes: the sediment influx into this area is lower due to upwind deposition and to slabs being diverted around the building. As upwind deposition becomes higher over time, slabs avalanche towards the building, filling up the initial erosion. For the 4 m wide buildings in Fig. 5.6, this results in deposition against the upwind building edge after two years, while wider buildings still show erosion at the building edge.

Adjacent to the buildings (i.e. left and right of the buildings in Fig. 5.6), scour occurs, often causing erosion directly against the building walls. However, the area adjacent to the buildings also receives extra sand due to slabs being diverted around a building, which can also lead to extra deposition, especially in the grid cells slightly further from the building. Further downwind, beyond the building, the extra influx of sand remains while the scour stops, leading to the formation of deposition tails. The combination of scour and deposition beside a building, followed by deposition downwind of the building, matches the patterns that formed in the field experiments (Fig. 5.7). In the lee behind the buildings, the very first cells usually display some accretion: the strong lee protection causes deposition of the few slabs transported over the building, while it prevents erosion. Further downwind, the low influx of sediment remains, while the lee protection slowly decreases, leading to more slabs being picked up from the bed, and hence erosion. For the field experiment with the small scale models, this was usually not visible, but for the larger scale model placed at the beach for 5 weeks (Fig. 5.7a), some downwind erosion occurred.

In the field experiments of Chapter 3, the length and width of the upwind deposition and the downwind depositions tails were observed to scale with building factor B. Upwind deposition in the field experiments had a width of approximately 2.8B, so clearly wider than the buildings. In comparison, in the CA model upwind deposition forms straight upwind of

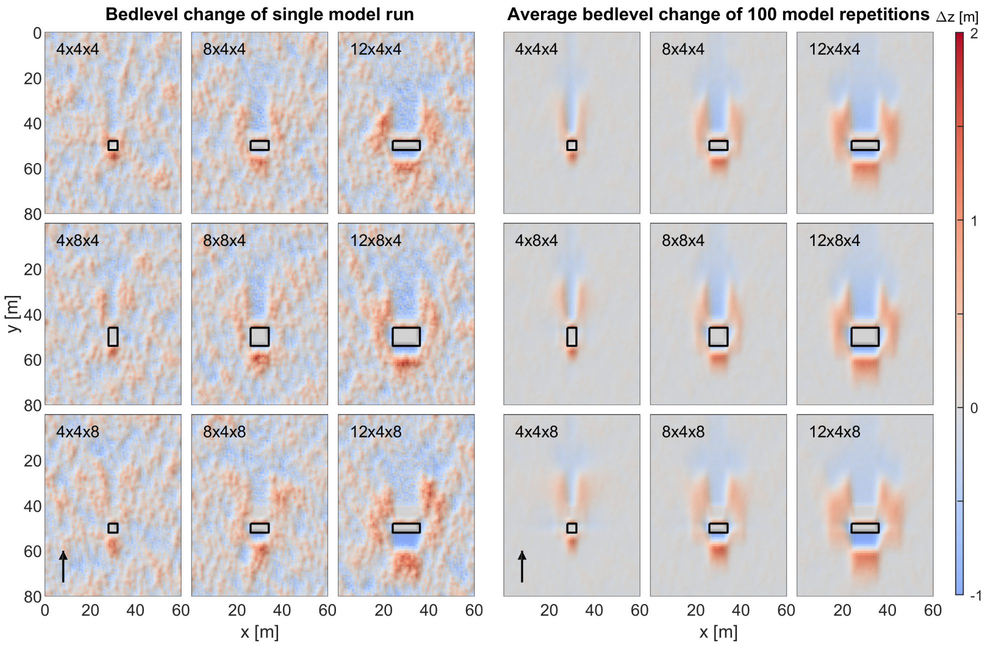

Figure 5.6: The topography around single buildings of various sizes after 2 years. Wind is coming from below, building sizes are indicated as $w \times l \times h$ in metres. The first three columns display the result of a single model repetition, showing both natural bedform dynamics and building-induced effects. The last three columns show the average of 100 model repetitions, to filter out natural bedforms and show consistent building-induced effects.

the building, as it depends on the horizon angle toward the building, and then extends a few cells to the side due to avalanching. Modelled upwind deposition length is similar to that in the experiments (2.3B), as the horizon angle at which upwind deceleration starts to occur was directly chosen based on the experiment.

The lateral and downwind deposition areas in the CA model form as a result of sediment slabs being diverted around the building. This sediment is spread to between 1 cell and a distance B besides the building. Hence, the width of the modelled lateral and downwind deposition increases with B, fitting with experimental observations. However, the quantitative effect of B on downwind deposition width differs: the width of the modelled deposition tails becomes somewhat larger than B due to avalanching spreading out the sediment, but remains well below widths of 2.5B as reached at the widest point in the field experiments. The length of the modelled tails is mostly building-independent: about 20 m, so between 2B (for the 12×4×8 m building) and 5B (the 4×4×4 m building). The field experiment showed tail length to scale with B and reach lengths of over 4B. This means that modelled lengths compare well to the experimental results for smaller buildings, but are clearly shorter for the larger buildings.

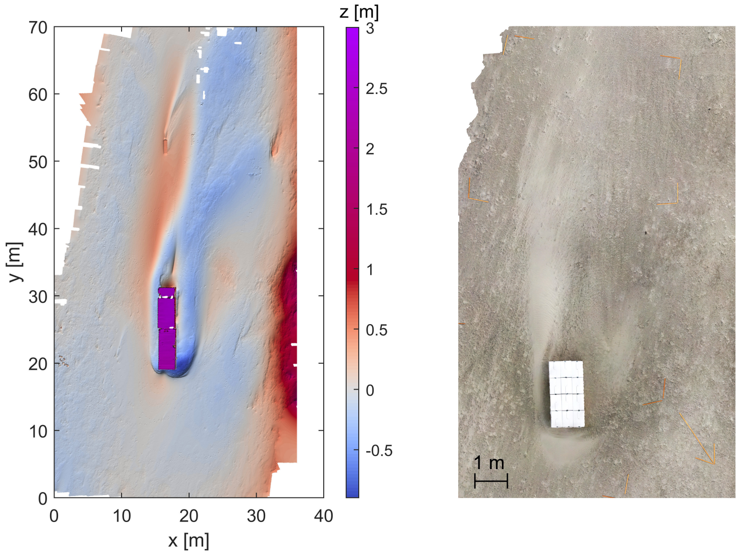

Figure 5.7: Examples of results around scale models in the field, with the dominant wind direction from below. Left: A DEM around a scale model of 2.5×12×2.5 m after 5 weeks in the field. High elevations at the righthand edge of the graph are the dune toe. Deposition is further affected by a small scale model at x;y=17;52. For details, see Chapter 3. Right: An orthophoto of the deposition around a scale model of 1×2×0.35 m, with lighter colours indicating deposition. Result after 1 day.

5

5.4.2 Multiple buildings

The general bed level dynamics around building groups are captured quite well by the model. The smallest building spacing yields deposition behind the gaps, which we refer to as inner tails, that is smaller than the deposition at the outside of the building group, referred to as outer tails (Fig. 5.8). As the building spacing increases, sediment transport through the gaps increases, resulting in larger inner tails and smaller outer tails. The inner tails first become both higher and wider, because both buildings next to a gap create deposition in exactly the same area. As the gap width increases further, the tails of both buildings form right next to each other, together resulting in a very wide inner tail. This agrees with the developments observed in the field experiment (Fig. 5.9).

A more detailed comparison of the size of the inner and outer tail at all gap widths, performed in Table 5.2, shows some differences. Modelled inner and outer tails always have the same length: approximately 20 metres, as for the individual buildings modelled before, whereas deposition length clearly showed variation in the field experiments. The underestimation of the deposition tail length results in very wide and short inner tails at the largest gap widths, whereas the field experiment showed tails that were longer than they were wide. In addition, some transitions between deposition topologies occur at a smaller gap ratio (g^*) in the CA model than in the field experiment. This is the case for the gap ratio at which

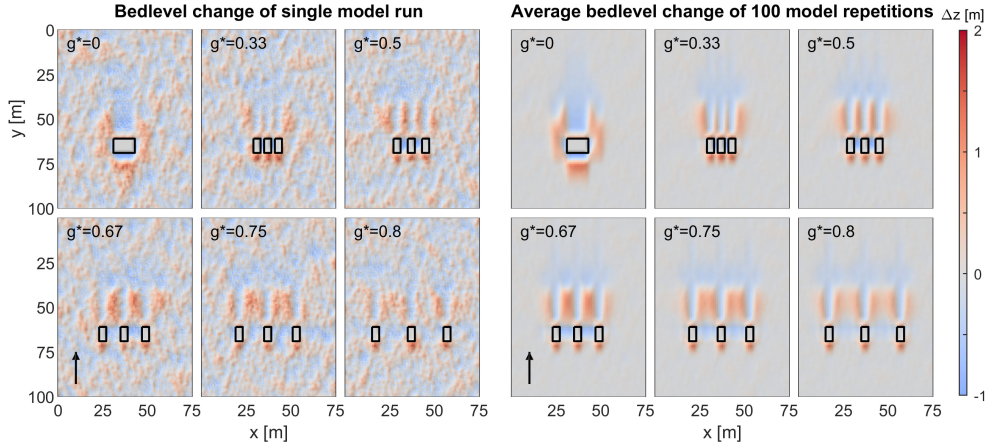

Figure 5.8: Modelled deposition and erosion patterns around groups of scale models, with individual scale models 4×8×4 m ($w \times l \times h$). Building spacing is indicated by the gap ratio g^*.

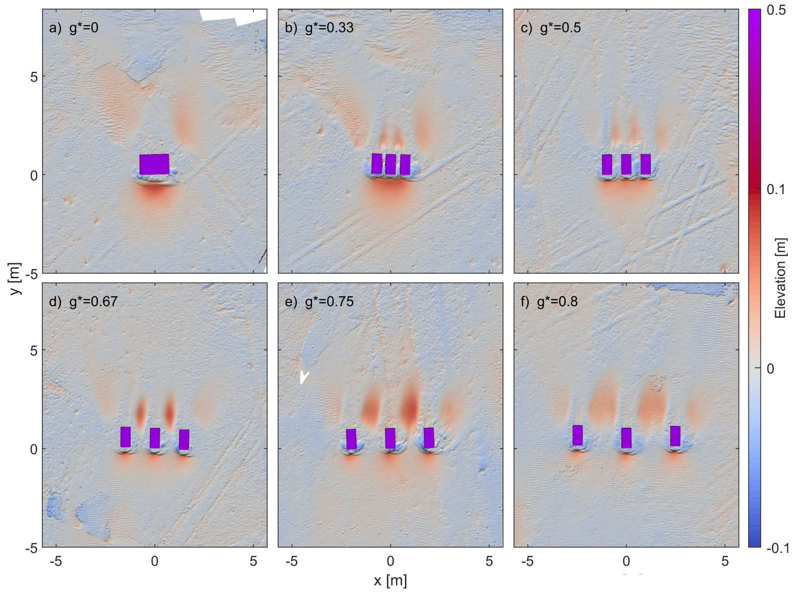

Figure 5.9: Elevation maps of the scale model experiments of Chapter 4. Elevation is relative to a fitted linear surface, to highlight local differences caused by erosion and deposition.

Table 5.2: Comparison of the effect of gap width on the downwind deposition pattern around rows of buildings in the field experiment (Chapter 4) and in the CA model

Gap ratio	Field experiment	CA model
0.33	Inner tail is shorter and narrower than outer tail, but slightly higher.	Inner tail is narrower and lower than outer tail.
0.5	Inner tail is somewhat shorter and narrower than outer tail, but higher.	Inner tail is somewhat narrower than outer tail, but higher.
0.67	Inner tail is shorter and narrower than outer tail, but clearly higher.	Inner tail is clearly wider than outer tail, slightly higher.
0.75	Inner tail is slightly wider than outer tail and clearly higher.	Inner tail is clearly wider than outer tail, slightly higher.
0.8	Inner tail is wider and higher than outer tail. Compared to $g^* = 0.75$, inner tail is wider and lower.	Inner tails start to separate. Individual inner tails equal to outer tails.

the inner tail becomes wider than the outer tail ($g^* = 0.75$ vs 0.5) and for the gap ratio at which the inner tail can be recognized as consisting of two adjacent tails from two buildings ($g^* = 0.75$ vs 0.8).

5.4.3 Wind direction

Next, we use the CA model to examine the effects of multi-directional wind regimes. Again initial bed level change is examined, so after a period of 2 years (Fig. 5.10). For a unidirectional wind from the south, the resulting deposition patterns are symmetrical, with two deposition tails of equal length. If the wind regime changes to bidirectional, from the south and west, the sediment dynamics and deposition pattern change. At the southern wall, transport to the north (during southern wind) is impeded by upwind deceleration, while transport to the east (during western wind) is increased by lateral scour. Conversely, at the eastern wall, transport to the north is increased by scour, while transport to the east is limited by the lee protection. The same processes occur at the western and northern wall. As a result sand is redirected around the building to the north-east corner.

For a square building and wind regime that is 50% south, 50% west, this leads to a diagonally oriented deposition tail at the northeast corner and symmetrical pattern around the southwest-northeast axis (Fig. 5.10p). Upwind deposition, which occurs at the southern and western wall, is blown to the eastern respectively northern end of these walls, limiting deposition at the south-west upwind corner. Instead deposition collects at the south-east and north-west corner, where it forms lee protection zones to the east (during western wind)

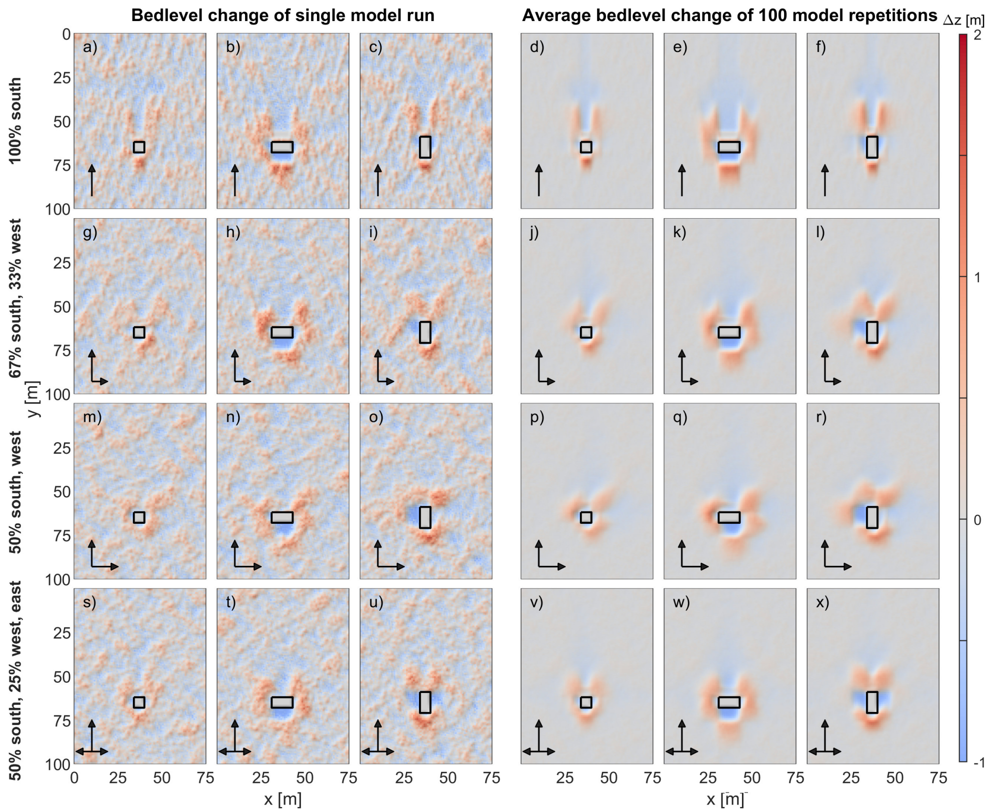

Figure 5.10: Effect of different wind regimes on the topography around buildings of 6×6×6, 12×6×6 and 6×12×6 m. Y-axis labels indicate the wind regime for each row.

and to the north (during southern wind), making the areas grow in the northeast direction.

If the building is rectangular instead of cubic, the larger building factor B in one direction causes upwind deposition in that direction to occur further from the building. This happens for instance at the southern wall in Fig. 5.10, subplot q. In addition, we see here that the deposition areas at the northeast and northwest corner are more clearly separated due to the larger distance between these corners. If the wind regime is 67% south, 33% west (subplot j), the resulting topography lies between the results for a 50%-south-50%-north regime and a unidirectional wind regime: two deposition tails develop, with the largest deposition tail at the northeast downwind corner, oriented to the north-northeast.

For a wind regime with 50% southern, 25% western and 25% eastern wind, the morphology develops similarly to that of a fully southern wind. However, the eastern and western wind spread out sediment to the east and west, while the sediment transport rate to the north is lower. This results in a pattern that is smeared out east-west, with especially the deposition tails becoming shorter but wider.

5.4.4 Long-term interactions

To explore the interactions between buildings and natural bedform dynamics, dynamics over a longer period and with a larger building are examined. Fig. 5.11 shows how the morphological development around a building is affected by bedform dynamics in the surrounding area, with wind unidirectional from the south. After 9 years, a dune is present directly upwind of the building. This decreases the horizon angle towards the building, which in turn decreases sideward slab transport around the building and increases transport over the building. As a result, strong deposition occurs in the lee protection zone behind the building, which reaches the same height as the building and clearly surpasses the height of bedforms unaffected by the building. After 13 years, the dune in front of the building disappears. This decreases sediment transport over the building, which causes the deposition area in the lee to become smaller.

Natural bedform dynamics are also affected by buildings. Fig. 5.12 shows a building shaping the location and direction of bedform growth. It presents the annual slab transport around a building as well as the bedform development for a bidirectional wind regime, with wind direction alternating equally between south and west. The transport pattern shows the redirection of sediment around a building, as explained before (section 5.4.3). The 1.5m elevation contour shows that bedform migration and evolution follow this pattern. For instance, the deposition initially present at the south-eastern corner shows diagonal development south of the building, but east of the building it deviates from the average wind direction and grows to the north.

5

Looking at even larger buildings and time spans of up to 15 years, dune migration Is affected in an even wider area of influence. In Fig. 5.13, the migration of four dune crests is indicated, for the same bidirectional wind regime as Fig. 5.12. The building here is 25×25×15 m, such that the building is wider than the dunes and can affect (the horizon angles of) all dune cells simultaneously. The dune crests initially form a straight line, and without a building these sand dunes would all migrate in the average wind direction, so diagonally to the north-east.

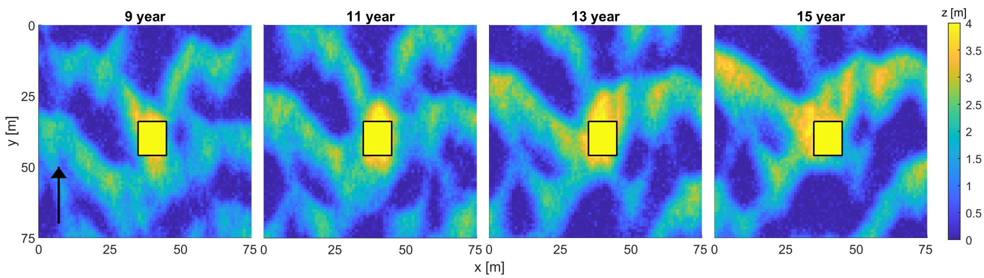

Figure 5.11: Snapshots of the morphology around a building, sized 10×12×3 m, showing how a migrating bedform that arrives in front of a building (after 9 years) and migrates past the building affects deposition in the building lee. Wind is coming from below.

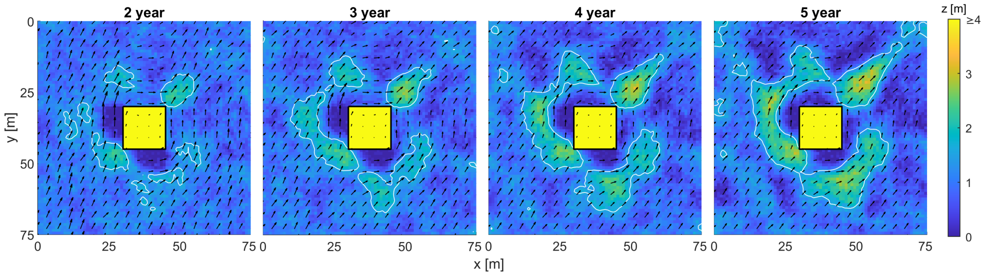

Figure 5.12: Snapshots of the morphology around a building, sized 15×15×6 m and the annual sediment transport pattern. White lines indicate the 1.5m contour line. Black arrows indicate the flow pattern of sand slabs, averaged over 1 year. The wind regime is 50% south, 50% west.

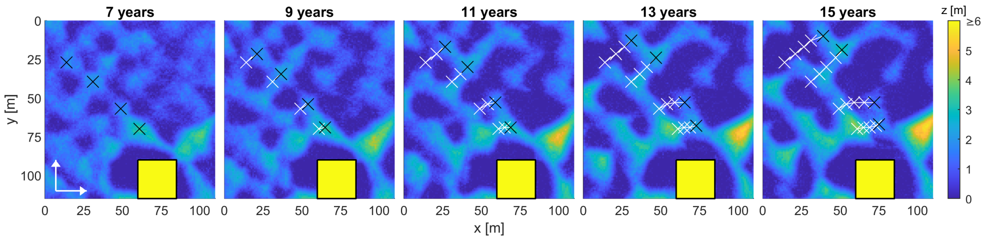

Figure 5.13: Snapshots of the morphology around a building, sized 25×25×15 m. The location of the crest of four dunes is indicated to emphasize the migration direction in the lee protection zone downwind of a building. Black crosses indicate the dune location in the current snapshot, white crosses the location of the previous snapshots. The wind regime is 50% south, 50% west.

The dunes furthest from the building indeed migrate north-east, but the dunes closer to the building migrate to the east, because their northward migration is decelerated by the lee protection behind the building, while the eastward migration is accelerated by lateral scour. 5

Finally, we examine how a group of buildings affects bedform development over a larger area (Fig. 5.14). For a unidirectional wind from the south, transverse dunes develop in the area without buildings, at the right side of the domain. The building group at the left locally causes increased deposition, which decreases the sediment transport to the area downwind of the buildings. As a result of the lower sediment supply, barchan dunes instead of transverse dunes develop in this area. For a bidirectional wind regime (67% south, 33% west), the area without buildings develops a dune topology resembling star dunes, i.e. a grid of dunes oriented perpendicular and parallel to the mean wind direction. Behind the buildings, the deposition tails grow to the north, in a manner similar to linear dunes and reaching lengths of 50 m.

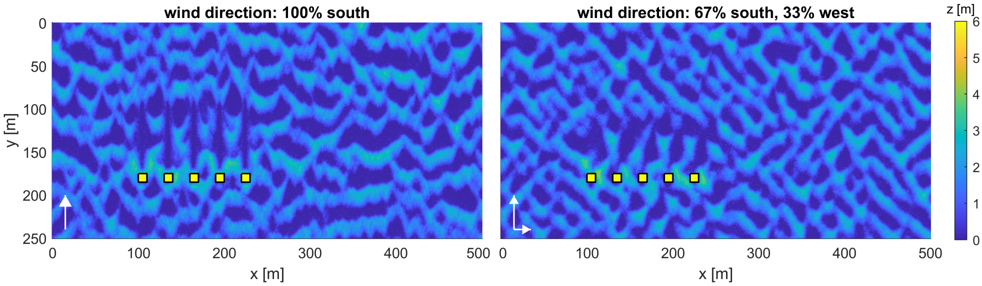

Figure 5.14: The morphological development after 12 years, around a row of 5 buildings of 10×10×6 m with gaps of 20 m between buildings and for two different wind regimes.

5.5 Discussion

The new CA rules for sediment dynamics around buildings replicate observed deposition and erosion patterns around buildings qualitatively well. They result in a realistic flux pattern around obstacles (Fig. 5.5). Moreover, the modelled shape of the morphological patterns around single buildings and building groups is comparable to that observed in field experiments. Quantitative comparison between CA model results and field experiments shows that modelled deposition around buildings is often smaller than observed deposition in field experiments. This is particularly notable for the upwind deposition width. In addition, the downwind deposition length is almost independent of building size in the CA model, whereas it increased with building width and height in the field.

5

These discrepancies partly follow from differences between field conditions and the cellular automaton environment. In the field, the wind direction fluctuates, whereas the CA model has a constant wind direction (or orthogonal variations). Slightly oblique winds that occur in the field can disperse sediment, causing deposition and erosion patterns to become wider. This also matches the CA simulation with 50% western wind and 25% northern and southern wind, which shows deposition tails that are slightly wider than for unidirectional wind. In addition, field experiments and the CA model differ in building size. The CA simulations replicate real building sizes rather than the smaller scale models because of the cell size at which DECAL was calibrated (Nield & Baas, 2008a). The duration of the CA simulations was also longer. First, the longer duration follows from deposition taking more time to develop for large buildings than for small scale models. Second, the field experiments were by design performed on days with abundant sediment transport, whereas DECAL and all derivative CA models employ a constant sediment flux and weekly to monthly timesteps (Baas, 2002; Keijsers et al., 2016) to model average long-term evolution.

Discrepancies partly result from the new model rules simplifying the complex processes around a building. They capture the general morphological dynamics around buildings well, including the shape of the deposition and erosion patterns, interactions between multiple buildings and feedback effects over time with natural dune dynamics. These rules are based on the horizon angle in the four cardinal directions. So cells that are not horizontally or vertically in line with a building are not directly affected, apart from some grid cells receiving sideward sediment transport. Hence the probability of deposition and erosion at the deposition tails, obliquely downwind of a building, are *not* changed by the building. Instead, deposition tails form due to a surplus of sediment transport, persisting from the obliquely upwind cells having received sideward sediment transport. The distance over which this surplus decays, and hence the initial deposition tail length, depends on the deposition probability p_d. In reality, this deposition is also aided by horizontal flow convergence in the horseshoe vortex tails (Pourteimouri et al., 2022).

The choice for idealized horizon-angle-based rules, without including all details of building effects, is linked to the nature of the CA model. The model rules do not specifically enforce effects around buildings. Instead, universally applicable rules evaluate the horizon angle throughout the entire domain in order to change the local sediment transport. This leads to *self-organizing* behaviour, where the morphological impact of a building emerges as the combined effect of all model rules. However, for a more precise quantitative replication of the morphological effects of specific buildings, locally *forced* building effects might need to be explicitly defined in addition to the general domain-wide rules currently used.

This means that the general horizon-angle-based rules fit the objective of this study, to explore possible interactions between building-induced morphological patterns and self-organized aeolian bedform dynamics. The success in simulating general morphological dynamics around buildings makes the model suitable to obtain insights on mechanisms of how building effects and natural dune dynamics interact. For example, the model helps to understand how sediment collecting around buildings affects downwind sediment transport and dune topology. When desired, such simulations can even be performed in a scenario study or sensitivity analysis, thanks to the relatively low computational cost (e.g. a 12-year simulation like in Fig. 5.14 takes 5 minutes[1]).

The general horizon-based rules might also be applicable to other processes and environments. The flow recirculation and deceleration that occur in front of buildings can also be found in natural environments that have steep slopes. They occur at cliffs that border beaches (Tsoar & Blumberg, 1991), steep dune scarps created by storms (George et al., 2021; Nishi et al., 1995), or foredunes with steep slopes that hamper landward sediment transport (Christiansen & Davidson-Arnott, 2003). In addition, horizon angles could offer an elegant mechanism to change the modelled steepness of the stoss slope of dunes, which tends to be quite high in the Werner and DECAL algorithm (Momiji et al., 2000). Moreover, the examined building-bedform interaction shows strong parallels to the interaction of marine sand waves with fixed structures such as pipelines (Morelissen et al., 2003), so there are

[1] With a grid size of 650×400 cells and 50 aeolian iterations per year, run on an Intel i7-8750H hexacore CPU.

5

opportunities to apply these rules in subaqueous environments.

There are some limitations stemming from the chosen model rules. The rules assume a steep upwind slope creates sediment transport *around* an obstacle. This is only true for obstacles of limited width. For relatively wider buildings, airflow increasingly flows *over* instead of *around* the building, until, at an aspect ratio (w/h) of about 10, the flow fundamentally changes, with additional vortices over the building breaking up the simple horseshoe vortex structure (Martinuzzi & Tropea, 1993). Hence the model should not be applied to very wide buildings. In addition, the current algorithm for determining the obstacle width looks for the number of consecutive neighbouring cells, perpendicular to the wind direction, with at least the same elevation. This works well for wind perpendicular to the building. However, for oblique wind directions this algorithm would have to be adapted.

Oblique wind directions were examined in the model with wind alternatingly coming from the south and the west, so on average diagonal to the building. However, this is not the same as an oblique wind direction in the field. In the CA model, this alternating wind results in a single deposition tail behind the downwind building corner (Fig. 5.10). In the field experiments of Chapter 4, wind consistently blowing obliquely to a building created the usual horseshoe deposition with two tails, instead of forming a singe deposition tail behind the downwind corner. This also shows that the net sediment transport direction and average wind direction do not necessarily coincide. If buildings or dunes are present, they can shelter the bed during specific wind directions, such that wind is decelerated, while wind is unaffected or even accelerated during other wind directions. As a result, the net sediment transport direction around obstacles, being manmade buildings or natural bedforms such as dunes, can differ from the average or dominant wind direction.

5.6 Conclusion

In this study, we examined how building-induced deposition and erosion patterns interact with self-organized aeolian bedform dynamics. Novel cellular automaton rules were developed to characterize sediment transport around bluff obstacles such as buildings. The rules use the horizon angle in the four cardinal directions to describe the acceleration and deceleration of sediment around obstacles, as well as sideward transport around obstacles. These general rules, which are applied throughout the entire model domain to both sandy cells and buildings, result in self-organizing behaviour that creates natural dune formation, but also patterns of deposition and erosion around bluff objects such as buildings. Combined, the rules give rise to a realistic sediment flux pattern around buildings. Comparison of model results to field experiments show that the modelled morphological development around buildings is realistic in terms of the shape of deposition and erosion patterns, as well as the interactions that occur around rows of buildings. However, some quantitative differences exist between the field experiments and model results. Especially downwind deposition tails are shorter in the CA results than in the field experiment, and do not show the desired dependency on building dimensions.

With this model, the effect of buildings on their environment and interactions with natural bedform dynamics can be studied. This is especially relevant for coastal settings where dunes need to have a certain height or volume for protection against flooding. In addition, there are broader applications to the new rules, as sediment dynamics in front of steep slopes are also important for natural cliffs or dune scarps forming due to storm erosion.

The simulations performed in this study showed interactions between local building-induced effects and natural aeolian bedform dynamics. The local morphological pattern around buildings responds to the bedform dynamics in their surroundings, with modelled deposition in the lee behind buildings increasing when a migrating sand dune is temporarily located in front of a building. Conversely, buildings also affect bedform dynamics in their surroundings. By diverting sediment around a building, the lee behind buildings receives less sediment, while sediment transport next to a building increases. For multi-directional wind regimes, sediment is redirected around a building. By providing shelter against the wind in a specific direction, buildings can steer sediment transport in their surroundings, and thereby steer the location and direction of dune growth. Larger buildings can hereby also change the dune migration trajectory. In essence, this means the local *net* sediment transport direction around buildings can diverge from the *average* wind direction.

5.7 Acknowledgements

This research forms part of the ShoreScape project. It is funded by the Netherlands Organization for Scientific Research (NWO), contract number ALWTW.2016.036, co-funded by Hoogheemraadschap Hollands Noorderkwartier and Rijkswaterstaat, and in kind supported by Deltares, Witteveen&Bos, and H+N+S.

Appendix 5A Detailed description CA rules for buildings

5.7.1 The representative downwind horizon angle

The CA model uses the *representative* downwind horizon angle to include the effect of both obstacle width and height. For the CA implementation, the model first determines for every cell which downwind cell causes the horizon angle, i.e. which cell touches the imaginary horizon line. The obstacle height is equal to the height difference Δh between both cells, while obstacle width w is determined from the number of consecutive neighbouring cells perpendicular to the wind direction that have at least the same elevation as the horizon-causing cell (Fig. 5.3). This gives building factor B and distance Δx between both cells, which allows for calculating the representative downwind horizon angle $\alpha_{rep,\ downw}$ (Eq. 5.2-5.5).

In the calculation, the aspect ratio (w/h-ratio) of the buildings is limited to range between 0.2 and 4, because for very tall or very wide buildings, the smaller building dimension becomes increasingly dominant for the size of airflow patterns (Martinuzzi & Tropea, 1993) and the resulting morphological patterns (see section 3.5.2).

$$w = \min(w, 4h) \tag{5.2}$$

$$\Delta h = \min(h, w/0.2) \tag{5.3}$$

$$B = \begin{cases} w^{2/3} \cdot \Delta h^{1/3}, & \Delta h \geq 0 \\ 0, & \Delta h < 0 \end{cases} \tag{5.4}$$

$$\alpha_{rep,\, downw} = \tan^{-1}\left(\frac{B}{x}\right) \tag{5.5}$$

5.7.2 Upwind deposition

The representative horizon angle ($\alpha_{rep,\, downw}$) affects the erosion and deposition probabilities through the *upwind deposition effectiveness* (η_{upw}), following the curve shown in Fig. 5.4a. Deposition, and hence η_{upw}, start to increase at a representative horizon angle of about 20°, based on upwind deposition in field experiments starting at a distance of approximately 2.3B from the building (Chpater 3). This also fits with observations of sediment transport being able to traverse mildly sloping dune fronts, while forming dune ramps (i.e. upwind deposition) at dunes steeper than approximately 20° (Christiansen & Davidson-Arnott, 2003) and with the limited sediment transport over such steep foredunes observed by Arens et al. (1995) and Bauer et al. (2012). Maximum upwind deposition effectiveness occurs at 55°, based on the observation in Chapter 3 that the crest of the upwind deposition occurs at a distance of 0.78B from buildings (using $\tan^{-1}\frac{1}{0.78}$). The maximum deposition effectiveness is set to 25% to allow for sediment transport past a building, as deposition and sediment transport behind buildings show that transport over a building is not zero. Directly in front of a building, there is little deposition or even erosion as the strong airflow blows most sand around a building, so the deposition effectiveness returns to zero at a horizon angle of at 90°.

5.7.3 Lateral scour

Airflow is only accelerated in the proximity of buildings, so a minimum lateral horizon angle is required before scour occurs. The same value is used as for the upwind deposition: 20°. At $\alpha_{lat} = 180°$, $\eta_{lat} = -1$, so peak scour effectiveness is reached at the maximum possible horizon angle, which approaches 180° for a cell in between two very tall buildings. For $20° < \alpha_{lat} \leq 180°$, p_e and p_d depend quadratically on the horizon angle (Fig. 5.4b).

5

The quadratic interpolation is applied because airflow returns faster to the undisturbed conditions perpendicular to the wind direction than in the wind direction, and hence scour is concentrated closer to a building than upwind or downwind deposition.

5.7.4 Lee protection zone

Previous CA models implemented the effect of obstacles sheltering the bed in their lee as shadow zones, so zones with full deposition ($p_d = 1$) and no erosion ($p_e = 0$) in all cells with an upwind horizon angle of more than 15° (Baas, 2002; Keijsers, 2015). This means that for a cell size of 1 m, a shadow zone forms as soon as a cell is 30 cm lower than the previous cell. In more physical terms, a bedform of 30 cm high would catch all aeolian sediment transport over it, so streamers cannot pass it (within a single aeolian iteration). In practice, such small bedforms would only catch a part of the sediment transport over a cell. For a larger dune most sediment would indeed deposit in its lee, but this sediment would still not all deposit in the very first cell behind a dune. In case of natural dune systems, these inaccuracies of binary shadow zones are mitigated by bedforms migrating constantly, spreading out deposition on the long term, even if it is too concentrated in a single iteration. However, buildings have a fixed position and a substantial height difference with their surroundings, making it more important to implement a more realistic and gradual sheltering mechanism. Therefore, a gradual *lee protection effectiveness* replaces the old binary shadow zones, with zero effectiveness if the upwind horizon angle is 0°, 100% at 45° or more and linearly interpolated effectiveness in between (Fig. 5.4c).

The full lee protection effectiveness for horizon angles larger than 45° denotes the recirculation zone, in which the wind direction is reversed, causing full deposition of incoming slabs at the start of the recirculation zone. The 45° value is chosen because the length of the recirculation zone is approximately equal to the obstacle height, for obstacles that are similar in height and width (Wilson, 1979). The lee protection effectiveness is affected up to horizon angles of 0° due to the persistence of the velocity deficit in the wake of obstacles. After the reattachment point the local wind *direction* matches the undisturbed wind direction again, but the wind *velocity* remains lower. This velocity deficit can persist very far behind obstacles, and has been observed 30 obstacle heights behind a building (Peterka et al., 1985), which is equivalent to an upwind horizon angle of about 2°. In the CA model, the lee protection effectiveness nevertheless applies to upwind horizon angles ranging between 0° and 45°, where effectively the 0 degree angle will not occur because there will always will be some self-organized bedforms developing.

5.7.5 Sideward sediment transport

Directly upwind of a building, a rolling vortex blows sand against the general wind direction, creating the (crest of the) upwind deposition area, while simultaneously transporting sand to

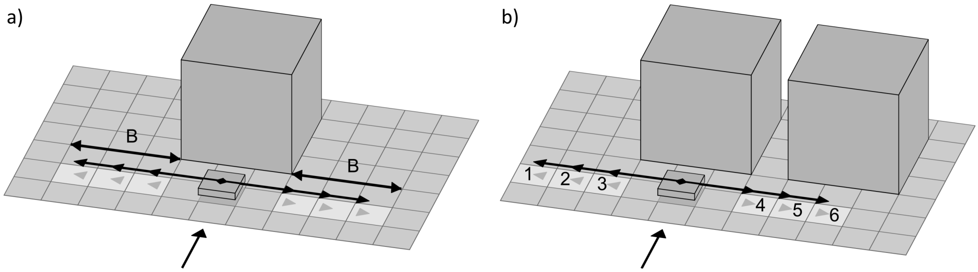

Figure 5.15: A slab in transport upwind of a building. If this slab is moved sideward, it is shifted to a random cell in of the destination area, i.e. the lighter coloured cells of the same grid row (the same distance upwind of the building), at between 1 cell and a distance B to the side of the building. Cell numbers are referred to in the text.

the side, around the building. In the field experiments of Chapter 3, the crest of the upwind deposition occurred at a distance of approximately 0.78B from the building, fitting quite well with the aerodynamic upwind separation distance of $0.7\sqrt{wh}$ as reported by Beranek (1984). Because experiments (Beranek, 1984; Martinuzzi & Tropea, 1993) and numerical modelling (Gao & Chow, 2005; Thiis & Jaedicke, 2000) show that streamlines already start to deflect to the side before the upwind separation point is reached, a slightly larger distance of 1B is employed as the starting distance for sideward sediment transport. This results in a minimum required representative horizon angle ($\alpha_{rep,\, downw}$) of $45°$. In cells where $\alpha_{rep,\, downw} > 45°$, the probability of sideward transport is set to 50%, to keep a portion of the sediment flux available for further downwind transport, thereby allowing for some deposition closer to the building, and a small sediment flux over the building.

To determine *to which cell* sidewards transported slabs are shifted, scaling length B is used once more. The vortex in front of the building, with a diameter proportional to B, is wrapped around the building. So it transports sediment to at most a distance B next to the building. Therefore, a sidewards shifted slab is shifted to a cell that is between 1 cell and a distance B (rounded to an integer number of cells) at either side of a building (Fig. 5.15a). The actual cell where a slab is transported to is selected randomly from this destination area.

The mechanism of randomly selecting one of the cells from the destination area is designed to also model situations with multiple buildings. For a single building oriented perpendicular to the wind, this mechanism results in an (on average) even distribution of sediment between both building sides. For a row of adjacent buildings with a building spacing smaller than B, this changes. Let us assume a slab in transport upwind of a building group as sketched in Fig. 5.15b. If the slab is shifted sideward to a grid column in front of the gap or outside of the building group (cell 1, 2 3 or 4 in Fig. 5.15b), the slab will remain in this column. However, if the slab is placed upwind of a neighbouring building (cell 5 or 6), it can be subject to sideward transport again in the next row. This effectively entails a repeated possibility for sideward slab transport to the outside of a building group, resulting in increased sediment transport around a building group and decreased sediment transport trough the gaps. This fits the results of wind tunnel experiments (Luo et al., 2014) and field experiments (Chapter 4) with a row of buildings, in which a small building spacing resulted in smaller deposition areas behind the gaps than at the outside of a group.

6

Discussion

6

Discussion

Figure previous page: Sand transport around a beach restaurant at Noordwijk, The Netherlands.

THE AIM OF THIS THESIS is to determine and understand quantitatively how buildings at a sandy beach affect the wind-driven morphological development of the beach environment. In Chapter 2 to 4, scale model experiments at the beach were used to examine morphological changes around buildings at the beach on the time scale of a single wind event up to several weeks. In Chapter 5, the insights and results from the experiments were used to model long-term (annual to decadal) interactions between these local building-induced effects and natural aeolian beach dynamics. The current chapter first discusses the results and conclusions from the field experiments, relates these to the airflow around buildings and compares them to existing literature. Next, it considers the nature and applications of the CA model, followed by the implications of all results for the beach-dune system and for coastal management.

6.1 Morphological patterns around buildings on a sandy beach

Field experiments with scale models of buildings at the beach were used to determine the patterns of aeolian erosion and deposition around buildings. In particular, the experiments aimed to quantitatively link the size and shape of the initial morphological patterns to the building characteristics. To focus on the initial patterns that arise locally on the timescale of a single wind event, most experiments were conducted with scale models placed at the beach for a day. These experiments examined how these deposition and erosion patterns are affected by building size and shape, by the spacing of buildings, and by the building orientation to the wind. In addition, a longer-term experiment was conducted, with a small scale model and a full-scale model of similar shapes, placed at the beach for 5 weeks, with two goals: to examine the cumulative effect of several wind events over a longer period and to investigate the relative effects of building size.

To understand the formation of the deposition and erosion patterns observed in the field experiments, these can be linked to the known airflow patterns observed around cubes or buildings as described in literature. Airflow towards the building face is diverted downwards and reverses near the bed. This creates a rolling vortex in front of the building, which is then wrapped around the building, resulting in the horseshoe vortex structure (Hunt, 1971; Peterka et al., 1985). Flow deceleration and flow reversal upwind of the building create the upwind deposition observed in the experiments, similar to the echo dunes that occur in front of natural cliffs (Qian et al., 2011; Tsoar & Blumberg, 1991; Tsoar, 1983). Higher wind velocity at the surface around a building (Depardon et al., 2005; Pourteimouri et al., 2022) can create scour at the upwind building face and at the sides of the building. This scour is exacerbated by airflow having been diverted downward at the upwind building face (see the rolling vortex in Fig. 5.1): this means that airflow at the bed level partly originates from higher elevations and hence has a relatively low sediment concentration compared to its velocity.

6

Simultaneously, deposition can also occur at the building sides, usually at the outside of zone where the scour can occur. Airflow and sediment transport upwind of a building already start to diverge sideward before the rolling vortex at the upwind building face is reached (Beranek, 1984; Gao & Chow, 2005; Martinuzzi & Tropea, 1993). So a part of the sediment is transported around the horseshoe vortex rather than in the vortex. This increases the sediment flux to the side of the building and can lead to deposition as the airflow velocity and sediment transport slowly decrease and revert to undisturbed conditions.

Downwind of the building, in or at the outside of the horseshoe vortex tails, deposition tails usually occur, as the excess wind velocity slowly decreases (Hansen & Cermak, 1975; Peterka et al., 1985), hence reducing the sediment transport capacity. In the lee directly behind a building, both erosion and deposition were observed. Sediment influx into this area is limited, so often the lee area shows no bed level change or even erosion, especially for wind perpendicular to the building. However, sand can be blown into this area, e.g. by the horizontal recirculation cells (Luo et al., 2012), by sand transport over the building or due to fluctuations in the wind direction. Due to flow deceleration and recirculation in the lee, sediment brought into this area is likely to deposit and accumulate over time, explaining the central deposition tail as visible during the large scale experiment in Chapter 3.

Compared to pre-existing research, the field experiments have in the first place added direct observations of windblown sand deposition and erosion around bluff obstacles at the beach, rather than observations of sand in a wind tunnel (Iversen et al., 1990; Luo et al., 2016; McKenna Neuman et al., 2013); measured airflow (Luo et al., 2012, 2014) or CFD-modelled airflow (Pourteimouri et al., 2022; Smith et al., 2017b) as proxies for the expected sediment dynamics; or studies on snow instead of sand (Liu et al., 2018; Oikawa & Tomabechi, 2000; Thiis, 2003; Tominaga, 2017). The importance of directly studying sediment dynamics and morphological development rather than only using airflow as a proxy for sediment transport is highlighted by the varied occurrence of deposition and erosion that we observed in the lee behind scale models, likely caused by variations in the presence of sediment in the airflow patterns around buildings. Hereby, these observations also show the added value of testing under variable field conditions. Secondly, the field experiments resulted in new *quantitative* knowledge, on the systematic relations between the geometric characteristics, of buildings and building groups, and the size of the induced aeolian deposition and erosion patterns.

Regarding the reliability of the field experiments and their applicability to other locations, several aspects are worth considering. A typical concern for the reliability of scaled experiments is unwanted effects from scaling issues. However, given that the developed quantitative relations apply to the full range of scale model sizes tested and match reasonably with the full-scale model (see section 3.5.1), such scaling issues seem of limited importance for the conducted field experiments. This is aided by the developed quantitative relations for deposition size acting more as an *indication* of the expected extent of initial deposition than as fundamental law, with wind speed, sediment availability, development time and variations in the wind conditions all affecting the (size of) morphological patterns around buildings. This also aids when generalizing the results to beaches other than the experimental locations. In addition, the consistency in the results obtained at different experimental locations instills confidence in the wider applicability of the results. The experiments for the effect of building geometry were performed at two different locations: Terschelling and the Sand Motor, with average grain sizes of approximately 200 μm resp. 335 μm (Chapter 3). Despite this substantial difference in the grain sizes, the size of the deposition patterns was similar.

Overall, the morphological patterns that develop around buildings at the beach are usually dominated by deposition. In the short-term experiments with small scale models this was definitely the case, with local erosion limited to the area directly along the building front and sides, while deposition was visible multiple building sizes away from a building. In the experiments with building groups (Chapter 3), this resulted for instance in deposition volumes that were on average 5 times as large as the erosion volumes. For the 5-week experiment with the full-scale model, erosion developed more strongly (fig. 3.14), but deposition remained dominant. Substantial scour occurred especially directly against the upwind wall (>0.5 m), and along the side walls. Moreover, erosion also occurred in the area surrounding the deposition tails– although it is difficult to say to what degree this was *building-induced* erosion, or due to the storm event during the experiment, that caused windblown erosion over the entire beach.

From a physical perspective, it makes sense for erosion to be more pronounced around larger buildings. The length and height of upwind deposition increases with building size. This means the upwind deposition volume per meter of building width increases, so the deposition volume becomes more substantial compared to the total sediment transport flux. This decreases the amount of sediment that remains in transport, potentially resulting in transport that is (more) below the transport capacity, hence enhancing erosion.

By mass balance, sand is not being created nor being destroyed, it is only redistributed. So the observed deposition, in front of buildings and directly around buildings, inherently means that the area further downwind receives less sediment. Looking at how this sediment is distributed alongshore, the lee area straight downwind of a building receives less sediment due to sand being diverted around the building. For the area obliquely downwind of a building, at or downwind of the deposition tails, the net effect on the local sediment flux is less clear: the sediment flux is increased by sand being diverted around the building, but decreased by sand being intercepted by the deposition areas. Regardless, summed over the full width where a building affects the sediment transport, the sediment flux must be lower. In the CA model results (Chapter 5), this sediment balance effect was clearly visible, with erosion occurring both downwind of the building and downwind of the deposition tails. In the field experiments, only the erosion behind the scale models themselves was occasionally visible (see also Appendix 4B). This may be attributed to a difference in bed erodibility between both approaches. The CA model contains an erodible bed, while groundwater or shell content (armour layer formation) prevented deeper erosion in the field experiments, thereby spreading the erosion over a larger area and making it less noticeable.

6.2 CA modelling of beach-dune dynamics around building

The results and insights from the experiments were used to develop new cellular automaton (CA) model rules for the sediment transport around buildings. These were combined with an existing CA model for beach-dune dynamics to study the interactions between the morphological patterns created by buildings and natural bare-sand bedform dynamics. For the interpretation of the results and possible future applications of the model, a number of model characteristics should be considered.

The strength of the model lies in its simplicity and its relatively low computational cost (Fonstad, 2013; Galiforni Silva, 2019; Keijsers et al., 2016). The simplicity allows for a relatively easy addition of new processes, in this case the sediment transport that occurs around buildings. The low computational cost makes it feasible to study long-term (e.g. decadal) morphological development or to do multiple model runs for a sensitivity analysis. However, the general nature of the model rules make the model more suitable to examine the *mechanisms* through which buildings shape their surroundings than to derive *quantitative* answers or predictions. For example, it gives insight in how buildings can change dune typology or how the sediment dynamics around buildings affect dune migration, but it should not be used to give detailed projections of how the sediment flux into the dunes behind a planned building depends on e.g. the building dimensions.

In this thesis, the CA model examined the sediment dynamics around buildings on an open beach, without a dune profile or vegetation present. However, as the model is based on Dubeveg, it already contains rules for vegetation, groundwater and hydrodynamic beach erosion (Keijsers et al., 2016). Hence, it has the potential to model more realistic situations than the scenarios considered thus far, for example with buildings placed in front of a vegetated dune. In addition, more dynamic building placement strategies can be implemented, for example with seasonally present buildings.

For example, fig. 6.1 below compares, as a first start, the morphological development around year-round buildings and seasonally present buildings. Other settings are still identical to Chapter 5, with open beach conditions, no vegetation and unidirectional wind from the south. This shows more limited upwind deposition and downwind deposition tails around seasonal buildings than around year-round buildings, while the downwind area shows no transition to barchan dunes, nor the extended eroded lines in grid columns downwind of the

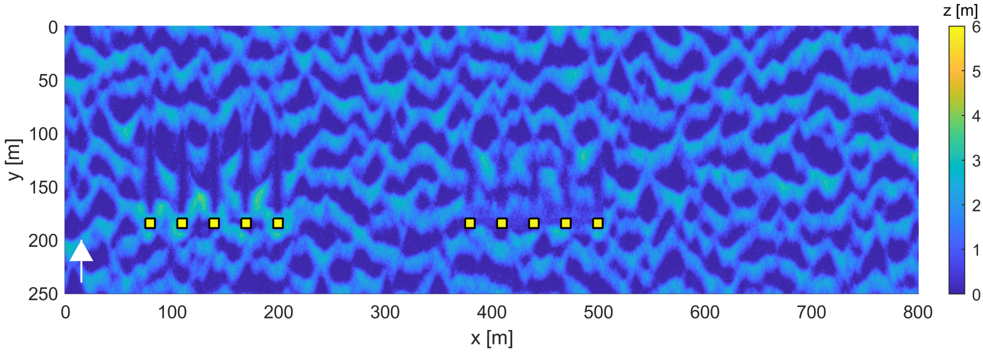

Figure 6.1: The morphological development after 12 years, around two rows with each 5 buildings of 10×10×6 m and gaps of 20 m between buildings. The left building row is present year-round, so essentially the same as fig. 5.14, while the righthand building row is only present in summer. The right side of the domain shows the morphological development unaffected by buildings.

buildings. However, dune shapes are still more irregular than in the area without buildings on the right, with more defects (interruptions) in the transverse dunes. Such a scenario helps to understand to what degree seasonal buildings can still shape their surroundings.

6.3 Implications for the beach-dune system

The conducted field experiments and CA modelling examined buildings on an open beach, to focus on direct building-induced effects. To determine the effects of buildings on the development a real-beach-dune system, at a larger spatial and temporal scale and in interaction with other processes, a number of characteristics and limitations of the followed methods should be considered. The field experiments consisted of scale models on a flat open beach; in practice buildings are usually placed close to the dune foot. In addition, field experiments mostly looked at *initial* patterns that develop on the timescale of a wind event and under a constant wind direction. In practice, buildings are present longer, so morphological patterns have time to develop and evolve over time, under influence of varying wind speeds and directions. Long-term (annual to decadal) sediment dynamics around buildings were examined in the CA model in Chapter 5, but scenarios were relatively simple, with only orthogonal wind directions, constant sand transport and no vegetation or hydrodynamic erosion. In addition, human interference plays a role in practice, in the form of people actively moving sand around buildings, but this was absent in the field experiment and CA model. These factors will be considered below to derive implications of our results for the effects of buildings in a setting with an actual beach-dune system.

6

Implications for long-term morphology

The experiments focused on the initial deposition patterns around buildings. In the experiments with scale models these patterns developed within a day. For full-scale buildings, this may take a few days – as also shown by deposition around the full-scale model (Chapter 3) that took a few days to develop – but it can still occur on the timescale of a single wind event. Over time, as deposition height increases, this topography starts to affect the local wind flow and sediment transport. Assuming constant wind direction, local topography can partly shelter the bed and damp effects induced by the building (McKenna Neuman & Bédard, 2015; McKenna Neuman et al., 2013). Substantial upwind deposition can for instance partly shelter the beach surface at the upwind building wall, thereby damping scour development. In the CA model, this effect is included by using horizon angles, with the effects visible in fig. 5.11. In essence, substantial deposition around a building can be regarded as an aerodynamic wrapping for the building that smooths sharp building edges and reduces building effects. This decrease in the building effects over time also showed in the full-scale experiment, by the relatively limited growth of the deposition around the full-scale model from three days to three weeks after the start of the experiment (Chapter 3). This reduction in the deposition rate around buildings implies that the building impact, in the form of a decrease in sediment flux further landward, decreases over time.

As part of the focus on initial patterns, the examined wind conditions where relatively constant, whereas wind conditions in the field vary over time. The small scale one-day experiments (Chapter 2-4) had almost constant wind direction, and also the full-scale experiment (Chapter 3) had a relatively constant wind direction. If the wind direction changes, the bed around a building has to adapt to the new conditions. In Chapter 5, a combination of alternating *orthogonal* wind directions, parallel and perpendicular to the building, was shown to steer sediment around a building, creating one dominant deposition tail at the downwind building corner. This means that onshore sediment transport that would normally be more uniform alongshore is now concentrated in the deposition tail; the building locally redistributes (concentrates) sand in the alongshore direction. In practice, the effect might even extend over a larger area, especially with prolonged periods of alongshore or onshore wind. Sediment transport rates are usually larger during alongshore wind conditions than during onshore wind, due to the larger fetch length (Bauer et al., 2009; Delgado-Fernandez, 2010). So especially during alongshore (or obliquely onshore) wind, sediment is expected to be collected as deposition around buildings, somewhat similar to how groynes collect alongshore hydrodynamic sediment transport. During onshore wind, this sediment collected around a building could potentially form an extra supply for sediment transport toward the dunes.

Implications for buildings in front of dune

In the field experiments, scale models were placed on the open beach. For the implications for buildings placed in front of an existing coastal dune, the sediment flux past a building into the dune is crucial. When looking at the total sediment flux over the full width where a building affects sediment transport, the upwind deposition that occurred in the field experiments leads to a reduction of the sediment flux directly downwind of a building. For buildings placed in front of a coastal dune, this reduced sediment flux means buildings have a negative effect on the dune volume.

The more detailed effects depend on how the observed deposition and erosion patterns around buildings change by placing buildings close to the dune foot. If the foredune has a steep slope, this impedes sediment transport over the dune until deposition in front of the dune forms a dune ramp for further sediment transport (Christiansen & Davidson-Arnott, 2003). Likewise, dune vegetation increases deposition by capturing aeolian sediment transport (Feagin et al., 2015; Ruggiero et al., 2018). In both cases, the increased deposition rate and reduced transport over the dune would likely limit the length of the deposition tails, and consequently increase their height and width. Possibly, the concentrated deposition in the deposition tails could also promote the formation of dune ramps and thereby enhance sediment transport into the dunes.

Implications of human interventions around buildings

Human interventions around buildings placed in front of a dune also affect the beach-dune environment. The experiments showed deposition behind buildings, either in tails to the side or in in the lee directly behind a building. Especially for larger beach buildings such as restaurants, the area behind a building is often used for access roads or for storage. So deposition directly behind buildings will form a hindrance and be removed mechanically. In contrast, deposition slightly further behind the building lands on the dune, where it is allowed to remain. If human intervention keeps the dune toe location fixed, while dune elevation continuously increases, the dune slope becomes steeper, possibly impeding landward sediment transport. At a Dutch beach pavilion where deposition between the building and dune toe was removed, elevation measurements indeed showed a steeper dune slope and less dune growth behind the pavilion compared to a neighbouring dune without building (De Klerk, 2019).

In addition, human intervention can also affect the sediment balance around buildings in a larger area. Deposition around buildings that blocks paths, roads or access to the buildings is often removed mechanically (Nordstrom, 1994; Jackson & Nordstrom, 2011; see also the news articles Crump, 2018; NH Nieuws, 2019). This increases the effect a building has, by restarting the strong initial effect, rather than allowing the deposition rate to decrease over time. Upwind deposition is often bulldozered to the sea or to the side of a building or

6

building group: especially for building groups this can be easier than bulldozering sand to the dune behind the buildings. In the stretch of coast with the buildings, this decreases the net sediment transport to the upper beach and dunes. In addition, for sediment moved to the side of a building group, concentrated disposal of sand in the form of sand piles near the foredune can create hummocky disposal dunes (Nordstrom & Arens, 1998).

Implications of buildings geometry and configuration

In this thesis, field experiments and CA modelling were used to examine the effect of building size, orientation and spacing on the morphological development around buildings. Larger buildings proved to create larger deposition and erosion patterns and affect the beach over a larger area. Experiments showed the area of influence with direct deposition to easily stretch to more than four times the building factor B behind a building. For building groups, buildings placed close together act in a manner similar to a single large building, dominantly sending sediment around the entire building group. This especially occurs for a spacing of up to half a building width. Larger building spacings increase airflow and sediment transport through the gaps, resulting in larger deposition tails behind the gaps and smaller tails at the outside of a building row. This effect becomes especially important for longer rows of buildings, as these have a larger number of gaps behind which the inner tails form (see also Appendix 6A, for a field experiment with longer rows of buildings).

In practice, buildings are often placed at the beach seasonally, because permits only allow summer placement or because winter storms could damage the building. In this case the deposition observed around buildings could be regarded as delayed sediment transport: sand that is temporarily collected around buildings during summer, but can be transported further landward in the winter. However, this only holds if the deposition is actually blown further landward. It should not be eroded by waves before it has had the time to actually be picked up by the wind, or be moved mechanically. Moreover, even if the local deposition is transported further once the building is removed, this is not the same as having no buildings at all. Buildings do not only induce deposition in their surroundings (and hence decrease the landward sediment flux), but were also shown to redistribute sediment alongshore. Some locations receive more sediment transport, especially behind the deposition tails, while the area in the lee of a building receives less sediment. This process still occurs during half a year for seasonally present buildings, so sediment can still be concentrated in one spot, while another location receives less sediment, potentially creating a weaker spot in the dunes.

Lastly, the construction of buildings may vary. While this research focused on buildings placed directly on the ground, in practice several buildings are constructed on poles. In some cases these raised buildings actually act as buildings placed on the ground. If buildings are placed on short poles, only a small amount of deposition is needed to fill up the space between the building and the ground, effectively making buildings act as buildings on the ground again. This is even more likely, because low poles can result in a deceleration of the airflow underneath buildings (Van Onselen, 2018), similar to a small horizontal spacing between buildings. For buildings on higher poles, building owners often close off the space between poles to use as storage, effectively turning the raised buildings into buildings on the ground (Nordstrom & McCluskey, 1984). However, if this is not the case and pole height is sufficient for the space between building and ground to remain open, that sediment transport can pass underneath the buildings. Scale experiments by us (Appendix 6B) and by Van Bergen et al. (2021), and observations around actual buildings (Nordstrom & McCluskey, 1984, 1985) as well as CFD modelling (Beyers et al., 2004) indicate that this creates some erosion under the building and directly around the building, where airflow is accelerated. In the lee some distance behind the building, airflow is decelerated, creating deposition.

6.4 Implications for coastal management

Coastal management is responsible for flood safety, the preservation of ecological values of dunes and beaches, economic development of the coast and access to beaches and buildings in the beach-dune interface. The obtained insights on the morphological patterns around different spatial layouts of buildings may be of benefit to achieve these goals.

First regarding flood safety, especially in light of a rising sea level: this requires minimally interrupted sand transport into the dunes to maintain safety standards. This sand input simultaneously contributes the ecological values of the dunes. The building design and configuration may be used to minimize the impact of buildings on the sediment flux into the dunes. Following the effects of building geometry described above, this foremost entails using a sufficiently large building spacing. The field experiments suggest that – for buildings with a square wind-facing surface – buildings placed at least one building width apart create less upwind deposition than buildings placed closer together. Hence, maintaining this building spacing would minimize the smaller building impact on the sediment transport to the dunes.

An alternative approach to ensuring minimally interrupted sediment transport into the dunes is making sure that buildings simply cannot intercept sediment before it reaches the dunes. This could be done by placing buildings *in* the dunes instead of in front of the dunes, such that any intercepted sediment will by definition end up in the dune. For example, on Long Beach Island, USA, houses built directly behind the primary dune acted as a sand fence, with deposition in front of the houses raising the height of the foredune (Canning, 1993). However, scour directly around buildings in the dunes also has the potential to cause local weak spots in the dunes (Nordstrom & McCluskey, 1984, 1985). So this approach seems more suitable for a row of small buildings, which could act as a kind of sand fence while only causing relatively limited scour around each building, than for a single large building,

6

which would create a proportionally larger scour zone around it. In addition, this approach entails a trade-off of management goals, as placing buildings and the required access ways in the dunes would be negative for the natural quality of a dune.

Instead of minimizing the negative effects of building on sediment transport, the results suggest that there might even be opportunities to actively use buildings to stimulate sediment transport into the dunes. In case of a steep foredune slope that impedes sediment transport into the dunes, the building layout might be designed such that deposition tails behind buildings form a dune ramp, allowing for more transport into the dunes. Through similar effects, buildings might provide synergy when used in combination with foredune notches or blowouts. Artificial notches or blowouts in the foredune are used to stimulate inland sediment transport and to create more dynamic, ecologically diverse dunes (Laporte-Fauret et al., 2021; Riksen et al., 2016). Buildings create a zone with a higher windspeed and sediment transport rate, by diverting wind and sediment transport around a building and by creating vortices that convey higher-velocity wind from higher elevations to the beach surface. If large buildings are placed such that this zone with extra sediment transport lines up with the blowout during the dominant wind direction, buildings could increase the sediment transport through the blowout. Alternatively, Van Bergen et al. (2021) suggested buildings placed in a funnel or V-shape could be used to mobilize sediment, increasing sediment transport into the dunes and thereby dune height. However, in the absence of blowouts, care should be taken to ensure that the dune profile allows for sediment transport across the foredune, such that increased sediment transport *at the beach* can actually result in increased transport *into the dunes*.

Next, guaranteeing easy access to the beach and the buildings in a dynamic sandy environment requires a recurrent effort to remove sediments blocking the access. The presented knowledge about the effect of building characteristics on the size and location of initial deposition can help to develop spatial designs that minimize the required management efforts, for instance by choosing suitable locations for roads or walkways. One straightforward option would be to place walkways far enough away from the buildings that they are outside the main deposition zone. Conversely, one could also make use of our observation of small areas with less deposition directly against the upwind building face. Accordingly, deposition would probably be less frequent on a path built directly in front of a building than on a path located a few metres in front of a building. However, given that only the crest of upwind deposition stays at a relatively fixed distance from a building (Chapter 3; Tsoar, 1983), larger deposition events can still reach the area directly in front of a building. The latter is also evidenced anecdotally by news articles on beach huts partly buried after storms (Crump, 2018; NH Nieuws, 2019).

Lastly, considering the need to preserve ecological and landscape values, the morphological effects of buildings could also be used to produce more spatial variation in a dune. Dunes that are artificially constructed or promoted through the planting of marram grass, often have a very straight shape and uniform appearance. Alongshore variation induced by bed level change patterns around buildings and varying building locations through time can be used to break up the uniformity of such dike-like dunes and create a more hummocky, natural appearance.

Appendix 6A Experiment with longer building rows

This appendix shows elevation maps of an experiment on how group size affects the morphological patterns around buildings. This experiment took place at 11-05-2019 at the Sand Motor, as part of the experiments for the effect of building spacing and orientation (chapter 4). Four different set-ups were tested, to compare the morphological patterns with group sizes of 3 and 6 buildings, and building spacings of 0.5 m and 1 m (gap ratios of 0.5 and 0.67). The elevation maps show that for a larger group size, the outer deposition tails become slightly larger, as a result of an increase in the total airflow and sediment transport diverted around a building group.

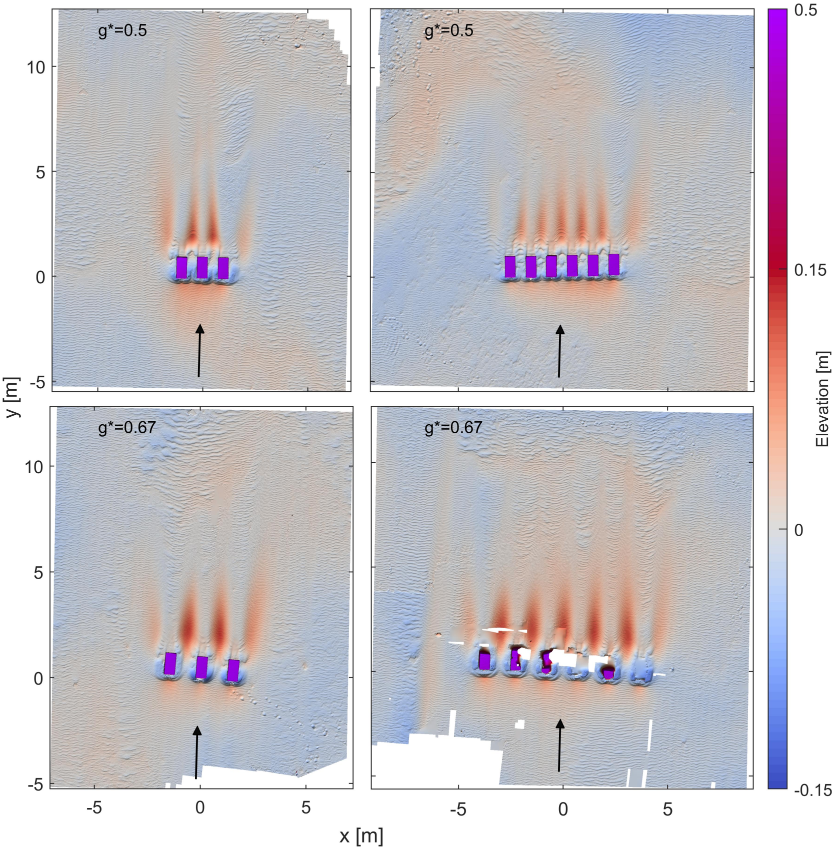

Figure 6.2: The effect of group size on deposition and erosion patterns. Scale models are 0.5×1×0.5 m. Elevation is relative to a linear surface fitted per subplot, to highlight local differences caused by erosion and deposition.

Appendix 6B Experiment with buildings on poles

This appendix shows elevation maps of an exploratory experiment on the effect of pole height on the morphological patterns around buildings. This experiment took place at 11-05-2019 at the Sand Motor, as part of the experiments for the effect of building spacing and orientation (chapter 4). Six individual scale models, sized 0.5×1×0.5 m, were placed on poles ranging from 0 to 50 cm. The elevation maps suggest that deposition and erosion areas becomes more smeared out if buildings are placed on poles, with deposition and erosion areas that are smaller in height, but seem to extend over a larger area. In addition, some cases show deposition in the lee behind scale models (e.g. for the poles of 10 and 20 cm), likely due to sediment transport underneath scale models. Downwind deposition tails seem to move somewhat downwind for the larger pole heights: tails start next to the scale model for the model placed on the surface, but some distance downwind for the highest set-ups.

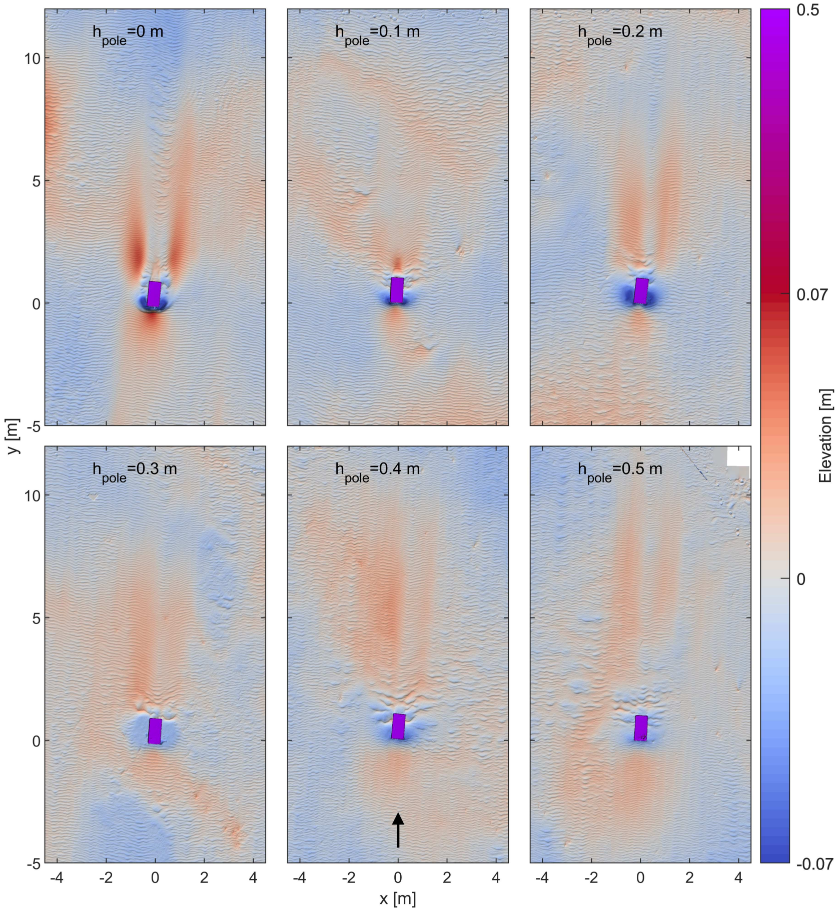

Figure 6.3: The effect of pole height on deposition and erosion patterns. Elevation is relative to a linear surface fitted per subplot.

7

Conclusions and recommendations

7

Conclusions and recommendations

Figure previous page: The beach at Noordwijk, the Netherlands. © Thomas Steenvoorden.

The aim of this thesis is *to determine and understand quantitatively how buildings at a sandy beach affect the wind-driven morphological development of the beach environment.* To investigate the effect of buildings, the deposition and erosion patterns that arise around buildings were examined using scale experiments on the beach. Next, the insights obtained in the experiments were used in a cellular automaton computer model to examine the long-term effect of buildings on the beach and interactions between building-induced effects and natural bedform dynamics. Based on these results, the current section answers the research questions formulated in Chapter 1, uses this to reflect on the overall research aim and gives recommendation for future research and for practice.

7.1 Answers to research questions and aim

Q1 *Which morphological patterns arise on the timescale of a wind event around a single building on a sandy beach?*

For a building placed at ground-level on a sandy beach, the main deposition forms as the result of the horseshoe vortex wind structure, and follows this shape. The dominant deposition areas are the area upwind of the building, and two deposition tails extending outward obliquely behind a building (i.e. the upwind horseshoe deposition and downwind horseshoe deposition in fig. 2.1). Sometimes deposition occurs next to a building, such that the deposition forms a full horseshoe shape around the building in which the upwind deposition area and downwind deposition tails are connected. Scour occurs at the upwind building walls and especially at the upwind building corners due to accelerated airflow. This can lead to undercutting of the building, i.e. erosion occurring not only in front of a building, but also underneath a building. Along the side walls, scour can occur as well. During winds perpendicular to a building, the lee area directly downwind of a building oftentimes shows little morphological development, due to the building blocking most sediment from entering this area. However, some sediment may enter the lee, for instance during variable winds obliquely to the building. Over time, deposition of this incoming sand due to the recirculation and low wind speed in the lee can lead to a substantial ridge-shaped deposition area behind the building.

Q2 *How does the initial size of the deposition pattern around a single building depend on the building geometry?*

The deposition patterns around a building become larger with increasing building size. The width and length of initial deposition patterns depend primarily on the frontal area of a building, so on the building width w – measured perpendicular to the wind direction – and the building height h. The combined effect of w and h can be expressed by the building factor B, with $B = w^{2/3}h^{1/3}$. The initial horizontal deposition size scales linearly with B. This scaling factor is valid for building aspect ratios (w/h)

between 0.2 and 4: for very wide or very tall buildings, the smallest dimension of w and h becomes increasingly dominant for airflow patterns that develop, breaking down the scaling with B. Building length, measured in the wind direction, has little effect on the size of deposition patterns. In addition, wind speed also affects the size of deposition patterns, by changing the sediment transport rate. Especially the initial downwind deposition length is affected, and increases approximately linear with wind speed.

Q3 *How do initial morphological patterns depend on the spatial configuration of buildings?*

Starting with individual buildings, placed at ground-level on a sandy beach: the orientation of a building modifies the shape of the deposition pattern that develops. If the upwind wall is at a right angle to the wind, deposition develops symmetrically, with upwind deposition straight in front of the building, and downwind deposition in two approximately equal deposition tails. If the building is at an oblique angle to the wind, this picture changes. Wind and sand diverted around a building are no longer split evenly between the left and right side of the building. This leads to asymmetrically developing deposition tails. The orientation of the wind-facing building walls and their effective width (measured perpendicular to the wind) together determine how asymmetrical the deposition tails become.

For rows of buildings, the *spacing* between buildings predominantly determines the shape of the deposition patterns. Gap ratio g^* can be used to quantify the porosity of a building group, with $g^* = \frac{G}{G+w}$, gap width G and building width w. Buildings placed close together obstruct airflow and sediment transport through the gaps between buildings. For buildings that have a height and width that are approximately equal, this is especially true for gap ratios of up to 0.33, assuming wind perpendicular to the building group. Then airflow and sediment transport are diverted mainly around a building group rather than through the gaps, making the building group in essence act similar to a single large building. Upwind, this results in deposition that extends further upwind and becomes higher than for an individual building or a more widely spaced building group. Downwind, the consequence of sediment predominantly being diverted around the building group is that deposition occurs mainly as outer tails at the outside of the building group. If the building spacing increases, sediment transport through the gaps increases, leading to larger deposition areas behind the gaps (inner tails) and smaller outer tails. For a gap ratio of 0.5 to 0.67, inner and outer tails are more equal in size, but they still differ in shape and location, due to the airflow still being affected by neighbouring buildings. For a gap ratio of 0.75 and larger, these interactions decrease and downwind morphology develops as the summed effect of independent buildings. The specific gap ratios at which all these transitions in the airflow regime occur, would become larger for A) oblique wind directions, which decrease the effective width between buildings open to the wind, or B) relatively taller buildings ($h > w$), which create a larger vortex in front of a building, expanding the horseshoe vortex.

Q4 *How do building-induced morphological patterns interact over time with natural aeolian bedform dynamics?*

In a dynamic beach environment, the local bed patterns that develop around buildings can interact with natural bedform dynamics. Buildings cause net deposition in their surroundings, which decreases the sediment transport further downwind. The reduced sediment supply to the area downwind of a building can affect the dynamics behind buildings. Bedforms such as dunes can decrease in height. Dune topology can change as well, especially in regions without vegetation to stabilize the dunes: the decreased supply behind buildings can cause defects (interruptions) in transverse dunes or a regime change from transverse dunes to barchan dunes. In additions, buildings can redirect sediment: the area behind a building is sheltered when it is in the lee of the building, but not when the wind blows from a different direction. As a result, the local direction of the effective sediment transport field around buildings differs from the undisturbed wind direction. By changing the sediment transport direction around buildings, buildings can affect the location and direction of dune growth. And if buildings are sufficiently large, such that dunes fit in their entirety in the lee zone behind a building, the direction of dune migration can be affected as well.

Reflection on aim

This thesis aimed to *determine and understand quantitatively how buildings at a sandy beach affect the wind-driven morphological development of the beach environment.* It revealed that systematic relations exist between geometric characteristics of buildings and of building groups, and the aeolian bed patterns they create. Quantitative relations were derived for the extent of initial deposition around buildings using a new building factor B, as well as for the asymmetry of the downwind deposition tails as a factor of the building shape and orientation. For configurations with multiple buildings, distinct regimes of deposition and erosion patterns were distinguished, with the building spacing determining if patterns can be regarded as the summed effect of independent individual buildings, or as a shared complex pattern caused by the combined building group. The deposition and erosion patterns around buildings and the associated reduction in the sediment supply to the area downwind of buildings were found to affect the bedform dynamics behind buildings. Through their effect on the sediment transport field, buildings can change the location and direction of dune growth and migration. Through all these effects, the building size, shape, orientation and distance to other buildings can serve as parameters for coastal managers to affect and steer beach-dune development.

7.2 Recommendations

The recommendations are divided in recommendations for further research and recommendations for coastal management.

7.2.1 Recommendations for future research

Examine effect dune behind buildings

All field experiments in this thesis are performed on a flat, open beach. In practice, buildings are often placed on the highest or artificially raised (safest) part of a beach, directly in front of the dune. Dunes affect the airflow in their surroundings, inducing local flow acceleration and deceleration (Wiggs et al., 1996), but also flow deflection, especially for obliquely onshore winds (Bauer et al., 2012; Hesp et al., 2015). Consequently, the airflow around a building placed in front of a dune may deviate from the airflow around a building on the open beach. Similar deposition patterns have been observed around buildings in front of a dune as around buildings at an open beach (see fig. 1.3 but changes in the wind field in front of a dune may to some extent change the morphological patterns around buildings. Therefore, future research should examine the effect of buildings in front of a dune, using for example CFD modelling (see e.g. Pourteimouri et al., 2022) or field experiments placed in front of a real dune.

Analyse monitoring data

Water authorities have extensive data series of yearly elevation monitoring of the Dutch coast. This data shows that dune volume growth behind buildings is lower than in undisturbed areas (De Zeeuw, 2017; Hoonhout & Van Thiel de Vries, 2013; Van der Valk & Van der Meulen, 2013). Previous studies had difficulties drawing statistically significant conclusions on this effect as it depends on specific building characteristics, such as building size, building spacing or summer placement versus year-round placement (Hoonhout & Van Thiel de Vries, 2013; Hoonhout & Waagmeester, 2014; Huisman, 2013). However, the amount of data available increases every year, and the spatial resolution of the data has increased as well. So monitoring data should be examined to determine if the data support the conclusions of this research. For example: previous studies concluded that a small building spacing decreases dune growth behind buildings (Hoonhout & Van Thiel de Vries, 2013; Hoonhout & Waagmeester, 2014; Van Westen, 2019), but were unable to quantify at which point the building spacing becomes too small. The preliminary advise of Hoonhout and Van Thiel de Vries (2013), to keep a building spacing of at least one building width, matches nicely with the recommendation of this thesis (see section 7.2.2 below), but maybe new data can also quantify these effects in the field. In addition, monitoring data could shed further light on the effect of placing buildings on poles or on differences between summer placement and year-round placement of buildings.

CA model: examine interaction building with vegetation and coastal dunes

In Chapter 5, the morphological effects of buildings are implemented in a cellular automata model and this model is used to examine the interactions between building-induced effects and natural bedform dynamics. These natural bedform dynamics were modelled on an initially flat domain without vegetation, similar to a wide beach or a desert. By combining the new rules for building effects with the existing Dubeveg model (Dune-Beach-VEGetation, Keijsers et al., 2016), the effect of buildings in a coastal environment with vegetation dynamics, groundwater and hydrodynamic erosion can be examined.

CA model: examine building placement strategies

When using the CA model in a realistic coastal setting as suggested above, the effect of different building placement strategies can be examined. Buildings are often only present in the summer season, with for example permits for beach houses in the Netherlands often only allowing placement between the beginning of April and the beginning of October. This prevents damage and loss of beach buildings during stronger winter storms, but also allows for half a year with unimpeded sediment transport to the dunes. However, especially for beach restaurants there is increasing demand for year-round present buildings (Buth, 2016; Province of Noord-Holland, 2017). In addition, regulations against year-round buildings have been suspended for the winters of 2020-2021 and 2021-2022 to decrease the (de)construction costs of restaurants and hence their financial losses due to Covid-19 (H2O, 2021; Ollongren, 2020). Therefore, it would be interesting to investigate the effect of seasonal versus year-round building placement. In addition, adaptive building placement strategies have been proposed (Van Bergen et al., 2021), in which a dynamic set-up of seasonal beach buildings is used, with building location shifting depending on the dune development in order to build up the foredune. The potential of such adaptive strategies could be examined further with the CA model.

7.2.2 Recommendations for coastal management

Use building spacing to modulate landward sediment transport

Depending on the situation, it can be desirable to increase or decrease the windblown sediment transport from the beach to the dune or hinterland. For a coastal dune, a large sediment transport into the dunes is desirable for coastal safety. Conversely, minimizing the local landward sediment transport becomes preferable if the beach is directly bordered by a road or coastal town, to minimize sand blown onto roads or other infrastructure. These management goals can be supported by different building spacings.

To express the building spacing relative to the building dimensions, scaling length R can be used, where $R = \min(w, h)^{2/3} \cdot \max(w, h)^{1/3}$ (with building width w and height h, see also section 4.4.2). Buildings placed a distance of $0.5R$ apart create upwind deposition that is higher than for buildings placed at least $1R$ apart, and also extends further upwind (Chapter 4). This stems from closely spaced buildings restricting the airflow in between buildings, causing stronger airflow deceleration upwind of the building and hence extra upwind deposition. So if you want to decrease the sediment transport and deposition downwind, building spacing should at most equal $0.5R$. Conversely, to decrease upwind deposition and allow for a larger sediment flux into the dunes, building spacing should at least equal R. The same minimal building spacing also applies when aiming to reduce sand hinder in front of a building group. A building spacing larger than R has little effect on the deposition right in front of the buildings, but is still beneficial to the dunes as building effects are spread over larger area, reducing the effect per meter dune. Furthermore, for wind that is at an oblique angle to the building, the effect is determined by the effective width between buildings that is open to the wind. This means that buildings should be angled to face the dominant wind direction, or alternatively, that the spacing between buildings should be increased until the gaps reach a width of $1R$, measured perpendicular to the dominant wind direction (see also fig. 4.13c). For buildings with an approximately square wind-facing surface and oriented to the dominant wind direction, this advise can be simplified: use a building spacing of at most $0.5w$ to reduce sediment transport downwind, or at least $1w$ to minimize negative building effects on the sediment transport downwind.

Experiment with synergy between buildings and blowouts

One of the aims of coastal management is to preserve or improve the natural values of the dunes. Hereto artificial notches or blowouts are sometimes made in the foredune. Sediment transport through these blow-outs into the dunes can improve the natural dynamics and biological quality of the dune (Laporte-Fauret et al., 2021; Riksen et al., 2016). In addition, the additional sediment transport into the dunes is also beneficial for coastal safety. Synergy might be possible between buildings and these blow-outs. Buildings create a zone with increased wind velocity and sediment transport. If buildings are placed such that this zone lines up with the blowout during dominant wind directions, they could enhance blow-out development and sediment transport through the blow-out. This effect might be achieved with a single large beach building, but a funnel or V-shape configuration of buildings might be even more effective to steer sediment towards a blowout. Therefore, pilot cases should be used to explore to what degree synergy between buildings and blowouts can be achieved.

Bibliography

Abbasi, H. R., Opp, C., Groll, M., Rohipour, H., & Gohardoust, A. (2019). Assessment of the distribution and activity of dunes in Iran based on mobility indices and ground data. *Aeolian Research*, *41*, 100539. https://doi.org/https://doi.org/10.1016/j.aeolia.2019.07.005

Anderson, R. S. (1987). A theoretical model for aeolian impact ripples. *Sedimentology*, *34*(5), 943–956. https://doi.org/10.1111/j.1365-3091.1987.tb00814.x

Arens, S. M., Van Kaam-Peters, H. M. E., & Van Boxel, J. H. (1995). Air flow over foredunes and implications for sand transport. *Earth Surface Processes and Landforms*, *20*(4), 315–332. https://doi.org/https://doi.org/10.1002/esp.3290200403

Ash, J. E., & Wasson, R. J. (1983). Vegetation and sand mobility in the Australian desert dunefield. *Zeitschrift fur Geomorphologie*, *45*(Supp.), 7–25.

ASHRAE. (2005). 2005 ASHRAE Handbook: Fundamentals - SI edition. American Society of Heating Refrigerating and Air-Conditioning Engineers.

Baas, A. C. W. (2002). Chaos, fractals and self-organization in coastal geomorphology: simulating dune landscapes in vegetated environments. *Geomorphology*, *48*(1), 309–328. https://doi.org/10.1016/S0169-555X(02)00187-3

Baas, A. C. W. (2007). Complex systems in aeolian geomorphology. *Geomorphology*, *91*(3), 311–331. https://doi.org/10.1016/j.geomorph.2007.04.012

Bagnold, R. A. (1941). *The Physics of Blown Sand and Desert Dunes*. Chapman & Hall.

Bai, H., & Alam, M. M. (2018). Dependence of square cylinder wake on Reynolds number. *Physics of Fluids*, *30*(1), 15102. https://doi.org/10.1063/1.4996945

Barchyn, T. E., & Hugenholtz, C. H. (2012). *A new tool for modeling dune field evolution based on an accessible, GUI version of the Werner dune model* (Vol. 138). https://doi.org/10.1016/j.geomorph.2011.09.021

Baskaran, A., & Kashef, A. (1996). Investigation of air flow around buildings using computational fluid dynamics techniques. *Engineering Structures*, *18*(11), 861–875. https://doi.org/10.1016/0141-0296(95)00154-9

Bauer, B. O., Davidson-Arnott, R. G. D., Hesp, P. A., Namikas, S. L., Ollerhead, J., & Walker, I. J. (2009). Aeolian sediment transport on a beach: Surface moisture, wind fetch, and mean transport. *Geomorphology*, *105*(1), 106–116. https://doi.org/10.1016/j.geomorph.2008.02.016

Bauer, B. O., Davidson-Arnott, R. G. D., Walker, I. J., Hesp, P. A., & Ollerhead, J. (2012). Wind direction and complex sediment transport response across a beach-dune system. *Earth Surface Processes and Landforms*, *37*(15), 1661–1677. https://doi.org/10.1002/esp.3306

Becker, S., Lienhart, H., & Durst, F. (2002). Flow around three-dimensional obstacles in boundary layers. *Journal of Wind Engineering and Industrial Aerodynamics*, *90*(4), 265–279. https://doi.org/10.1016/S0167-6105(01)00209-4

Beranek, W. J. (1984). Wind environment around single buildings of rectangular shape. *Heron*, *29*(1), 4–31.

Beyers, J. H. M., Harms, T. M., & Sundsbø, P. A. (2004). Numerical simulation of snow drift around an elevated structure. *Snow Engineering V: Proceedings of the Fifth International Conference on Snow Engineering, 5-8 July 2004, Davos, Switzerland*, 185.

Beyers, J. H. M., & Waechter, B. (2008). Modeling transient snowdrift development around complex three-dimensional structures. *Journal of Wind Engineering and Industrial Aerodynamics*, *96*(10-11), 1603–1615. https://doi.org/10.1016/j.jweia.2008.02.032

Blocken, B., Stathopoulos, T., Carmeliet, J., & Hensen, J. L. M. (2011). Application of computational fluid dynamics in building performance simulation for the outdoor environment: an overview. *Journal of Building Performance Simulation*, *4*(2), 157–184. https://doi.org/10.1080/19401493.2010.513740

Brunier, G., Fleury, J., Anthony, E. J., Gardel, A., & Dussouillez, P. (2016). Close-range airborne Structure-from-Motion Photogrammetry for high-resolution beach morphometric surveys: Examples from an embayed rotating beach. *Geomorphology*, *261*, 76–88. https://doi.org/10.1016/j.geomorph.2016.02.025

Buth, G.-J. (2016). *Analyse van recent gerealiseerde bebouwing en nieuwe bouwplannen aan de Nederlandse kust*. Natuurmonumenten.

Canning, D. J. (1993). Dunes management plan: Long Beach Peninsula, Washington. In O. T. Magoon, W. S. Wilson, H. Converse, & L. T. Tobin (Eds.), *Coastal zone '93* (pp. 1938–1950). ASCE.

Carter, R. W. G. (1991). Near-future sea level impacts on coastal dune landscapes. *Landscape Ecology*, *6*(1), 29–39. https://doi.org/10.1007/bf00157742

Castro, I. P., & Robins, A. G. (1977). The flow around a surface-mounted cube in uniform and turbulent streams (2006/04/11). *Journal of Fluid Mechanics*, *79*(2), 307–335. https://doi.org/10.1017/S0022112077000172

Charbonneau, B. R., Dohner, S. M., Wnek, J. P., Barber, D., Zarnetske, P., & Casper, B. B. (2021). Vegetation effects on coastal foredune initiation: Wind tunnel experiments and field validation for three dune-building plants. *Geomorphology*, *378*, 107594. https://doi.org/10.1016/j.geomorph.2021.107594

Cheng, H., Liu, C., & Kang, L. (2020). Experimental study on the effect of plant spacing, number of rows and arrangement on the airflow field of forest belt in a wind tunnel. *Journal of Arid Environments*, *178*, 104169. https://doi.org/10.1016/j.jaridenv.2020.104169

Chiba, T., & Thiis, T. K. (2016). Accuracy of snow depth measurements on roofs measured with photogrammetry. In P. Deplpech & T. K. Thiis (Eds.), *Snow engineering, recent advances* (pp. 334–338).

Christiansen, M. B., & Davidson-Arnott, R. (2003). Effects of dune ramps on sediment supply to coastal foredunes: Skallingen, SW Denmark. *International conference on coastal sediments 2003*.

Cooke, R. U., Warren, A., & Goudie, A. S. (1993). *Desert geomorphology*. CRC Press.

Coulthard, T. J., Hicks, D. M., & Van de Wiel, M. J. (2007). Cellular modelling of river catchments and reaches: Advantages, limitations and prospects. *Geomorphology*, *90*(3), 192–207. https://doi.org/https://doi.org/10.1016/j.geomorph.2006.10.030

Crump, E. (2018). Abersoch beach hut owners have their work cut out before they can enjoy Easter break. *Daily Post*. www.dailypost.co.uk/news/north-wales-news/abersoch-beach-hut-owners-work-14435963

De Groot, A. V., Berendse, F., Riksen, M., Baas, A., Slim, P. A., Van Dobben, H. F., & Stroosnijder, L. (2011). Modelling coastal dune formation and associated vegetation development. *EGU 2011*, *13*.

De Klerk, R. P. (2019). *The influence of buildings on aeolian coastal dune development (MSc. Thesis)*. Technical University Delft.

7

De Winter, R. C., & Ruessink, B. G. (2017). Sensitivity analysis of climate change impacts on dune erosion: case study for the Dutch Holland coast. *Climatic Change*, *141*(4), 685–701. https://doi.org/10.1007/s10584-017-1922-3

De Zeeuw, R. C. (2017). *Effecten strandbebouwing op strand- en duinontwikkeling* (tech. rep.). Den Haag, Shore Monitoring and Research.

Delgado-Fernandez, I. (2010). A review of the application of the fetch effect to modelling sand supply to coastal foredunes. *Aeolian Research*, *2*(2-3), 61–70. https://doi.org/10.1016/j.aeolia.2010.04.001

Depardon, S., Lasserre, J. J., Boueilh, J. C., Brizzi, L. E., & Borée, J. (2005). Skin friction pattern analysis using near-wall PIV. *Experiments in Fluids*, *39*(5), 805–818. https://doi.org/10.1007/s00348-005-0014-8

Dong, Z., Liu, X., Wang, H., Zhao, A., & Wang, X. (2003). The flux profile of a blowing sand cloud: a wind tunnel investigation. *Geomorphology*, *49*(3), 219–230. https://doi.org/10.1016/S0169-555X(02)00170-8

Duarte-Campos, L., Wijnberg, K. M., & Hulscher, S. J. M. H. (2021). Field test of the accuracy of laser particle counters to measure aeolian sediment flux. *Aeolian Research*, *50*, 100676. https://doi.org/10.1016/j.aeolia.2021.100676

Duran, O., & Moore, L. J. (2013). Vegetation controls on the maximum size of coastal dunes (2013/10/09). *Proc. Natl. Acad. Sci. U. S. A.*, *110*(43), 17217–17222. https://doi.org/10.1073/pnas.1307580110

Duthinh, D., & Simiu, E. (2011). The use of wind tunnel measurements in building design. In J. C. Lerner (Ed.), *Wind tunnels and experimental fluid dynamics research* (pp. 282–300). InTech. https://doi.org/10.5772/1867

Dwyer, L., & Edwards, D. (2000). Nature-based tourism on the edge of urban development. *Journal of Sustainable Tourism*, *8*(4), 267–287. https://doi.org/10.1080/09669580008667364

Eastwood, E., Nield, J., Baas, A., & Kocurek, G. (2011). Modelling controls on aeolian dune-field pattern evolution. *Sedimentology*, *58*(6), 1391–1406. https://doi.org/10.1111/j.1365-3091.2010.01216.x

Fackrell, J. E. (1984). Parameters characterising dispersion in the near wake of buildings. *Journal of Wind Engineering and Industrial Aerodynamics*, *16*(1), 97–118.

Feagin, R. A., Figlus, J., Zinnert, J. C., Sigren, J., Martínez, M. L., Silva, R., Smith, W. K., Cox, D., Young, D. R., & Carter, G. (2015). Going with the flow or against the grain? The promise of vegetation for protecting beaches, dunes, and barrier islands from erosion. *Frontiers in Ecology and the Environment*, *13*(4), 203–210. https://doi.org/10.1890/140218

Fonstad, M. A. (2013). Cellular automata in geomorphology. *Treatise on Geomorphology*, *2*, 117–134. https://doi.org/10.1016/B978-0-12-374739-6.00035-X

Fonstad, M. A., Dietrich, J. T., Courville, B. C., Jensen, J. L., & Carbonneau, P. E. (2013). Topographic structure from motion: a new development in photogrammetric measurement. *Earth Surface Processes and Landforms*, *38*(4), 421–430. https://doi.org/10.1002/esp.3366

Galiforni Silva, F. (2019). *Beach-dune systems near inlets: Linking subtidal and subaerial morphodynamics* (Doctoral dissertation). Enschede, University of Twente. https://doi.org/10.3990/1.9789036547598

Galiforni Silva, F., Wijnberg, K. M., de Groot, A. V., & Hulscher, S. J. M. H. (2018). The influence of groundwater depth on coastal dune development at sand flats close to inlets. *Ocean Dynamics*, *68*(7), 885–897. https://doi.org/10.1007/s10236-018-1162-8

Galiforni Silva, F., Wijnberg, K. M., de Groot, A. V., & Hulscher, S. J. M. H. (2019). The effects of beach width variability on coastal dune development at decadal scales. *Geomorphology*, *329*, 58–69. https://doi.org/https://doi.org/10.1016/j.geomorph.2018.12.012

Gao, Y., & Chow, W. K. (2005). Numerical studies on air flow around a cube. *Journal of Wind Engineering and Industrial Aerodynamics*, *93*(2), 115–135. https://doi.org/10.1016/j.jweia.2004.11.001

García Romero, L., Hernández-Cordero, A. I., Fernández-Cabrera, E., Peña-Alonso, C., Hernández-Calvento, L., & Pérez-Chacón, E. (2016). Urban-touristic impacts on the aeolian sedimentary systems of the Canary Islands: conflict between development and conservation. *Island Studies Journal*, *11*(1), 91–112.

George, E., Lunardi, B., Smith, A., Lehner, J., Wernette, P., & Houser, C. (2021). Short communication: Storm impact and recovery of a beach-dune system in Prince Edward Island. *Geomorphology*, *384*, 107721. https://doi.org/10.1016/j.geomorph.2021.107721

Goossens, D., Nolet, C., Etyemezian, V., Duarte-Campos, L., Bakker, G., & Riksen, M. (2018). Field testing, comparison, and discussion of five aeolian sand transport measuring devices operating on different measuring principles. *Aeolian Research*, *32*, 1–13. https://doi.org/10.1016/j.aeolia.2018.01.001

Guillén, J., & Hoekstra, P. (1997). Sediment distribution in the nearshore zone: Grain size evolution in response to shoreface nourishment (Island of Terschelling, The Netherlands). *Estuarine, Coastal and Shelf Science*, *45*(5), 639–652. https://doi.org/10.1006/ecss.1996.0218

H2O. (2021). Strandpaviljoens mogen vanwege corona nogmaals overwinteren. https://www.h2owaternetwerk.nl/h2o-actueel/strandpaviljoens-mogen-vanwege-corona-nogmaals-overwinteren

Hall, C. M. (2001). Trends in ocean and coastal tourism: the end of the last frontier? *Ocean & Coastal Management*, *44*(9), 601–618. https://doi.org/10.1016/S0964-5691(01)00071-0

Hallin, C., Huisman, B. J. A., Larson, M., Walstra, D.-J. R., & Hanson, H. (2019). Impact of sediment supply on decadal-scale dune evolution — Analysis and modelling of the Kennemer dunes in the Netherlands. *Geomorphology*, *337*, 94–110. https://doi.org/10.1016/j.geomorph.2019.04.003

Hansen, A. C., & Cermak, J. E. (1975). Vortex-containing wakes of surface obstacles.

Hernández-Calvento, L., Jackson, D. W. T., Medina, R., Hernández-Cordero, A. I., Cruz, N., & Requejo, S. (2014). Downwind effects on an arid dunefield from an evolving urbanised area. *Aeolian Research*, *15*, 301–309. https://doi.org/10.1016/j.aeolia.2014.06.007

Hesp, P. A. (1981). The formation of shadow dunes. *Journal of Sedimentary Petrology*, *51*(1), 101–112. https://doi.org/10.1306/212F7C1B-2B24-11D7-8648000102C1865D

Hesp, P. A., Smyth, T. A. G., Nielsen, P., Walker, I. J., Bauer, B. O., & Davidson-Arnott, R. (2015). Flow deflection over a foredune. *Geomorphology*, *230*, 64–74.

Hoonhout, B. M., & De Vries, S. (2016). A process-based model for aeolian sediment transport and spatiotemporal varying sediment availability. *Journal of Geophysical Research: Earth Surface*, *121*(8), 1555–1575. https://doi.org/https://doi.org/10.1002/2015JF003692

Hoonhout, B. M., & De Vries, S. (2019). Simulating spatiotemporal aeolian sediment supply at a mega nourishment. *Coastal engineering*, *145*, 21–35. https://doi.org/10.1016/j.coastaleng.2018.12.007

Hoonhout, B. M., & Van Thiel de Vries, J. (2013). *Invloed van strandbebouwing op zandverstuiving, Adviezen voor vergunningverlening*. Deltares.

Hoonhout, B. M., & Waagmeester, N. (2014). *Invloed van strandbebouwing op zandverstuiving, Een verkenning naar methoden, meetgegevens en modellen*. Deltares.

Hugenholtz, C. H., & Barchyn, T. E. (2011). Laboratory and field performance of a laser particle counter for measuring aeolian sand transport. *Journal of Geophysical Research: Earth Surface*, *116*(F1). https://doi.org/10.1029/2010JF001822

Huisman, M. (2013). *De effecten van strandbebouwing op de ontwikkeling van de eerste duinenrij - Evaluatie en advies monitoringsprogramma HHNK (MSc. Thesis)*. VU Amsterdam.

Hunt, J. C. R. (1971). The effect of single buildings and structures. *Phil. Trans. R. Soc. Lond. A*, *269*(1199), 457–467. https://doi.org/10.1098/rsta.1971.0044

Hunt, J. C. R., Abell, C. J., Peterka, J. A., & Woo, H. (1978). Kinematical studies of the flows around free or surface-mounted obstacles; applying topology to flow visualization (2006/04/12). *Journal of Fluid Mechanics*, *86*(1), 179–200. https://doi.org/10.1017/S0022112078001068

Iversen, J. D., Wang, W. P., Rasmussen, K. R., Mikkelsen, H. E., Leach, R. N., Barndorff-Nielsen, O. E., & Willetts, B. B. (1991). Roughness element effect on local and universal saltation transport. *2*, 65–75.

Iversen, J. D., Wang, W.-P., Rasmussen, K. R., Mikkelsen, H. E., Hasiuk, J. F., & Leach, R. N. (1990). The effect of a roughness element on local saltation transport. *Journal of Wind Engineering and Industrial Aerodynamics*, *36*, 845–854.

Jackson, N. L., & Nordstrom, K. F. (2011). Aeolian sediment transport and landforms in managed coastal systems: A review. *Aeolian Research*, *3*(2), 181–196. https://doi.org/10.1016/j.aeolia.2011.03.011

Keijsers, J. G. S. (2015). *Modelling foredune dynamics in response to climate change* (Doctoral dissertation). Wageningen University.

Keijsers, J. G. S., De Groot, A. V., & Riksen, M. J. P. M. (2016). Modeling the biogeomorphic evolution of coastal dunes in response to climate change. *Journal of Geophysical Research: Earth Surface*, *121*(6), 1161–1181. https://doi.org/10.1002/2015jf003815

Kim, H., Ahn, E., Cho, S., Shin, M., & Sim, S.-H. (2017). Comparative analysis of image binarization methods for crack identification in concrete structures. *Cement and Concrete Research*, *99*, 53–61. https://doi.org/10.1016/j.cemconres.2017.04.018

KNMI. (2020). Klimatologie: Uurgegevens van het weer in Nederland. http://projects.knmi.nl/klimatologie/uurgegevens/

Kok, J. F., Parteli, E. J. R., Michaels, T. I., & Karam, D. B. (2012). The physics of wind-blown sand and dust (2012/09/18). *Rep. Prog. Phys.*, *75*(10), 106901. https://doi.org/10.1088/0034-4885/75/10/106901

Kothari, K. M., Peterka, J. A., & Meroney, R. N. (1979). Stably stratified building wakes.

Kothari, K. M., Peterka, J. A., & Meroney, R. N. (1986). Perturbation analysis and measurements of building wakes in a stably stratified turbulent boundary layer. *Journal of Wind Engineering and Industrial Aerodynamics*, *25*(1), 49–74.

Laporte-Fauret, Q., Castelle, B., Michalet, R., Marieu, V., Bujan, S., & Rosebery, D. (2021). Morphological and ecological responses of a managed coastal sand dune to experimental notches. *Science of The Total Environment*, *782*, 146813. https://doi.org/10.1016/j.scitotenv.2021.146813

Leenders, J. K., Boxel, J. H. v., & Sterk, G. (2007). The effect of single vegetation elements on wind speed and sediment transport in the Sahelian zone of Burkina Faso. *Earth Surface Processes and Landforms*, *32*(10), 1454–1474. https://doi.org/10.1002/esp.1452

Liu, M., Zhang, Q., Fan, F., & Shen, S. (2018). Experiments on natural snow distribution around simplified building models based on open air snow-wind combined experimental facility. *Journal of Wind Engineering and Industrial Aerodynamics*, *173*, 1–13. https://doi.org/10.1016/j.jweia.2017.12.010

Lorenz, R. D., Gasmi, N., Radebaugh, J., Barnes, J. W., & Ori, G. G. (2013). Dunes on planet Tatooine: Observation of barchan migration at the Star Wars film set in Tunisia. *Geomorphology*, *201*, 264–271. https://doi.org/https://doi.org/10.1016/j.geomorph.2013.06.026

Luo, W., Dong, Z., Qian, G., & Lu, J. (2012). Wind tunnel simulation of the three-dimensional airflow patterns behind cuboid obstacles at different angles of wind incidence, and their significance for the formation of sand shadows. *Geomorphology*, *139*, 258–270. https://doi.org/10.1016/j.geomorph.2011.10.027

Luo, W., Dong, Z., Qian, G., & Lu, J. (2014). Near-wake flow patterns in the lee of adjacent obstacles and their implications for the formation of sand drifts: a wind tunnel simulation of the effects of gap spacing. *Geomorphology*, *213*, 190–200. https://doi.org/10.1016/j.geomorph.2014.01.008

Luo, W., Lu, J., Qian, G., & Dong, Z. (2016). Influence of the gap ratio on variations in the surface shear stress and on sand accumulation in the lee of two side-by-side obstacles. *Environmental Earth Sciences*, *75*(9), 766. https://doi.org/10.1007/s12665-016-5588-3

Malavasi, M., Santoro, R., Cutini, M., Acosta, A. T. R., & Carranza, M. L. (2013). What has happened to coastal dunes in the last half century? A multitemporal coastal landscape analysis in Central Italy. *Landscape and Urban Planning*, *119*, 54–63. https://doi.org/10.1016/j.landurbplan.2013.06.012

Malvárez, G., Jackson, D., Navas, F., Alonso, I., & Hernandez-Calvento, L. (2013). A conceptual model for dune morphodynamics of the Corralejo dune system, Fuerteventura, Spain. *Journal of Coastal Research*, *65*(sp2), 1539–1544. https://doi.org/10.2112/SI65-260.1

Martinuzzi, R., & Tropea, C. (1993). The flow around surface-mounted, prismatic obstacles placed in a fully developed channel flow (Data bank contribution). *Journal of Fluids Engineering*, *115*(1), 85–92. https://doi.org/10.1115/1.2910118

McKenna Neuman, C., & Bédard, O. (2015). A wind tunnel study of flow structure adjustment on deformable sand beds containing a surface-mounted obstacle. *Journal of Geophysical Research: Earth Surface*, *120*(9), 1824–1840. https://doi.org/10.1002/2015jf003475

McKenna Neuman, C., Sanderson, R. S., & Sutton, S. (2013). Vortex shedding and morphodynamic response of bed surfaces containing non-erodible roughness elements. *Geomorphology*, *198*, 45–56. https://doi.org/10.1016/j.geomorph.2013.05.011

Mitteager, W. A., Burke, A., & Nordstrom, K. F. (2006). Restoring natural landscapes on private shorefront properties in New Jersey, USA. *Journal of Coastal Research*, 890–897.

Momiji, H., Carretero-González, R., Bishop, S. R., & Warren, A. (2000). Simulation of the effect of wind speedup in the formation of transverse dune fields. *Earth Surface Processes and Landforms*, *25*(8), 905–918. https://doi.org/10.1002/1096-9837(200008)25:8<905::AID-ESP112>3.0.CO;2-Z

Morelissen, R., Hulscher, S. J. M. H., Knaapen, M. A. F., Németh, A. A., & Bijker, R. (2003). Mathematical modelling of sand wave migration and the interaction with pipelines. *Coastal engineering*, *48*(3), 197–209. https://doi.org/10.1016/S0378-3839(03)00028-0

Moreno, A., & Amelung, B. (2009). Climate change and coastal & marine tourism: review and analysis. *Journal of Coastal Research*, 1140–1144. http://www.jstor.org/stable/25737965

Morton, R. A., Paine, J. G., & Gibeaut, J. C. (1994). Stages and durations of post-ptorm beach recovery, southeastern Texas coast, USA. *Journal of Coastal Research*, *10*(4), 884–908.

Namikas, S. L., & Sherman, D. J. (1995). A review of the effects of surface moisture content on aeolian sand transport. In V. P. Tchakerian (Ed.), *Desert aeolian processes* (pp. 269–293). Springer Netherlands. https://doi.org/10.1007/978-94-009-0067-7{_}13

NH Nieuws. (2019). *Strandhuisjes en paviljoens IJmuiden ontoegankelijk door dikke laag zand.* NOS. www.nos.nl/artikel/2297339-strandhuisjes-en-paviljoens-ijmuiden-ontoegankelijk-door-dikke-laag-zand.html

Nield, J. M., & Baas, A. C. W. (2008a). Investigating parabolic and nebkha dune formation using a cellular automaton modelling approach. *Earth Surface Processes and Landforms*, *33*(5), 724–740. https://doi.org/10.1002/esp.1571

Nield, J. M., & Baas, A. C. W. (2008b). The influence of different environmental and climatic conditions on vegetated aeolian dune landscape development and response. *Global and Planetary Change*, *64*(1), 76–92. https://doi.org/10.1016/j.gloplacha.2008.10.002

Nield, J. M., Wiggs, G. F. S., & Squirrell, R. S. (2011). Aeolian sand strip mobility and protodune development on a drying beach: examining surface moisture and surface roughness patterns measured by terrestrial laser scanning. *Earth Surface Processes and Landforms*, *36*(4), 513–522. https://doi.org/10.1002/esp.2071

Nishi, R., Sato, M., & Wang, H. (1995). Field observation and numerical simulation of beach and dune scarps. *Coastal engineering 1994* (pp. 2434–2448).

Nishimori, H., & Ouchi, N. (1993). Formation of ripple patterns and dunes by wind-blown sand. *Physical Review Letters*, *71*(1), 197.

Nordstrom, K. F., & Arens, S. M. (1998). The role of human actions in evolution and management of foredunes in The Netherlands and New Jersey, USA. *Journal of Coastal Conservation*, *4*(2), 169–180. https://doi.org/10.1007/bf02806509

Nordstrom, K. F. (1994). Beaches and dunes of human-altered coasts. *Progress in Physical Geography: Earth and Environment*, *18*(4), 497–516. https://doi.org/10.1177/030913339401800402

Nordstrom, K. F. (2000). *Beaches and dunes of developed coasts.* Cambridge University Press.

Nordstrom, K. F., & Jackson, N. L. (1998). Effects of a high rise building on wind flow and beach characteristics at Atlantic City, NJ, USA. *Ocean & Coastal Management*, *39*(3), 245–263. https://doi.org/10.1016/S0964-5691(97)00036-7

Nordstrom, K. F., & McCluskey, J. M. (1984). Considerations for control of house construction in coastal dunes. *Coastal Management*, *12*(4), 385–402.

Nordstrom, K. F., & McCluskey, J. M. (1985). The effects of houses and sand fences on the eolian sediment budget at Fire Island, New York. *Journal of Coastal Research*, *1*(1), 39–46. http://www.jstor.org/stable/4297009

Oikawa, S., & Tomabechi, T. (2000). Daily observation of snowdrifts around a model cube. In E. Hjorth-Hansen, I. Holand, S. Løset, & H. Norem (Eds.), *Snow engineering: Recent advances and developments* (pp. 137–141). Balkema.

Oke, T. R., Mills, G., Christen, A., & Voogt, J. A. (2017). Airflow. *Urban climates* (pp. 77–121).

Cambridge University Press. https://doi.org/10.1017/9781139016476.005

Ollongren, K. H. (2020). *Kamerbrief over overwinteren strandpaviljoens*. Ministerie van Binnenlandse Zaken en Koninkrijksrelaties.

Orams, M. B., & Lück, M. (2014). Coastal and marine tourism. *The Wiley-Blackwell companion to tourism*, 479–489.

Peterka, J. A., Meroney, R. N., & Kothari, K. M. (1985). Wind flow patterns about buildings. *Journal of Wind Engineering and Industrial Aerodynamics*, *21*(1), 21–38. https://doi.org/10.1016/0167-6105(85)90031-5

Poppema, D. W. (2020). *The effect of buildings on the morphological development of the beach-dune system: Literature report*. Enschede, University of Twente.

Pourteimouri, P., Campmans, G. H. P., Wijnberg, K. M., & Hulscher, S. J. M. H. (2022). A numerical study on the impact of building dimensions on airflow patterns and bed morphology around buildings at the beach. *Journal of Marine Science and Engineering*, *10*(1), 13. https://doi.org/10.3390/jmse10010013

Province of Noord-Holland. (2017). *Toekomstperspectief 2040 Noord-Hollandse Noordzeekust, ruimte voor rust en reuring*.

Pye, K., & Tsoar, H. (2008). *Aeolian sand and sand dunes*. Springer Science & Business Media.

Qian, G., Dong, Z., Luo, W., & Lu, J. (2011). Mean airflow patterns upwind of topographic obstacles and their implications for the formation of echo dunes: A wind tunnel simulation of the effects of windward slope. *Journal of Geophysical Research: Earth Surface*, *116*(F4). https://doi.org/10.1029/2011JF002020

Reinders, J., Van der Valk, B., & Van der Meulen, F. (2014). *Effecten van tijdelijke strandbebouwing op de ontwikkeling van de jonge zeereep (H2130: Wit Duin) aan de zeezijde van de Duincompensie Delfstandse Kust (1206682-000-ZKS-0014)*. Deltares.

Riksen, M. J. P. M., Goossens, D., Huiskes, H. P. J., Krol, J., & Slim, P. A. (2016). Constructing notches in foredunes: Effect on sediment dynamics in the dune hinterland. *Geomorphology*, *253*, 340–352. https://doi.org/10.1016/j.geomorph.2015.10.021

Roelvink, D., & Costas, S. (2019). Coupling nearshore and aeolian processes: XBeach and duna process-based models. *Environmental Modelling & Software*, *115*, 98–112. https://doi.org/https://doi.org/10.1016/j.envsoft.2019.02.010

Rotnicka, J. (2013). Aeolian vertical mass flux profiles above dry and moist sandy beach surfaces. *Geomorphology*, *187*, 27–37. https://doi.org/10.1016/j.geomorph.2012.12.032

Ruggiero, P., Hacker, S., Seabloom, E., & Zarnetske, P. (2018). The role of vegetation in determining dune morphology, exposure to sea-level rise, and storm-induced coastal hazards: A U.S. Pacific Northwest perspective. In L. J. Moore & A. B. Murray (Eds.), *Barrier dynamics and response to changing climate* (pp. 337–361). Springer International Publishing. https://doi.org/10.1007/978-3-319-68086-6{_}11

Sauvola, J., & Pietikäinen, M. (2000). Adaptive document image binarization. *Pattern recognition*, *33*(2), 225–236.

Scarelli, F. M., Sistilli, F., Fabbri, S., Cantelli, L., Barboza, E. G., & Gabbianelli, G. (2017). Seasonal dune and beach monitoring using photogrammetry from UAV surveys to apply in the ICZM on the Ravenna coast (Emilia-Romagna, Italy). *Remote Sensing Applications: Society and Environment*, *7*, 27–39. https://doi.org/10.1016/j.rsase.2017.06.003

Schlacher, T. A., Schoeman, D. S., Dugan, J., Lastra, M., Jones, A., Scapini, F., & McLachlan, A. (2008). Sandy beach ecosystems: key features, sampling issues, management challenges and climate change impacts. *Marine Ecology*, *29*(s1), 70–90. https://doi.org/10.1111/j.1439-0485.2007.00204.x

Schulman, L. L., Strimaitis, D. G., & Scire, J. S. (2000). Development and evaluation of the PRIME plume rise and building downwash model. *Journal of the Air & Waste Management Association*, *50*(3), 378–390. https://doi.org/10.1080/10473289.2000.10464017

Senthilkumaran, N., & Vaithegi, S. (2016). Image segmentation by using thresholding techniques for medical images. *Computer Science & Engineering: An International Journal*, *6*(1), 1–13.

Shafait, F., Keysers, D., & Breuel, T. M. (2008). Efficient implementation of local adaptive thresholding techniques using integral images. *Document recognition and retrieval XV*, *6815*, 681510.

Sherman, D. J., & Nordstrom, K. F. (1994). Hazards of wind-blown sand and coastal sand drifts: a review. *Journal of Coastal Research*, 263–275. http://www.jstor.org/stable/25735603

Smith, A. B., Jackson, D. W. T., & Cooper, J. A. G. (2017a). Three-dimensional airflow and sediment transport patterns over barchan dunes. *Geomorphology*, *278*, 28–42. https://doi.org/10.1016/j.geomorph.2016.10.025

Smith, A. B., Jackson, D. W. T., Cooper, J. A. G., & Hernández-Calvento, L. (2017b). Quantifying the role of urbanization on airflow perturbations and dunefield evolution. *Earth's Future*, *5*(5), 520–539. https://doi.org/10.1002/2016ef000524

Stathopoulos, T., Wu, H., & Bédard, C. (1992). Wind environment around buildings: A knowledge-based approach. *Journal of Wind Engineering and Industrial Aerodynamics*, *44*(1), 2377–2388. https://doi.org/10.1016/0167-6105(92)90028-9

Sturdivant, E. J., Lentz, E. E., Thieler, E. R., Farris, A. S., Weber, K. M., Remsen, D. P., Miner, S., & Henderson, R. E. (2017). UAS-SfM for coastal research: Geomorphic feature extraction and land cover classification from high-resolution elevation and optical imagery. *Remote Sensing*, *9*(10), 1020.

Theil, H. (1961). *Economic forecasts and policy*. North-Holland Pub. Co.

Thiis, T. K., & Jaedicke, C. (2000). The snowdrift pattern around two cubical obstacles with varying distance, measurements and numerical simulations. In E. Hjorth-Hansen, I. Holand, S. Løset, & H. Norem (Eds.), *Snow engineering: Recent advances and developments* (pp. 369–375).

Thiis, T. K. (2003). Large scale studies of development of snowdrifts around buildings. *Journal of Wind Engineering and Industrial Aerodynamics*, *91*(6), 829–839. https://doi.org/10.1016/S0167-6105(02)00474-9

Thiis, T. K., & Gjessing, Y. (1999). Large-scale measurements of snowdrifts around flat-roofed and single-pitch-roofed buildings. *Cold Regions Science and Technology*, *30*(1), 175–181. https://doi.org/10.1016/S0165-232X(99)00021-X

Tominaga, Y. (2017). Computational fluid dynamics simulation of snowdrift around buildings: Past achievements and future perspectives. *Cold Regions Science and Technology*. https://doi.org/10.1016/j.coldregions.2017.05.004

Tominaga, Y., Okaze, T., & Mochida, A. (2018). Wind tunnel experiment and CFD analysis of sand erosion/deposition due to wind around an obstacle. *Journal of Wind Engineering and Industrial Aerodynamics*, *182*, 262–271. https://doi.org/10.1016/j.jweia.2018.09.008

Tsoar, H., & Blumberg, D. (1991). The effect of sea cliffs on inland encroachment of aeolian sand. In O. E. Barndorff-Nielsen & B. B. Willetts (Eds.), *Aeolian grain transport* (pp. 131–146). Springer Vienna. https://doi.org/10.1007/978-3-7091-6703-8{_}10

Tsoar, H. (1983). Wind tunnel modeling of echo and climbing dunes. In M. E. Brookfield & T. S. Ahlbrandt (Eds.), *Developments in sedimentology: Eolian sediments and processes* (pp. 247–259). Elsevier. https://doi.org/10.1016/S0070-4571(08)70798-2

Ungar, J. E., & Haff, P. K. (1987). Steady state saltation in air. *Sedimentology*, *34*(2), 289–299.

Van Bergen, J., Mulder, J. P. M., Nijhuis, S., Poppema, D. W., Wijnberg, K. M., & Kuschnerus, M. (2021). Urban Dunes: Towards BwN design principles for dune formation along urbanized shores. *Building with Nature perspectives: Cross-disciplinary BwN approaches in coastal regions.* TU Delft Open. https://doi.org/10.47982/rius.7.130

Van der Valk, B., & Van der Meulen, F. (2013). *Ecologisch en morfologisch advies strandbebouwing. Memo 30 juli 2013.* Deltares.

Van Onselen, E. P. (2018). *Analysing measures to improve beach-dune interaction in the presence of man-made structures using computational fluid dynamics (CFD)* (tech. rep.). Utrecht, Utrecht University, Hoogheemraadschap van Rijnland,

Van Puijenbroek, M. E. B., Nolet, C., De Groot, A. V., Suomalainen, J. M., Riksen, M. J. P. M., Berendse, F., & Limpens, J. (2017). Exploring the contributions of vegetation and dune size to early dune development using unmanned aerial vehicle (UAV) imaging. *Biogeosciences*, *14*(23), 5533–5549. https://doi.org/10.5194/bg-14-5533-2017

Van Westen, B. (2019). *Invloed strandbebouwing op duinontwikkeling*. Deltares.

Werner, B. T. (1995). Eolian dunes: Computer-simulations and attractor interpretation. *Geology*, *23*(12), 1107–1110. https://doi.org/10.1130/0091-7613(1995)023<1107:Edcsaa>2.3.Co;2

Westoby, M. J., Brasington, J., Glasser, N. F., Hambrey, M. J., & Reynolds, J. M. (2012). 'Structure-from-Motion' photogrammetry: A low-cost, effective tool for geoscience applications. *Geomorphology*, *179*, 300–314. https://doi.org/10.1016/j.geomorph.2012.08.021

White, B. R. (1996). Laboratory simulation of aeolian sand transport and physical modeling of flow around dunes. *Annals of Arid Zone*, *35*(3), 187–213.

Wiggs, G. F. S., Livingstone, I., Thomas, D. S. G., & Bullard, J. E. (1994). Effect of vegetation removal on airflow patterns and dune dynamics in the southwest Kalahari desert. *Land Degradation & Development*, *5*(1), 13–24. https://doi.org/10.1002/ldr.3400050103

Wiggs, G. F. S., Livingstone, I., & Warren, A. (1996). The role of streamline curvature in sand dune dynamics: evidence from field and wind tunnel measurements. *Geomorphology*, *17*(1), 29–46. https://doi.org/10.1016/0169-555X(95)00093-K

Wijnberg, K., Poppema, D., Mulder, J., Van Bergen, J., Campmans, G., Galiforni-Silva, F., Hulscher, S., & Pourteimouri, P. (2021). Beach-dune modelling in support of Building with Nature for an integrated spatial design of urbanized sandy shores. *Building with Nature perspectives: Cross-disciplinary BwN approaches in coastal regions* (pp. 241–260). TU Delft Open. https://doi.org/10.47982/rius.7.136

Wilson, D. J. (1979). Flow patterns over flat roofed buildings and application to exhaust stack design. *ASHRAE Trans.*, *85*, 284–295.

Winckel, P. R., Vrijling, J. K., & Van de Graaff, J. (2008). Developing a building policy for the erosion zone: Solutions to some key (Dutch) questions. *Coastal engineering*, *55*(1), 79–92. https://doi.org/10.1016/j.coastaleng.2007.09.004

Yan, N., & Baas, A. C. W. (2017). Environmental controls, morphodynamic processes, and ecogeomorphic interactions of barchan to parabolic dune transformations. *Geomorphology*, *278*, 209–237. https://doi.org/https://doi.org/10.1016/j.geomorph.2016.10.033

Yen, S. C., & Liu, C. T. (2011). Gap-flow patterns behind twin-cylinders at low Reynolds number. *Journal of Mechanical Science and Technology*, *25*(11), 2795–2803. https://doi.org/10.1007/s12206-011-0908-8

Zhang, D., Narteau, C., Rozier, O., & Courrech du Pont, S. (2012). Morphology and dynamics of star dunes from numerical modelling. *Nature Geoscience*, *5*(7), 463–467. https://doi.org/10.1038/ngeo1503

List of publications

Peer-reviewed journal articles

1. Poppema, D.W., Wijnberg, K.M., Mulder, J.P.M., & Hulscher, S.J.H.M. (2022). Deposition patterns around buildings at the beach: Effects of building spacing and orientation. Geomorphology, 401, 108114. https://doi.org/10.1016/j.geomorph.2022.108114
2. Poppema, D.W., Wijnberg, K.M., Mulder, J.P.M., Vos, S.E., & Hulscher, S.J.H.M. (2021). The effect of building geometry on the size of aeolian deposition patterns: Scale model experiments at the beach. Coastal Engineering, 168, 103866. https://doi.org/10.1016/j.coastaleng.2021.103866
3. Poppema, D.W., Willemsen, P.W., De Vries, M.B., Zhu, Z., Borsje, B.W., & Hulscher, S.J.H.M. (2019). Experiment-supported modelling of salt marsh establishment. Ocean & Coastal management, 168, 238-250. https://doi.org/10.1016/j.ocecoaman.2018.10.039

Book chapters

1. Wijnberg, K., Poppema, D., Mulder, J., Van Bergen, J., Campmans, G., Galiforni-Silva, F., Hulscher, S. & Pourteimouri, P. (2021). Beach-dune modelling in support of Building with Nature for an integrated spatial design of urbanized sandy shores. Building with Nature perspectives: Cross-disciplinary BwN approaches in coastal regions, 241-260. https://doi.org/10.47982/rius.7.136
2. Van Bergen, J., Mulder, J., Nijhuis, S., Poppema, D., Wijnberg, K., & Kuschnerus, M. (2021). Urban dunes: Towards BwN design principles for dune formation along urbanized shores. Building with Nature perspectives: Cross-disciplinary BwN approaches in coastal regions, 101-127. https://doi.org/10.47982/rius.7.130

Conference papers and abstracts

1. Poppema, D.W., Wijnberg, K.M., Mulder, J.P.M., & Hulscher, S.J.H.M. (2019). Scale experiments on aeolian deposition and erosion patterns created by buildings on the beach. Presented at Coastal Sediment 2019, Tampa, USA. Published in Coastal Sediments 2019: Proceedings of the 9th International Conference, 1693-1707. https://doi.org/10.1142/9789811204487_0146
2. Poppema D.W., Wijnberg K.M., Mulder J.P.M. & Hulscher S.J.M.H (2021). The effect of the orientation and spacing of buildings at the beach on aeolian deposition patterns. Coastal Dynamics 2021, Delft, the Netherlands.

3. Poppema, D.W., Wijnberg, K.M., Mulder, J.P.M., & Hulscher, S.J.H.M. (2020). The effect of building geometry on aeolian deposition and erosion patterns: a field experiment. Coastal Engineering Proceedings, (36v), sediment.21. Presented at vICCE2020. https://doi.org/10.9753/icce.v36v.sediment.21; https://youtu.be/hlcMP7Ev1m0

4. Poppema, D.W., Willemsen, P.W.J.M., De Vries, M.B., Zhu, Z., Borsje, B.W. & Hulscher, S.J.M.H. (2017). Experiment-supported modeling of salt marsh establishment: Applying the Windows of opportunity concept to the Marconi pioneer salt marsh design. ECSA Focus Meeting 2017, Shanghai, China.

5. Poppema, D.W., Baas, A.C.W., Hulscher, S.J.M.H. & Wijnberg, K.M. (2022). Modelling sediment dynamics around buildings in a cellular automaton model. NCK Days 2022, Enschede, the Netherlands.

6. Poppema D.W., Wijnberg K.M., Mulder J.P.M. & Hulscher S.J.M.H. (2021). How the spacing and orientation of buildings shape local sandy deposition patterns. NCK Days 2021, online.

7. Poppema D.W., Wijnberg K.M., Mulder J.P.M. & Hulscher S.J.M.H. (2019). Scale experiments on Aeolian deposition patterns around buildings on the beach. NCK Days 2019, Enkhuizen, the Netherlands.

8. Pourteimouri, P., Campmans, G.H.P., Poppema, D.W., Wijnberg, K.M., Hulscher, S.J.M.H. (2019). CFD modeling of airflow over urbanized beaches and the impact of built environment on aeolian sediment transport. NCK Days 2019, Enkhuizen, the Netherlands.

9. Poppema, D.W., Baas, A.C.W., Hulscher, S.J.M.H. & Wijnberg, K.M. (2022). Morphological effects of beach buildings: from field experiments to CA modelling. Accepted for EGU General Assembly 2022, Vienna, Austria.

Other

1. Poppema, D.W. (2020). The effect of buildings on the morphological development of the beach-dune system: Literature report. Enschede: University of Twente.

2. Poppema, D.W., Willemsen, P.W.J.M., Borsje, B.W., De Vries, M., Zhu, Z., Dankers, P., & Hulscher, S.J.H.M. (2018). Naar een grondiger begrip van vegetatievestiging. H2O, 2018(1), 34-35.

3. Poppema, D.W., Wijnberg, K.M., Mulder, J.P.M., & Hulscher, S.J.H.M. (2022). Experimental data of Deposition patterns around buildings at the beach: effects of building spacing and orientation. Dataset at 4TU.Centre for Research Data. https://doi.org/10.4121/16860145.v3

About the author

Daan Poppema grew up in Winsum and Eenrum, two villages in the north of the Netherlands. After graduating from the Willem Lodewijk Gymnasium in Groningen, he moved to Enschede in 2011 to start his bachelor Civil Engineering at the University of Twente. He combined his bachelor assignment with a minor in Sustainable Development in Guadalajara, Mexico. Here he studied urban rainwater drainage and flooding at an NGO founded by the local university. Next, Daan continued his studies at the University of Twente with the Civil Engineering and Management master, where he chose the Water Engineering and Management track. During this master, he also studied at the Norwegian University of Science and Technology (NTNU) in Trondheim for half a year. Back in the Netherlands, Daan conducted his master thesis at two research institutes: Deltares Delft and the NIOZ in Yerseke. Here he studied the establishment conditions of salt marsh vegetation, by testing the erosion resistance of saltmarsh seedlings in a wave flume and linking this to bed level dynamics in a morphodynamic Delft3D model. With this graduation research, he won multiple thesis prizes.

Daan started the PhD that culminated in this dissertation in November 2017, as part of the ShoreScape research program. During this PhD at the University of Twente, he attended the SAMO summer school and NCK summer school. He presented his work in international peer-reviewed journal articles and at conferences in Shanghai (China), Sint Petersburg (Florida, USA), Delft (Netherlands) and the online ICCE. Besides research, Daan was actively involved in education, by supervising BSc and MSc graduate students and giving tutorials and practicals for courses on wave dynamics, data analysis and morphology.